

University of Windsor

Scholarship at UWindor

Electronic Theses and Dissertations

Theses, Dissertations, and Major Papers

2011

Experimental Study on Bridge Stay Cable Vibration Mitigation Using External Viscous Damper

Le Huang
University of Windsor

Follow this and additional works at: <https://scholar.uwindsor.ca/etd>

Recommended Citation

Huang, Le, "Experimental Study on Bridge Stay Cable Vibration Mitigation Using External Viscous Damper" (2011). *Electronic Theses and Dissertations*. 80.
<https://scholar.uwindsor.ca/etd/80>

This online database contains the full-text of PhD dissertations and Masters' theses of University of Windsor students from 1954 forward. These documents are made available for personal study and research purposes only, in accordance with the Canadian Copyright Act and the Creative Commons license—CC BY-NC-ND (Attribution, Non-Commercial, No Derivative Works). Under this license, works must always be attributed to the copyright holder (original author), cannot be used for any commercial purposes, and may not be altered. Any other use would require the permission of the copyright holder. Students may inquire about withdrawing their dissertation and/or thesis from this database. For additional inquiries, please contact the repository administrator via email (scholarship@uwindsor.ca) or by telephone at 519-253-3000ext. 3208.

**EXPERIMENTAL STUDY ON BRIDGE STAY CABLE
VIBRATION MITIGATION USING EXTERNAL VISCOUS
DAMPER**

By

Le Huang

A Thesis
Submitted to the Faculty of Graduate Studies
through the Department of Civil and Environmental Engineering
in Partial Fulfillment of the Requirements
for the Degree of Master of Applied Science at the
University of Windsor

Windsor, Ontario, Canada

2011

© 2011 Le Huang

Experimental Study on Bridge Stay Cable Vibration Mitigation Using External Viscous
Damper

by

Le Huang

APPROVED BY:

J. Wu (External Reader)
Department of Electrical Engineering

B. Budkowska (Department Reader)
Department of Civil and Environmental Engineering

S. Cheng (Advisor)
Department of Civil and Environmental Engineering

C. Lee (Chair of Defence)
Department of Civil and Environmental Engineering

04 April 2011

Author's Declaration of Originality

I hereby certify that I am the sole author of this thesis and that no part of this thesis has been published or submitted for publication.

I certify that, to the best of my knowledge, my thesis does not infringe upon anyone's copyright nor violate any proprietary rights and that any ideas, techniques, quotations, or any other material from the work of other people included in my thesis, published or otherwise, are fully acknowledged in accordance with the standard referencing practices. Furthermore, to the extent that I have included copyrighted material that surpasses the bounds of fair dealing within the meaning of the Canada Copyright Act, I certify that I have obtained a written permission from the copyright owner(s) to include such material(s) in my thesis and have included copies of such copyright clearances to my appendix.

I declare that this is a true copy of my thesis, including any final revisions, as approved by my thesis committee and the Graduate Studies office, and that this thesis has not been submitted for a higher degree to any other University or Institution.

ABSTRACT

Selecting an optimum damper size for a specific cable with designed damper location is very important. An experimental study of cable vibration mitigation by using external viscous damper was carried out in the present work. A linear viscous oil damper with six adjustable damper sizes was designed and fabricated. The experimental work mainly focused on evaluating the equivalent structural damping ratio of a cable-damper system using forced vibration tests. General damper design curves based on the current experimental results have been developed and compared with those in the existing literature. In addition, the damper stiffness effect, which is ignored in the past work, has been extensively studied. Results show that the impact of damper stiffness on its efficiency is highly dependent on the damper location. An approximately linear relationship is found to exist between the damper stiffness and the damping ratio. As stiffness of the damper increases, the equivalent modal damping ratio of the system will decrease.

ACKNOWLEDGEMENTS

The thesis would not have been possible started without the support and guidance of Dr. Shaohong Cheng who has enriched my fundamental knowledge of structural dynamics. I would like to especially thank Dr. Cheng for her guidance every step of the way, constant support, advice and encouragement whenever it was needed. Secondly, I would also like to thank my thesis proposal committee, Dr. Budkowska, and Dr. Wu for their helpful comments on my thesis. Finally, I would like to thank laboratory technicians, Mr. Lucian Pop, Mr. Matt St.Louis, and Mr. Pat Seguin for their help during my experimental research.

TABLE OF CONTENTS

AUTHOR'S DECLARATION OF ORIGINALITY	III
ABSTRACT.....	IV
ACKNOWLEDGEMENTS.....	V
LIST OF FIGURES	IX
LIST OF TABLES.....	XIV
CHAPTER 1 INTRODUCTION	1
1.1 Background.....	1
1.2 Motivation.....	2
1.3 Objectives	3
CHAPTER 2 LITERATURE REVIEW	4
2.1 Various Types of Cable Vibration Phenomena	4
2.1.1 Rain-wind induced vibration	4
2.1.2 Vortex-induced vibration.....	7
2.1.3 High-speed vortex excitation.....	8
2.1.4 Buffeting	9
2.1.5 Wake galloping.....	9
2.1.6 Galloping for dry inclined cable	10

2.2 Cable Vibration Mitigation Methods.....	11
2.2.1 Aerodynamic control	11
2.2.2 Mechanical control	13
2.2.3 State-of-the-art on mitigating cable vibration using external damper	17
 CHAPTER 3 EXPERIMENTAL DETAILS	 30
3.1 Experimental Setup.....	30
3.2 Damper Design and Calibration	40
3.2.1 Damper Design	40
3.2.2 Damper Calibration	44
3.3 Free Vibration Tests	46
3.3.1 Testing procedures.....	47
3.3.2 Theoretical background	48
3.3.3 Potential problem found in the free vibration tests.....	50
3.4 Forced Vibration Tests	52
3.4.1 Testing procedures.....	53
3.4.2 Theoretical background	54
3.4.3 Advantage of forced vibration tests.....	55
 CHAPTER 4 RESULTS AND DISCUSSIONS.....	 57
4.1 Pre-processing of Experimental Data	57
4.2 Experimental Results	61

4.2.1 Damping ratio of a damped cable.....	61
4.3 Comparison with Other Studies.....	68
4.3.1 Universal damper design curve (Pacheco et al, 1993).....	68
4.3.2 Damper design curves (Cheng et al, 2010).....	71
4.4 Effect of Damper Stiffness	77
CHAPTER 5 CONCLUSIONS AND RECOMMENDATIONS	95
5.1 Conclusions for Current Study	95
5.2 Recommendations for Future Work	96
REFERENCE.....	98
APPENDIX A DAMPER PROPERTIES	102
APPENDIX B MATLAB CODE FOR DATA PROCESSING	109
APPENDIX C FILTERED AND CONVERTED DATA.....	111
APPENDIX D DAMPER DESIGN CURVES (CHENG ET AL, 2010).....	121
VITA AUCTORIS	124

LIST OF FIGURES

Figure 1-1 Sutong Bridge (Left) and Stonecutter Bridge (Right).....	2
Figure 2-1 Variation of the angle of formation of the water rivulet with wind speed $\theta = 45^\circ$ (Hikami and Shiraisi, 1988).....	5
Figure 2-2 Three different mechanisms of rain-wind induced excitation proposed by Verwiebe (1998).....	6
Figure 2-3 Qualitative trend of vortex shedding frequency with wind velocity during lock-in (Simiu, 1986).....	8
Figure 2-4 Illustration of the axial vortex and Karman vortex interaction in the wake of a yawed inclined cable (Matsumoto et al., 1995).....	9
Figure 2-5 Wind attacking a bluff body (Elsa, 2007).....	11
Figure 2-6 Indented surface used on the Tataru Bridge (Sun et al., 2010).....	12
Figure 2-7 Illustration of different types surface protrusions.....	13
Figure 2-8 Cross-ties System in Cable-stayed Bridges.....	14
Figure 2-9 MR damper installed on cable-stayed bridges.....	15
Figure 2-10 A picture of Rubber damper (left) and rubber damper installed on Tataru bridge(right).....	16
Figure 2-11 Friction damper installed on Uddevalla bridge in Sweden.....	16
Figure 2-12 Two oil dampers installed on second Nanjing Yangtze Bridge.....	17
Figure 2-13 Dynamic amplification curves (Kovács, 1982).....	19
Figure 2-14 Universal damper design curve by Pacheco et al.(1993).....	20
Figure 2-15 Variation of the maximum damping ratio with respect to the bending stiffness parameter (Tabatabai and Mehrabi, 2000).....	22

Figure 2-16 Schematic illustration of kinetic energy time history of the nth mode of a damped cable (Cheng et al., 2010).....	23
Figure 2-17 Damping ratio of the first mode in experimental model (Sulekh and Pacheco, 1990).....	25
Figure 2-18 Experimental test setups by Xu et al. (1999).....	26
Figure 2-19 Responses amplitude with and without damper (Xu et al., 1999).....	27
Figure 2-20 Taut Cable with Spring-mass Damper.....	28
Figure 3-1 Experimental setup.....	31
Figure 3-2 Iron mass.....	32
Figure 3-3(a) Universal Flat Load Cell Top View.....	33
Figure 3-3(b) Universal Flat Load Cell Front View.....	33
Figure 3-4 Hydraulic hand pump.....	34
Figure 3-5 Accelerometer placed in the middle of the cable.....	35
Figure 3-6 Back View of Shaker installed on cable.....	36
Figure 3-7 HP 15MHz function/Arbitrary Waveform Generator.....	37
Figure 3-8 AstroDAQ Xe Data Acquisition System.....	38
Figure 3-9 Realtime mode before testing.....	39
Figure 3-10 Capturing data in Realtime mode.....	39
Figure 3-11 Damper design sketch.....	40
Figure 3-12 Oil damper designed in the current study.....	41
Figure 3-13 Four Solid Aluminum Plates.....	42
Figure 3-14 Three Springs from McMaster.com.....	44
Figure 3-15 Damper Calibration Setup.....	46

Figure 3-16 Free Vibration Test Setup.....	47
Figure 3-17 Mass Block with wire tied on it.....	48
Figure 3-18 Sample of 1 st modal displacement decay curve.....	50
Figure 3-19 free vibration tests to determine friction existed between the plastic stick and the lid.....	52
Figure 3-20 Forced Vibration Test Setup.....	53
Figure 3-21 half power method illustration on frequency-response curve.....	56
Figure 4-1 First modal displacement time-history of B_3200_20500_S05_D06_A50_7.40 Hz.....	62
Figure 4-2 Frequency-response curve for case B_3200_20500_S05_D06_A50.....	64
Figure 4-3 Equivalent first modal damping ratio with damper installed at 4%L.....	66
Figure 4-4 Equivalent first modal damping ratio with damper installed at 6%L.....	67
Figure 4-5 Equivalent first modal damping ratio with damper installed at 10%L.....	68
Figure 4-6 Universal damper design curve proposed by Pacheco et al. (1993).....	69
Figure 4-7 Comparison between the current results and the universal damper design curve proposed by Pacheco et al. (1993).....	70
Figure 4-8 Layout of a cable-damper system studied by Cheng et al (2010).....	71
Figure 4-9 Schematic illustration of kinetic energy time history of the nth mode of a damped cable (Cheng et al., 2010).....	72
Figure 4-10 Comparison between the current study and Cheng et al's design curve at 4%L.....	74
Figure 4-11 Comparison between the current study and Cheng et al's design curve at 6%L.....	74

Figure 4-12 Comparison between the current study and Cheng et al's design curve at 10%L.....	75
Figure 4-13 Impact of damper stiffness on equivalent 1 st modal cable damping ratio (damper location 4%L).....	80
Figure 4-14 Impact of damper stiffness on equivalent 1 st modal cable damping ratio (damper location 6%L).....	80
Figure 4-15 Impact of damper stiffness on equivalent 1 st modal cable damping ratio (damper location 10%L).....	81
Figure 4-16 Damping ratio vs Damper stiffness (C = 18.4 N·s/m).....	82
Figure 4-17 Damping ratio vs Damper stiffness (C = 46.7 N·s/m).....	82
Figure 4-18 Damping ratio vs Damper stiffness (C = 70.3 N·s/m).....	83
Figure 4-19 Damping ratio vs Damper stiffness (C = 164.8 N·s/m).....	83
Figure 4-20 Damping ratio vs Damper stiffness (C = 275.5 N·s/m).....	84
Figure 4-21 Damping ratio vs Damper stiffness (C = 1463.8 N·s/m).....	84
Figure 4-22 Damping ratio decay rate of experimental results and Zhou's formula with damper size 18.4 N·s/m.....	92
Figure 4-23 Damping ratio decay rate of experimental results and Zhou's formula with damper size 46.7 N·s/m.....	92
Figure 4-24 Damping ratio decay rate of experimental results and Zhou's formula with damper size 70.3 N·s/m.....	93
Figure 4-25 Damping ratio decay rate of experimental results and Zhou's formula with damper size 164.8 N·s/m.....	93

Figure 4-26 Damping ratio decay rate of experimental results and Zhou's formula with
damper size 164.8 N·s/m.....94

Figure 4-27 Damping ratio decay rate of experimental results and Zhou's formula with
damper size 1463.8 N·s/m.....94

LIST OF TABLES

Table 2-1 Summary of empirical damper design formulae in the existing literature: Optimal damper coefficient and maximum damping ratio for a viscous damper.....	24
Table 3-1 Properties of Aluminum Plates.....	42
Table 3-2 Oil Properties.....	43
Table 3-3 Spring Properties.....	44
Table 3-4 Damper properties.....	45
Table 4-1 Summary of maximum displacements in case B_3200_20500_S05_D06 _A50	63
Table 4-2 Cable damping ratio for different damper sizes and locations.....	65
Table 4-3 Different damper size and its corresponding nondimensional damping parameter ψ	73
Table 4-4 Damper stiffness effect on cable damping ratio (%).....	74
Table 4-5 Damping ratio decay rate of experimental results and Zhou's formula with damper size 18.4 N·s/m.....	86
Table 4-6 Damping ratio decay rate of experimental results and Zhou's formula with damper size 46.7 N·s/m.....	87
Table 4-7 Damping ratio decay rate of experimental results and Zhou's formula with damper size 70.3 N·s/m.....	88
Table 4-8 Damping ratio decay rate of experimental results and Zhou's formula with damper size 164.8 N·s/m.....	89

Table 4-9 Damping ratio decay rate of experimental results and Zhou's formula with
damper size 275.5 N·s/m.....90

Table 4-10 Damping ratio decay rate of experimental results and Zhou's formula with
damper size 1463.8 N·s/m.....91

CHAPTER 1 INTRODUCTION

1.1 Background

With the development of modern structural materials and the advancement of construction technologies, it is possible to build structures which have longer span and taller height. This type of structures is usually flexible and thus very sensitive to environmental dynamic effects such as wind and earthquake. Cable is a common type of structural component. It has been widely used in various types of civil structures, such as cable-stayed bridge, suspension bridge, mesh antenna etc. Cable-stayed bridge has become more and more popular since 1950's because of its ease of construction, aesthetics, technology maturity and economy. The current longest cable-stayed bridge in the world is the Sutong Bridge in China, which was completed in 2008. It has a main span of 1088 m. The second longest span is the Stonecutter Bridge which is also in China and has a main span of 1018 m. The third longest is the Tataru Bridge in Japan. Its main span length is 890 m. Bridge stay cable is flexible and low in inherent damping. It is prone to dynamic excitation and exhibit large amplitude of vibrations. This is more pronounced for longer cables. The rapidly increased bridge span length in recent years requires longer length cable to support the superstructure. This causes more frequently observed cable vibration problem on bridge site! Cables can be excited by various mechanism such as rain-wind induced vibration, vortex-excited vibration, high-speed vortex excitation, galloping, buffeting etc (Yamaguchi and Fujino, 1998; Jiang, 2006; Zhou, 2005; Sun et al., 2010). Frequent and excessive cable vibrations will cause cable fatigue failure at its anchorage. There are lots of cable fault in the past. For example, it

was found on Maracaibo Bridge in Venezuela in 1978 that more than 500 steel wires were damaged. A year later, another 3 cables were totally failed (Zhou, 2005). In the case of Jinan Yellow River Bridge in China, all the cables were replaced after 13 years in service because of fatigue failure (Zhou, 2005). Stay cables account at least 15% of the total cost of a cable-stayed bridge project. Therefore, reducing the probability of stay cable failure caused by vibration is very important not only in terms of structural safety, but for economy as well.



Figure 1-1 Sutong Bridge (Left) and Stonecutter Bridge (Right)

1.2 Motivation

External damper is the most commonly used device for controlling bridge stay cable vibrations in field. Developments of empirical formulae for damper design were mostly conducted using numerical simulation or analytical method. Only limited numbers of experimental studies were performed. Besides studies on how damper stiffness could affect the damper efficiency are scarce in existing literatures.

These facts initiated the motivations to conduct an experimental study on the behavior of a cable-damper system, and utilized such a system to verify results reported

in the existing literatures. In addition, efforts will also be dedicated to investigating the effect of damper stiffness on the efficiency of its performance.

1.3 Objectives

The objectives of the current study are proposed as follows:

- 1) Design and develop an experimental setup to study the behavior of a cable-damper system. Based on the conditions of the current structures lab located in Essex Hall B-19, design and develop the arrangements to satisfy the requirements of the proposed experimental study.
- 2) Design and build a linear viscous damper which will allow having adjustable damper capacity.
- 3) Develop proper methodologies and procedures to process the experimental data. Data processing and analysis will be mainly conducted in the Matlab and Microsoft Excel environment.
- 4) Conduct cable free vibration tests to obtain modal properties of the studied cable-damper system.
- 5) Conduct forced vibration tests to obtain modal cable damping ratio and compare it with existing literature.
- 6) Study damper stiffness effect by adding springs to the damper in the tests and compare variation of modal cable damping ratio with and without springs.

CHAPTER 2 LITERATURE REVIEW

2.1 Various Types of Cable Vibration Phenomena

Cable vibrations can be classified into two main categories: wind-induced vibrations and non-wind-induced vibrations. Wind-induced vibrations include rain-wind induced vibration, vortex-induced vibration, high-speed vortex-excited vibration, buffeting, galloping etc., whereas non-wind-induced vibrations include parametric excitation and external excitation. Periodic bridge deck motion and traffic loads could induce vibration when the motion frequency approaches to natural frequency of stay cable. A brief review of various types of cable vibration phenomena is presented in the following subsection.

2.1.1 Rain-wind induced vibration

Although there are many reasons to excite vibrations of stay cables, it is believed about 95% of the reported vibration problems on cable-stayed bridges belong to rain-wind induced oscillations (Wagner and Fuzier, 2003). In the past 30 years, numerous cable-stayed bridges were observed exhibiting large amplitude of stay cable oscillations under certain environmental conditions. It became evident that these vibrations occurred when moderate rain was combined with moderate wind conditions (HNTB Corporation, 2007). The main feature of this complex phenomenon was concluded by Tanaka (2003). He indicated that under the combined action of rain and wind, at specific angles of attack and intensity of rainfall, water rivulets would form at the upper and lower surfaces of the

cable (Figure 2-1). The formation of these rivulets would cause the change of the balance of gravitational, aerodynamic and surface capillary forces, which eventually led to unsymmetrical cable cross-section. Therefore, under certain physical conditions, non-zero lift force would occur to excite the cable.

Hikami and Shiraish (1988) performed a wind tunnel test to simulate the generating mechanism of rain-wind induced vibration. In particular, the formation and role of the water rivulet along the cable in excitation mechanism was investigated. Results showed that a second rivulet was formed along the upper windward surface of the cable at an angle θ equal to 45° . The formation of this upper rivulet was associated with wind speed. As the wind speed increased to a certain value, the raindrops would overcome the gravity and friction forces to form the upper rivulet. The relationship between the angle of formation and wind speed is shown in Figure 2-1.

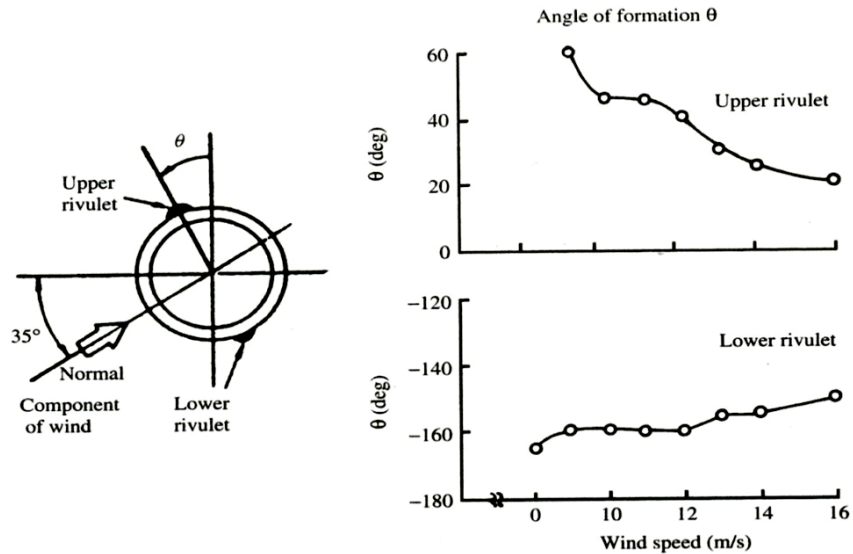


Figure 2-1 Variation of the angle of formation of the water rivulet with wind speed $\theta = 45^\circ$
(Hikami and Shiraisi, 1988)

The lower rivulet was found to have a stabilizing effect which would produce an aerodynamic damping force to suppress cable motion; whereas the upper rivulet would generate aerodynamic force to excite the cable motion.

Verwiebe (1998) further identified three different mechanisms of rain-wind induced excitation, the sketch of which are illustrated in Figure 2-2. The first mechanism occurred when wind was in the direction of cable motion. The oscillation of water rivulet intensified the cable vibration, and it reached the maximum vibration amplitude when wind speed is 25m/s.

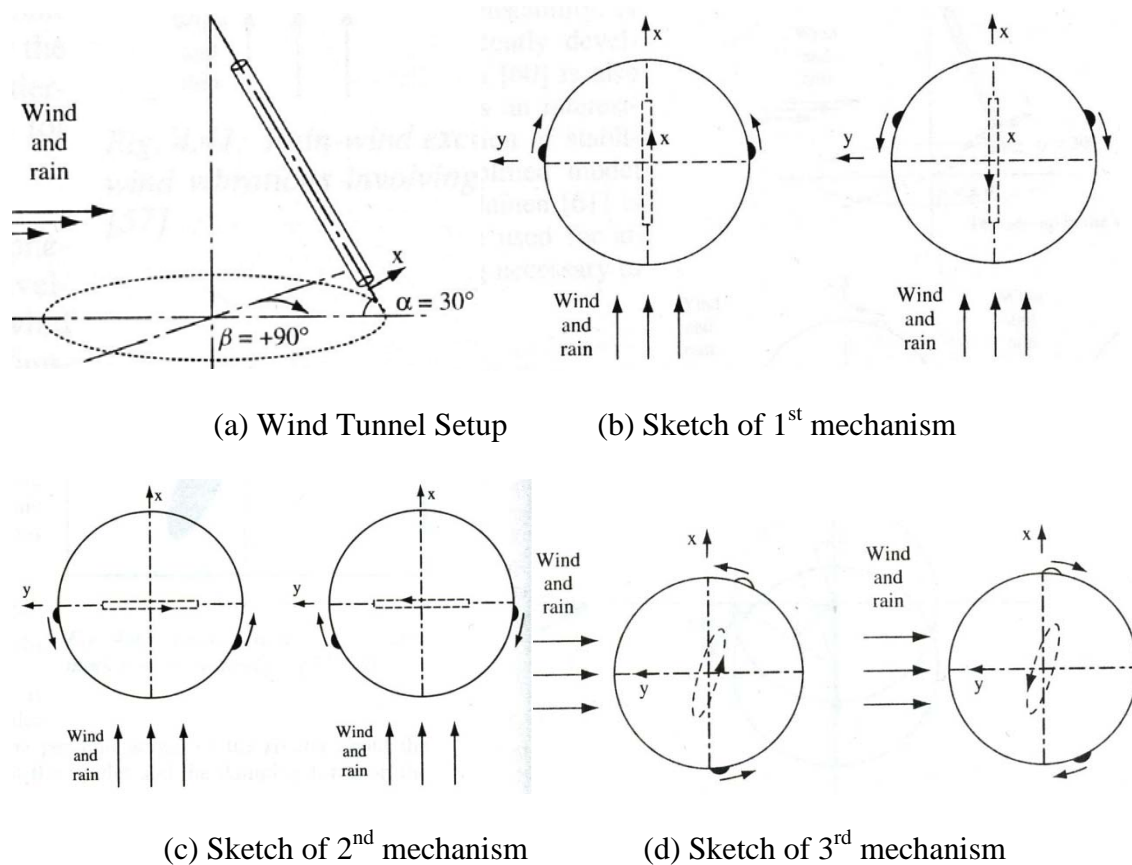


Figure 2-2 Three different mechanisms of rain-wind induced excitation proposed by

Verwiebe (1998)

The second mechanism occurred when wind velocity exceeded 18m/s and the cable vibrated in the cross-wind direction. The vibration stimulated the anti-symmetrical oscillation of the upper and lower rivulets. The third mechanism occurred when cable was inclined orthogonally to the wind direction. When speed of wind was smaller than 19m/s, only the underside rivulet oscillated. However, when wind speed was above 19m/s, oscillation of both upper and downside rivulet occurred.

2.1.2 Vortex-induced vibration

Vortex shedding (Matsumoto et al., 1995) is a common excitation phenomenon of stay cables. When flow passes cable, it will separate and form shedding vortices in the wake region. These vortices are well known as Kármán Vortices. When alternating shedding frequency of the vortices approaches to the natural frequency of the cable, resonance will occur and the cable will be excited. The vortex resonance drives cable to interact with surrounding flow even when the critical wind speed was exceeded by certain range. This is known as lock-in phenomenon as depicted in Figure 2-3. Although vortex-induced cable vibration is commonly observed on bridges, it was found that the amplitude of vibration was generally very small. Davenport (1994) stated that the amplitude of vortex-induced vibration rarely reached the size of the cable radius.

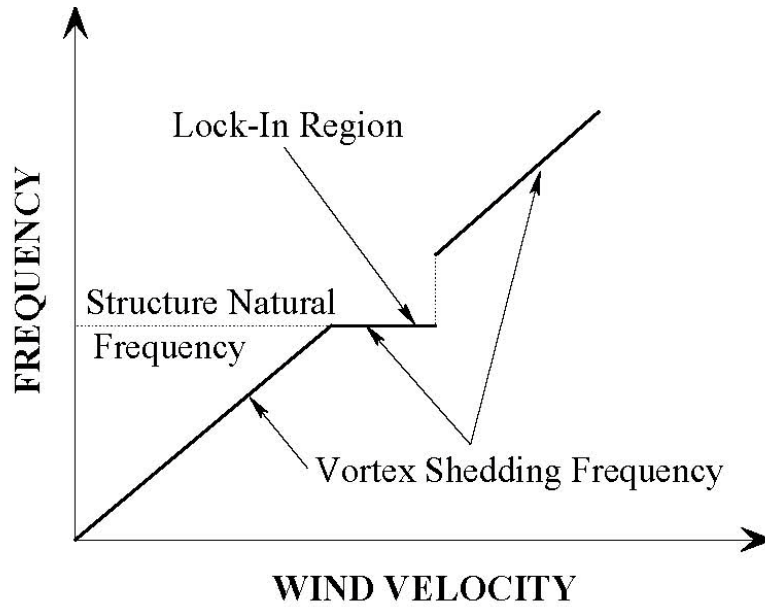


Figure 2-3 Qualitative trend of vortex shedding frequency with wind velocity during lock-in (Simiu, 1986)

2.1.3 High-speed vortex excitation

High-speed vortex excitation is a newly proposed mechanism of wind-induced cable vibrations in recent years. It was observed on inclined cables in several full-scale measurements in wind tunnel tests (Matsumoto, 1995), (Cheng et al., 2003), (Cheng et al. 2008). According to Matsumoto's research, it was found to be directly associated with the axial vortex shedding and its interaction with conventional Kármán Vortices shedding in the wake of the cable. Testing results showed a Kármán Vortex interacting with the axial flow as the illustration in Figure 2-4. However, the characteristics of this axial vortex have not been fully identified yet. Although this type of instability is also associated with vortex-shedding in the wake, it occurs at a wind speed much higher than the conventional Kármán Vortex-excited vibration discussed in section 2.1.2, it is therefore called high-

speed vortex excitation. This phenomenon is greatly affected by the intensity of turbulence in the upcoming wind.

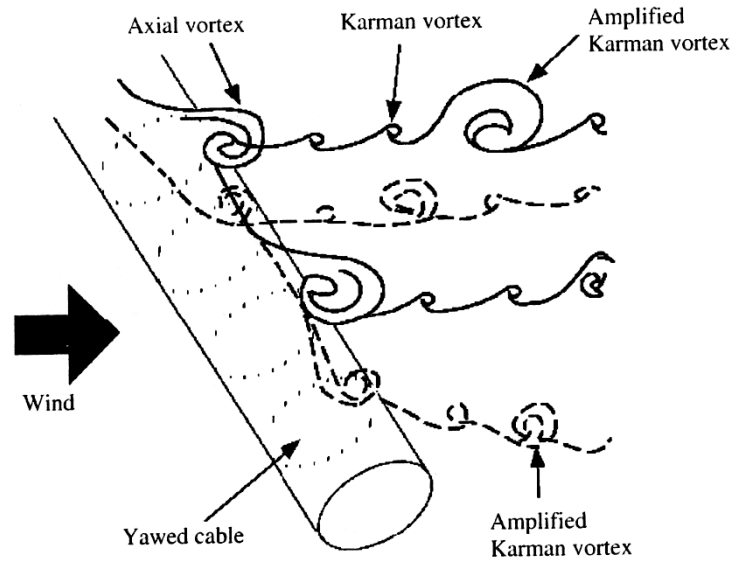


Figure 2-4 Illustration of the axial vortex and Karman vortex interaction in the wake of a yawed inclined cable (Matsumoto, 1995)

2.1.4 Buffeting

Buffeting is a type of random forced vibration induced by the turbulent component in the wind. It differs from other cable vibration mechanisms in that it does not deal with an aerodynamic or resonant phenomenon. The response characteristics are highly dependent on the turbulent nature of the wind. The vibration amplitude is relatively small. Though no violent cable motion would occur, the frequent low-amplitude of cable motion has the potential of inducing fatigue failure at cable anchorage.

2.1.5 Wake galloping

Wake galloping occurs when a cable locates in the wake of another cable or other

structural members. Aerodynamic forces acting on the cable change while wind angle of attack changes (HNTB, 2007). The main difference between wake galloping and vortex-induced vibration is that the former is a high amplitude vibration which occurs only at high wind speed. It will cause fatigue failure at cable anchorage. It was found that wake galloping could also happen and the hangers of suspension and arch bridges. However, up to date, fatigue failure at cable anchorage due to wake galloping has never been reported in literature for cable-stayed bridges.

2.1.6 Galloping for dry inclined cable

The divergent type of motion induced by wind for dry inclined cable was observed in wind tunnel tests by Saito et al. (1994) and Honda et al. (1995) in the subcritical Re regime; and Miyata et al. (1994) and Cheng et al. (2003, 2008a, 2008b) in the transition and critical Reynolds number regime. It was also reported in the field (Irwin et al., 1999; Virlogeux, 1998). The excitation mechanism was studied by Cheng et al. (2008b), she proved that mechanism was similar to that for Den Hartog criterion galloping. Glauert-Den Hartog criterion [Simiu, 1996] $\left(\frac{dC_L}{d\beta} + C_D \right)_{\beta=0} < 0$ clearly express galloping occurrence cases (Den Hartog, 1956). Where α is the attacking angel, C_L is Lift coefficient and C_d Drag coefficient. From the criterion, we known circular cross-section will never experience galloping if wind attacking direction is perpendicular to stay cable since α will be zero because of symmetry of circle. Figure 2-5 shows lift and drag forces when wind passing a bluff body with attacking angle α . Cheng et al. (2008b) also stated that the surrounding flow field of dry inclined cable against wind has strong 3D

characteristics. Therefore, driving mechanism of divergent motion was complicated; the Den Hartog criterion might only be part of the reason, and further investigation was recommended.

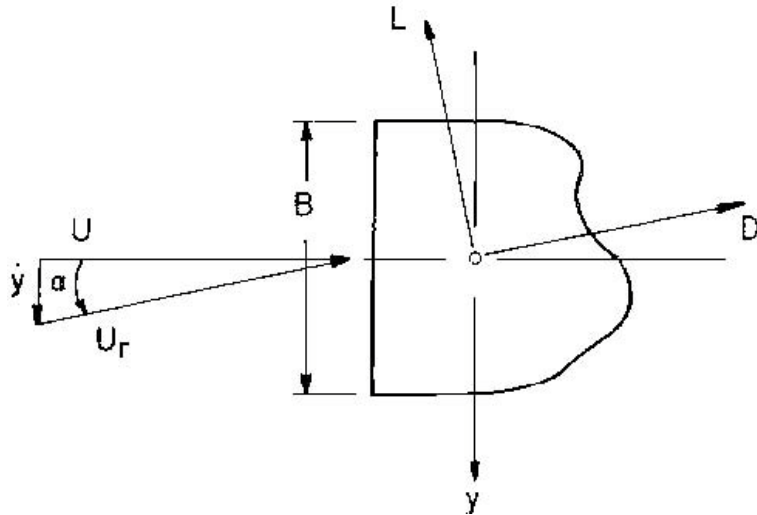


Figure 2-5 Wind attacking a bluff body (Elsa, 2007)

2.2 Cable Vibration Mitigation Methods

To suppress cable vibration on cable-stayed bridges induced by various mechanisms, many mitigation methods have been developed and applied in field with different levels of success. These methods can generally be classified as aerodynamic control method and mechanical control method.

2.2.1 Aerodynamic control

Aerodynamic control is a passive control method which modifies aerodynamic feature of the cable cross-section. It is most effective in controlling rain-wind-induced cable vibration by preventing accumulation of rain to form water stream on the surface of

stay cable. The surface modification should ensure no other aerodynamic instability would be excited. This method should be carefully considered not to increase the drag coefficient of cable cross-section. Many researchers conducted wind tunnel tests or numerical simulation to justify the effectiveness of aerodynamic control method. There are mainly two commonly used surface modification techniques for stay cables (Sun et al., 2010; Saito et al., 1994; Kleissl, 2009; Flamand, 1994; Bosdogianni, 1996; Virlogeux, 1998): Cable surface indentations (Figure 2-6) and cable surface protrusions (Figure 2-7). Aerodynamic control has the advantages that the repair and maintenance is easy and simple and the cost is low. However, the development and construction details of different cases need to be experimentally validated and developed. For example, the total damping ratio of the cable before and after applying surface modification needs to be tested based on site service conditions.

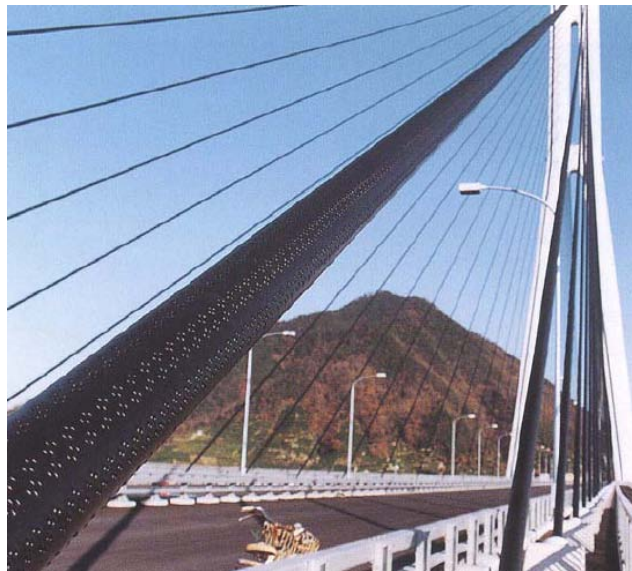


Figure 2-6 Indented surface used on the Tatara Bridge (Sun et al., 2010)



Figure 2-7 Illustration of different types surface protrusions

2.2.2 Mechanical control

Mechanical control is the most popularly used mitigation method on bridge site to control cable vibration. Cross-ties and external dampers are commonly used for this purpose.

Cross-ties have been installed on many cable-stayed. For example, it is applied on the Normandy Bridge in France, the Second Severn Bridge in the United Kingdom, the Helgeland Bridge in Norway, and the Meiko Nishi Bridge in Japan (Kumarasena, 2007). Stay cable normally has low natural frequencies and inherent damping. So it is easily excited by dynamic loads. By the addition of cross-tie system, two or more stay cables are interconnected. Therefore, the in-plane stiffness (natural frequencies) can be increased. This could effectively suppress stay cables vibration in low frequencies.

Besides, the internal damping of the cable can also be increased if cross-tie is used. Yamaguchi (1995) proposed in his research that if softer cross-ties were used, the cable damping could be increased more. Figure 2-8 shows two different cross-ties system in cable-stayed bridges.

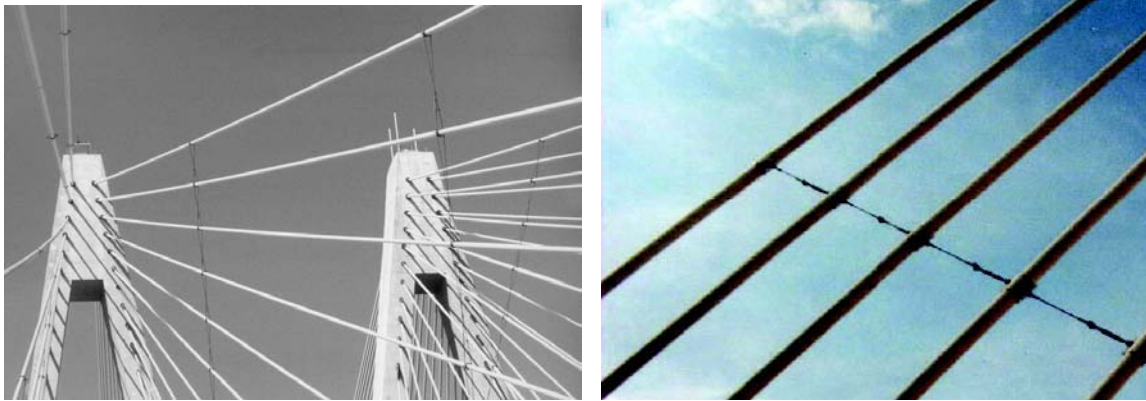


Figure 2-8 Cross-ties System in Cable-stayed Bridges

Based on the functioning characteristics external dampers can be active damper, semi-active damper and passive damper. Active damper control requires the input of external power. It is not commonly used in stay cable vibration mitigation.

Semi-active dampers are becoming more popular in recent years. MR damper is the most common type of semi-active control device in the field. MR damper is short for magnetorheological damper, it filled with magnetorheological fluid which could change its damper size by varying magnetic field (Zhou, 2005). Because of their mechanical simplicity, high dynamic range, low power requirements, large force capacity, and robustness, MR damper is considered as one of the most promising devices for mechanical vibration control (Jung, 2005). The only problem for MR damper is that it always requires an external power source. Figure 2-9 shows an MR damper installed on a cable-stayed bridge.



Figure 2-9 MR damper installed on cable-stayed bridges

At present, majority of the external dampers used on bridge site belong to passive damper. It has variety of types such as rubber damper, friction damper, and oil damper.

1. Rubber damper

Rubber damper consists of several high-damping rubber pads. The cable vibration energy is absorbed by shear deformation of the rubber pads (VSL, 2008). Damper is normally installed inside the cable casing between the cable and the steel tube near the bridge deck anchorage. It retains aesthetic appearance of the bridge since the size this rubber damper is small. Figure 2-10 shows a rubber damper installed on the Tatara bridge in Japan (Zhou, 2005).

2. Friction damper

Frictional forces arising from the relative motion of two contacting surfaces are a well-known source of energy dissipation. Friction damper was invented to increase the damping of cable-damper system in a simple and cost-effective way (Lopez, 2004).

Friction damper is used on Uddevalla bridge in Sweden, as shown in Figure 2-11.

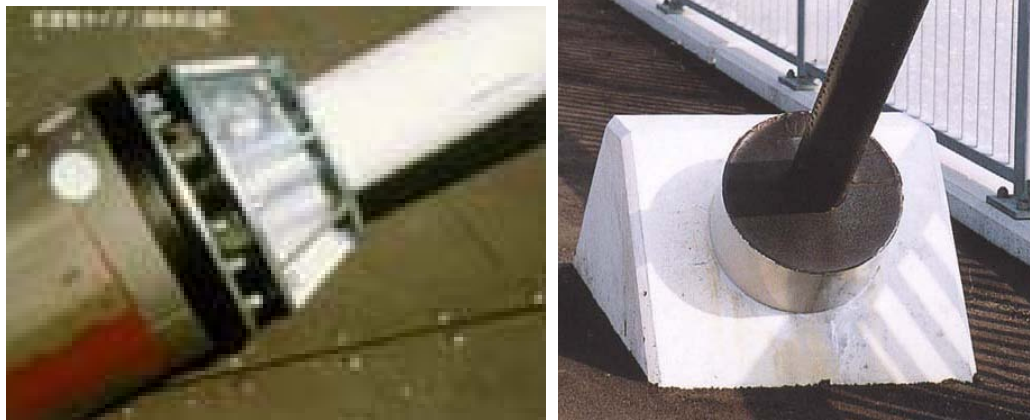


Figure 2-10 A picture of Rubber damper (left) and rubber damper installed on Tataru bridge(right)



Figure 2-11 Friction damper installed on Uddevalla bridge in Sweden

3. Oil damper

Mechanism of oil damper is very simple. Oil damper consists of a cylindrical container filled with viscous oil, and a piston which can move through the oil. oil provides viscous resistance while piston moves in the damper cylinder. The resistance force is the damping force. Oil dampers have many advantages such as wide range of

damping capacity, technology maturity, low cost etc. Its application on cable-stayed bridges is common. Since oil damper can only provide axial damping force along its cylindrical direction, in order to control both in-plane and out-of-plane cable vibration, two oil dampers are required to be installed on one cable at certain inclination angle. Figure 2-12 shows such an oil damper installation scheme on the second Nanjing Yangtze Bridge.



Figure 2-12 Two oil dampers installed on second Nanjing Yangtze Bridge

2.2.3 State-of-the-art on mitigating cable vibration using external damper

External damper is the most widely used external device to mitigate cable vibration because of aesthetic and practical reasons. As discussed earlier, external damper can be classified as active, semi-active, and passive dampers. Passive dampers generally are more cost effective, easier to maintain, and reliable in performance. The existing theoretical and numerical studies and field experience show that passive dampers can effectively increase cable modal damping ratio and suppress cable vibration without the requirement of external power source and complicated equipments. In order to evaluate efficiency of passive dampers on suppressing stay cable vibration, the attainable

maximum modal damping ratio was used as an index. Tabatabai and Mehrabi (2000) collected information of over one thousand bridge stay cables and concluded that undamped stay cable generally exhibit damping ratio in the range of 0.05% to 0.5%. This is not sufficient to avoid cable vibration problems on bridge site.

As mentioned in Section 2.1.1, 95% of stay cable vibrations belong to rain-wind-induced vibration. PTI Guide Specification (2000) and Federal Highway Administration (2007) both suggested that to avoid rain-wind-induced cable vibration, the Scruton number S_{c0} of the cable should be great than 10. Scruton number S_{c0} is defined as $S_{c0} = m\xi / \rho D^2$, where m is the mass of cable per unit length (kg/m or lbf/ft), ξ is the damping as ratio of critical damping, ρ is air density (kg/m³ or lbf/ft³), and D is cable diameter (m or ft). By inspecting the four variables in the definition of the Scruton number, cable mass and diameter are determined at the design stage, air density is a constant. Therefore, to satisfy the condition of $S_{c0} > 10$, the damping ratio ξ of the cable should be increased by installing external damper or other measures.

Achieving maximum modal damping ratio ξ_{max} was studied in recent two decades. A few researchers have found that damper coefficient of external damper can be optimized to yield a maximum modal damping ratio for an applied cable.

Kovács (1982) first introduced dynamic amplification curve and empirically defined the maximum attainable modal damping for the first mode. He illustrated the maximum first modal damping ratio when damper location was fixed. It is shown in Figure 2-13. He concluded that there is an optimal damper size for each cable. Very small damper size would not take any effect on mitigation of cable vibration. On the other hand, very large damper size would generate large damping force; therefore the damper would

act as a support at the location. He proposed that the maximum first modal damping ratio $\xi \approx 0.5x_c/L$ and the optimal damper size $c_{opt} \approx 1/(2\pi)mL\omega_{01}/(nx_c/L)$, where n is the mode number, c_{opt} is the optimal damper size, x_c is the damper location, L is the cable length.

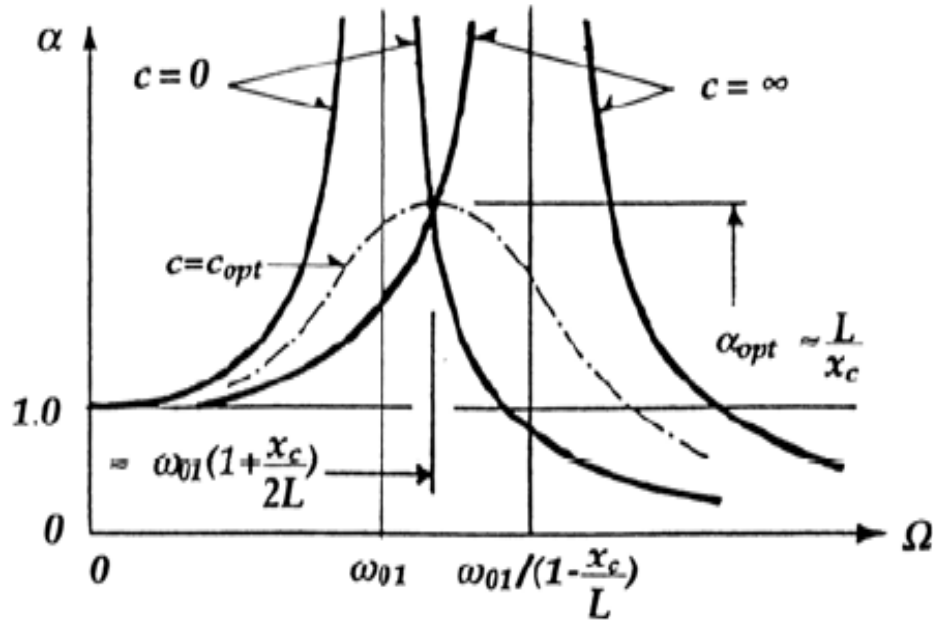


Figure 2-13 Dynamic amplification curves (Kovács, 1982)

Yoneda et al. (1989) developed an analytical model of a damped cable as a complex eigenvalue problem. The optimal damper size and the maximum damping ratio for different modes were calculated. He proposed that the optimal first modal damper size could be estimated by $c_{opt} = 6.25/(2\pi)(mL\omega_{01}nx_c/L)/[\sin^2(\pi nx_c/L)]$ and the maximum

first modal damper size could be determined from $\xi_{max} = \frac{6.25}{2\pi} \frac{x_c}{L} (0.45 + \frac{x_c}{L})$. It was found that the optimum damper coefficient decreased with the increase of vibration mode.

Pacheco et al.(1993) proposed a universal curve, as shown in Figure 2-14, in multi-modes which is very useful for selecting size and installation location of damper during preliminary design stage. In the analysis, the cable was treated as a taut cable, i.e.

its bending stiffness and sag were ignored. Without conducting large amount of numerical simulations, the universal damper design curve could be conveniently used to find the proper damper size and location for the required amount of damping ratio of a particular stay cable or estimate the attainable damping ratio of a particular stay cable for the given damper size and location.

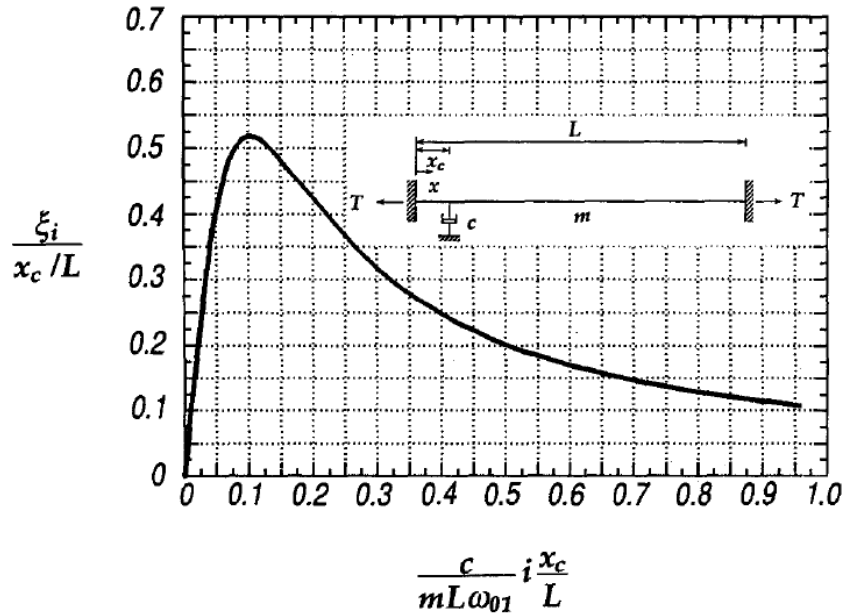


Figure 2-14 Universal damper design curve by Pacheco et al.(1993)

To verify the universal curve proposed by Pacheco et al.(1993), Krenk (2000) performed a numerical analysis in terms of complex eigenvalue problem. An asymptotic solution was obtained for the damping ratio of the lower modes, valid for damper location close to one support. In his analysis, when the nondimensional damper location x_c/L is larger than 0.05, differences between the proposed asymptotic results and the universal damper design curve by Pacheco et al. (1993) were found. The results by Krenk led to a slightly larger optimal external damper size. He proposed that the maximum modal damping could be estimated by $\xi \approx 0.5x_c/L$ and the attainable optimal damper

size by $c_{opt} \approx \sqrt{Tm}/(\pi n x_c/L)$, where T is the tension of modal cable, m is mass per units length of cable, n is the mode number.

Shallow cable was studied by Cremona (1997). He extended the concept of universal curve to sagging cable based on the formulation by Irvine (1974), of which the effect of the inclination of the cable chord was ignored. It was found that sagging effect would lead to reduction of attainable modal damping ratio. He proved that the damping ratios of anti-symmetric modes of shallow cables were identical to those of taut cables. On the contrary, the damping ratios of symmetric modes depended on the value of the Irvine parameter. This reduction mainly affected in the first symmetric mode. As an example, he further identified that for the longest cable of the Normandy bridge, the damping ratio reduction was 30% when compared to the taut cable solution. The reduction of damping ratio for the long cable was found to be significant because of the sagging effect due to cable self- weight.

Tabatabai and Mehrabi (2000) considered cable bending stiffness and sag extensibility in an analytical formulation by the finite difference method. The increase in the cable bending stiffness was found to result in a decrease of the damper efficiency. Figure 2-15 shows the variation of the maximum damping ratio with respect to the bending stiffness parameter. The bending stiffness parameter was defined as $\zeta = \sqrt{HL^2/EI}$, where E is the modulus of elasticity and I is the bending moment of inertia, and H is the cable tension. Non-dimensional damper size is defined as $\eta = c/\sqrt{Hm}$. The first modal damping ratio of the cable is denoted as ξ_1 . It can be deduced that the maximum attainable damping ratio is around 8%. This is higher than that obtained from

the universal damper design curve. It was also found that the bending stiffness effect was more relevant for dampers that were located closer to the cable end.

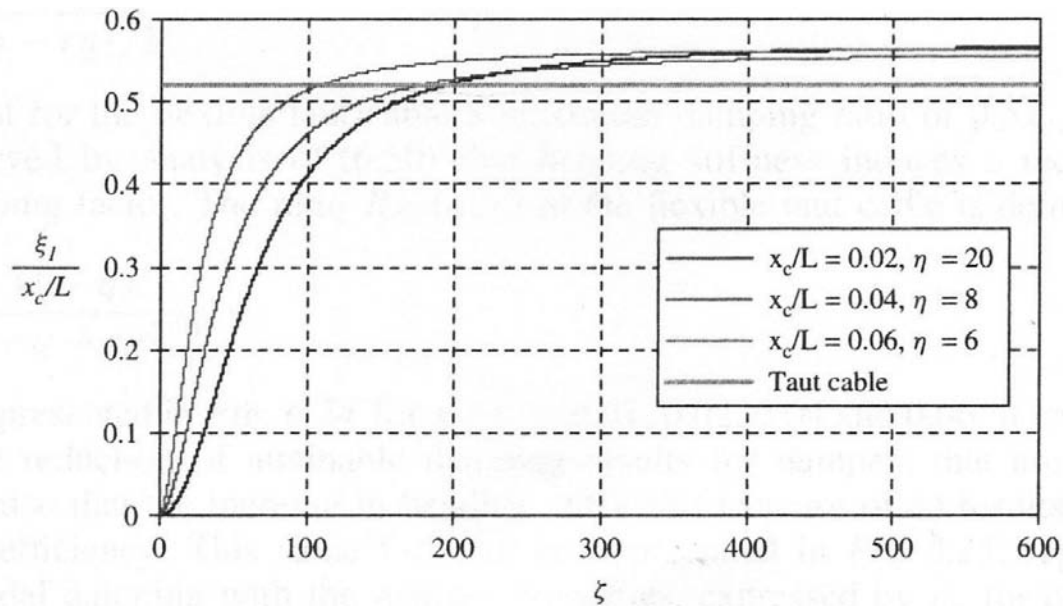


Figure 2-15 Variation of the maximum damping ratio with respect to the bending stiffness parameter (Tabatabai and Mehrabi, 2000)

Zhou (2005) derived a general equation for the optimal damper size associated with different modes by using complex modal analysis. The damper stiffness was also included in the formulation. A non-dimensional damper stiffness $\gamma = (kx_c)/H$ was introduced, where k is the damper stiffness in “N/m”; x_c is the distance between the damper and the near end of the cable anchorage in “m”; and H is the tension of cable in “N”. He concluded that the optimal damper size for different modes could be expressed as $c_{opt,i} = 1/(\pi^2)mL\omega_1(1+\gamma)/i/(l_1/L)$. This equation suggests that as the non-dimensional damper stiffness increases, the optimal damper size will increase linearly.

Hoang et al. (2007) proposed the effect of bending stiffness on the modal properties of a stay cable in an analytical study. An explicit asymptotic formula for the modal damping of a cable attached to a general type damper was derived. The study

focused mostly on the effectiveness of maximum modal damping ratio by considering the cable bending stiffness effect. Results showed that while the flexure property in the cable could reduce the maximum attainable modal damping ratio by 20%, it could significantly increase the optimal damping coefficient of the damper.

Cheng et al. (2010) derived the maximum damping ratio achievable by a cable-damper system in numerical simulation using an energy-based approach. The cable sagging effect and cable bending stiffness were considered in the analysis for determining the optimal damper property and maximum attainable cable modal damping ratio. The overall increase of the cable damping offered by the external damper was determined by examining the time history of the kinetic energy of a damped cable. The kinetic energy decay ratio was used to determine the efficiency of the damper. Figure 2-16 illustrates schematically kinetic energy decay time-history of the n^{th} mode of a damped cable. Where, the n^{th} kinetic energy decay ratio d_n was defined as follow:

$$d_n = \frac{1}{j} \sum_{i=1}^j \frac{(E_{ki,n})_{max} - (E_{k(i+1),n})_{max}}{(E_{ki,n})_{max}}, \text{ where } (E_{ki,n})_{max} \text{ and } (E_{k(i+1),n})_{max} \text{ are the}$$

maximum n^{th} modal kinetic energy of the cable in the i^{th} and the $(i+1)^{\text{th}}$ cycles, respectively, and j is the number of cycle pairs selected in the calculation. The damping ratio was derived to be $\xi_n = -\ln(1-d_n)/(4\pi)$. A set of damping estimation curves were developed for the practical parameter ranges of bridge stay cables, which directly relate a damper design with the corresponding attainable damping ratio in the damped cable. By applying regression analysis to the numerical simulation results, it was proposed that the maximum attainable damping ratio could be estimated by:

$$\xi_{n,max} = 48.52 (x_c/L)^{1.03} [L/(H/EI)^{1/2}]^{0.033}, \text{ and the optimal damper size by}$$

$$c_{opt,n} = 0.261 e^{-0.00061[L/(H/EI)^{1/2}]} (x_c/L)^{-1.192}.$$

There are other researchers who studied the cable vibration problems, such as Yoneda et al.(1989), Uno et al. (1991), Zhou(2005), Fujino and Hoang(2007) etc.. Table 2-1 summarizes the empirical formulae for estimating optimal damper size and maximum modal damping ratio suggested in these studies.

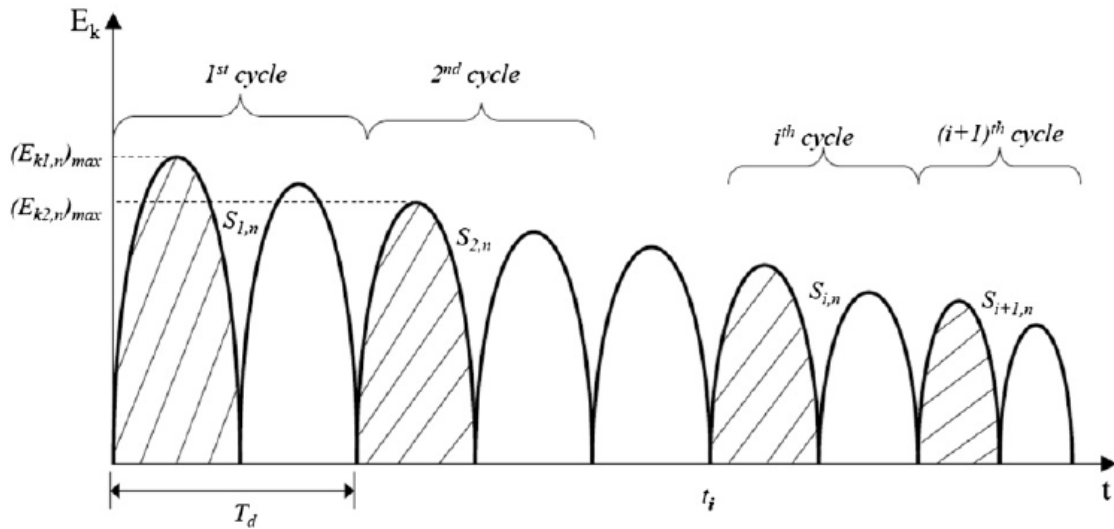


Figure 2-16 Schematic illustration of kinetic energy time history of the nth mode of a damped cable (Cheng et al., 2010)

Table 2-1 Summary of empirical damper design formulae in the existing literature:

Optimal damper coefficient and maximum damping ratio for a viscous damper

Literature	$c_{opt,n}$	$\xi_{n,max}$
Kovács (1982)	$1/(2\pi).mL\omega_{01}/(nx_c/L)$	$0.5.x_c/L$
Yoneda et al. (1989)	$6.25/(2\pi)(mL\omega_{01}nx_c/L)/[\sin^2(\pi nx_c/L)]$	$6.25/(2\pi).x_c/L.$ $[0.45 + x_c/L]$
Uno et al.(1991)	$6.25/(2\pi)(mL\omega_{01}nx_c/L)/[n \sin^2(\pi x_c/L)]$	$3.3/(2\pi).x_c/L$
Pacheco et al.(1993)	$0.10. mL\omega_{01}/(nx_c/L)$	$0.52.x_c/L$
Cheng et al. (2010)	$0.261e^{-0.00061[L/(H/EI)]^{1/2}} (x_c/L)^{-1.192}$	$48.52(x_c/L)^{1.03}[L/(H/EI)]^{1/2}]^{0.033}$

All the literature reviewed above are based on either analytical approach or numerical simulation. Experimental works are generally expensive and time consuming. But it can validate the results obtained in the theoretical analysis, or even lead to new findings. Therefore, a number of researchers conducted experiments to study cable vibration problems.

Sulekh and Pacheco (1990) developed a small-cable model. A steel-wire was fitted with improvised viscous damper, and the damping ratio was estimated from the displacement time-history obtained from free vibration tests using the logarithmic decrement method. The steel-wire was 2.08m long and the unit mass per length of the model cable was 0.07 kg/m. The tension was set to 59.4N. In order to provide additional damping to the cable, an oil viscous damper was built. The piston of the damper was simulated by a light wooden square plate with 0.02m on sides. The piston was placed in an open container with silicone oil. By attaching the damper at 6% of cable length from one end, a relation between the kinematic viscosity of the silicone oil (simulating damper property) and the obtained damping ratio was derived as shown in Figure 2-17.

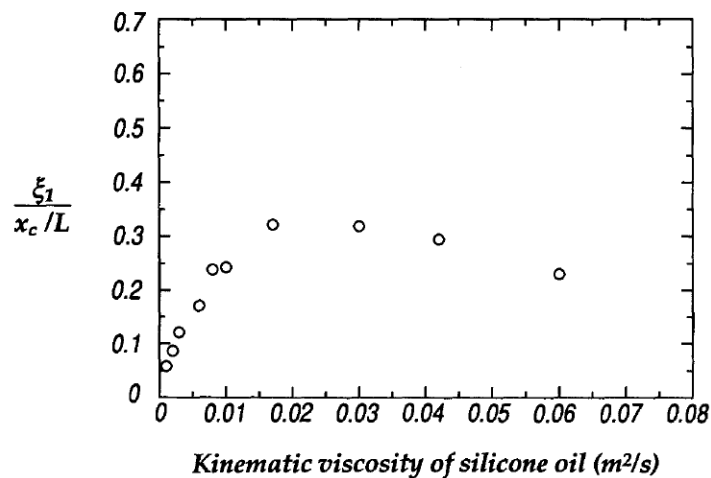


Figure 2-17 Damping ratio of the first mode in experimental model

(Sulekh and Pacheco, 1990)

It was commented that the calibration of the damper was difficult because of the design. From the figure, it can be seen that as kinematic viscosity of the silicon oil increased, damping ratio increased and reached to certain point and then decreased. This verified qualitatively that there existed an optimal damper size when the damper was installed at a certain location.

Xu et al.(1999) conducted an experimental study on vibration mitigation of stay cables in cable-stayed bridges using oil dampers. The experimental setup is shown in Figure 2-18. The two ends of a steel cable were cast into two steel cylinders. The upper end of the cable was then pin-connected to a smaller steel anchor that was able to slide vertically along a column. The lower end of the cable was pin-connected to a larger steel anchor via a load cell. A piston and silicone oil damper was made for experimental tests. The natural frequencies of cable measured by the free vibration tests were found in good agreement with the theoretical estimation by Irvine (1974). A series of large-amplitude force-controlled tests and displacement-controlled tests were also carried out. In the former, the excitation force generated by the shaker was a constant all the time which was 5N, and in the latter, the excitation displacement remained as a constant which is 0.141mm. Non-linear characteristics of cable vibration were observed in the forced vibration tests. A significant reduction in the cable response after attaching to a damper confirmed the necessary of installing external damper to suppress stay cable vibration on site. Figure 2-19 shows response amplitudes with and without damper

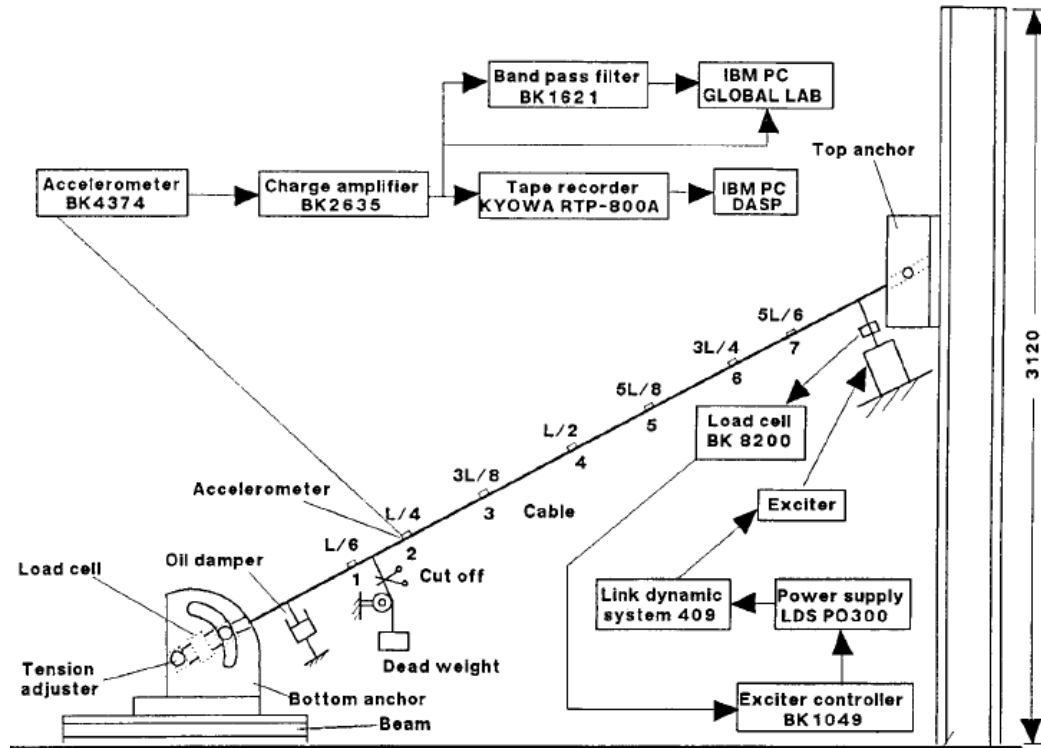


Figure 2-18 Experimental test setups by Xu et al. (1999)

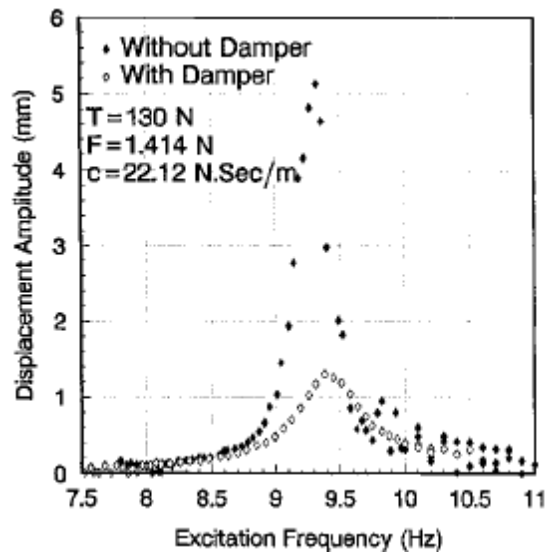


Figure 2-19 Responses amplitude with and without damper (Xu et al., 1999)

Tabatabai and Mehrabi (2000) performed an experimental study to justify their derivation on the effect of cable bending stiffness on its vibration control. The modal cable consisted of a bundle of seven-wires, 6.4 mm-diameter strands encased in a

polyvinyl chloride pipe. The length of the cable was 13.695 m, the equivalent axial rigidity $EA = 49,318$ kN (including grout and cover pipe), and equivalent flexural rigidity $EI = 2.28$ kN m² (including grout and cover pipe). These resulted in a bending stiffness parameter $\zeta = 100$, and the mass per unit length $m = 3.6$ kg/m. A small damper with two different damper sizes 1680 N·s/m and 15130 N·s/m were made. The damper was attached at 6% of the cable length from one end of the cable. Three cases were tested: a free vibration test without damper, and two free vibration tests with damper. The experimental results proved that the bending stiffness effect should be considered in the damper design.

In majority of the existing studies, the stiffness of the external damper is neglected when evaluating the efficiency of an external damper in controlling cable vibration. Only very few recent research addressed this issue. Krenk and Hogsberg (2005) used a system shown in Figure 2-20 to study the damper stiffness effect. As shown in the figure, the studied taut cable is assumed to be attached to a damper and a spring which are in parallel. The theoretical analysis results clearly indicated that the damper efficiency could be increased by introducing negative stiffness component.

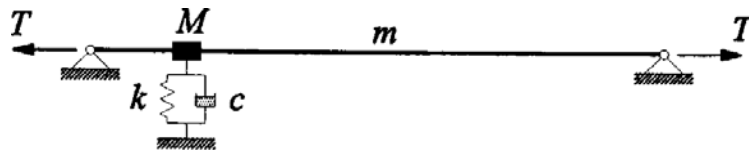


Figure 2-20 Taut Cable with Spring-mass Damper (Zhou, 2005)

Results by Zhou (2005) further suggested that damper stiffness and optimal damper size approximately had a linear relationship, i.e. a larger damper stiffness would lead to a larger optimal damper size. Zhou also proposed a maximum modal damping ratio decay rate $R_{\max} = 1/(1+\gamma)$, where $\gamma = (kx_c)/H$ is the non-dimensional damper

stiffness, k is the damper stiffness (N/m); x_c is the distance between the damper and the near end of cable anchorage(m); H is the tension of cable (N). It is worth noting that literature related to damper stiffness and its impact on damper efficiency of controlling cable vibration is scarce. Since this parameter could directly affect the effective performance of an external damper, a well planned systematic investigation is essential. In the current study, the impact of damper stiffness on the effectiveness of damper performance will be studied experimentally.

CHAPTER 3 EXPERIMENTAL DETAILS

In order to experimentally study the effectiveness of an external damper in suppressing cable vibration and better understand the behavior of a cable damper system, the design and set up of the current experimental study will be presented in this chapter. First, all the testing equipments and components of the cable-damper system will be described. The design and calibration of the damper will be presented next. The procedures of free vibration and forced vibration tests, including the methodologies to determine damping ratio of a damped cable based on these tests will be illustrated in the last part of this chapter.

3.1 Experimental Setup

The experimental study was performed in the Structures Lab at the University of Windsor (Essex Hall B-19). The equipments required for this experimental study are described as follows:

1. Model cable

A model cable was designed to simulate the behavior of a real bridge stay cable in the lab environment. The model cable has a length of 9.33m after mounting in place. It has 4.65mm in diameter and 0.092kg/m in unit mass. The moment of inertia of the cable is calculated to be 15.8 mm^4 . The cable was mounted horizontally onto two steel columns with one end connected with a load cell and another end connected with a hydraulic pumper to introduce tension load.

The fundamental frequency of a simple cable can be estimated based on $f = \frac{1}{2L} \sqrt{\frac{T}{m}}$, where L is length of the cable, T is the tension, and m is the mass per units length of cable. The cable modes which are easily excited by dynamic forces generally have frequencies lower than 15 Hz. Since the length of the modal cable is constrained by the column spacing in the lab, cable pretension and unit mass should be adjusted to render the fundamental frequency of the model cable to be less than 15 Hz. At early stage of tests, the cable was observed to exhibit elliptical motion when pretension was set too large. Further, if the pretension is too small, the cable was slack. After a number of trials, it was found that a preferable pretension range should be between 2500N to 4000N. In order to achieve the frequency range of a real cable, supplementary iron mass blocks was installed on cable to increase the unit mass of the modal cable. After adding the mass blocks, the fundamental frequency of cable in lab environment can be kept below 8 Hz.

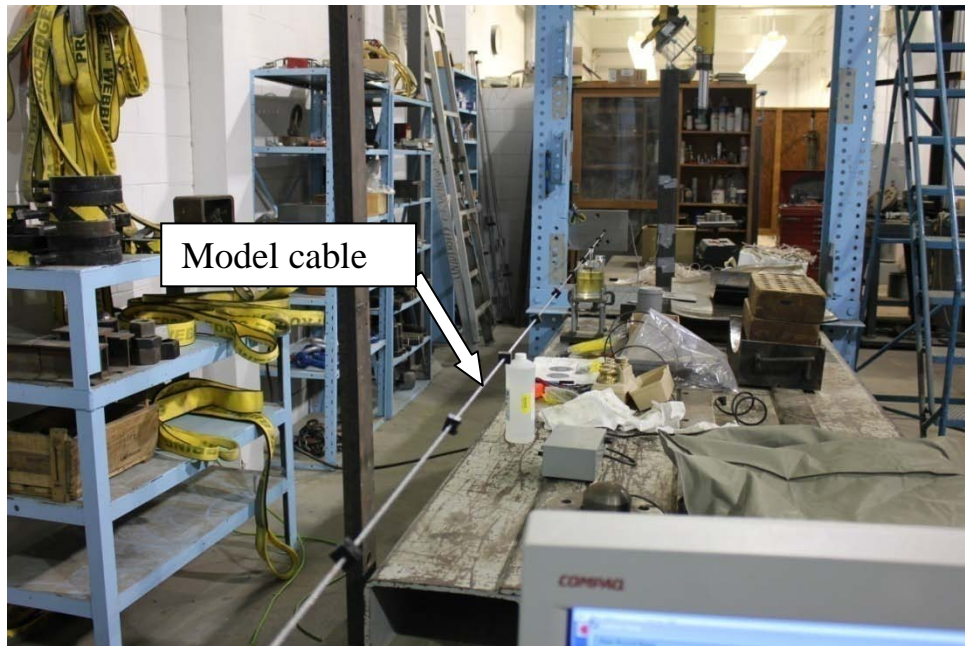


Figure 3-1 Experimental setup

2. Supplementary iron mass block

The supplementary iron mass block is shown in Figure 3-2. Twenty of 50g iron mass blocks were mounted onto the model cable with equal spacing to increase the unit mass of the model cable, so it would yield a fundamental frequency comparable to a full scale cable. After adding the mass blocks, the unit mass of the model cable became 0.2 kg/m.

$$m = (0.092 * 9.33 + 20 * 50 / 1000) / 9.33 = 0.2 \text{ (kg/m)}$$

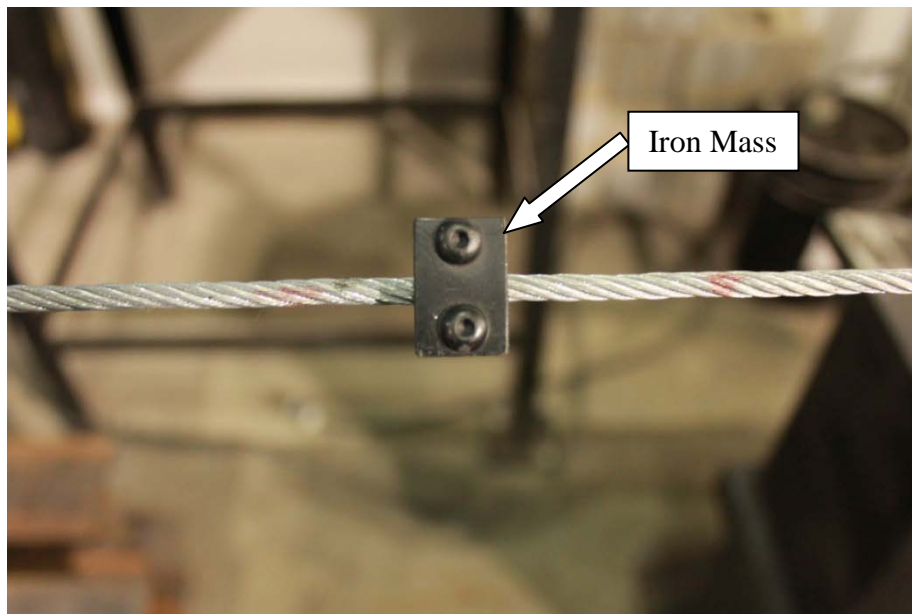


Figure 3-2 Iron mass

3. Universal flat load cell

A universal flat load cell (Model FL25U-2SG) was used in the experimental study to measure the pretension in the model cable. It has a maximum capacity 25000lbs, and a resolution of 10N. It is attached to one end of the cable. There is a piece of flat rubber placed between the load cell and the cramp, which is used for insulation as shown in Figure 3-3.

The load cell was calibrated by the universal tensile tester with a short sample of the model cable. By monitoring the voltage changes on the data acquisition system while increased the tension slowly, the linear relationship between the voltage and the applied tension gave a calibration constant of 5.458 kN/mV.

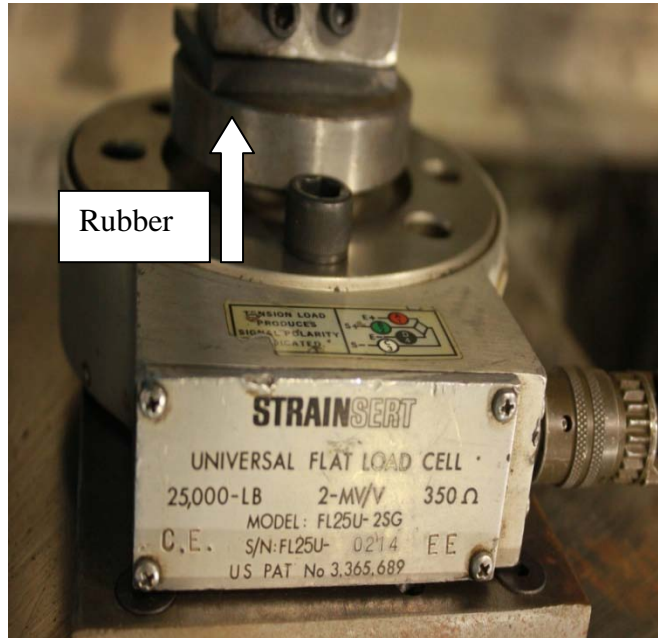


Figure 3-3(a) Universal Flat Load Cell Top View

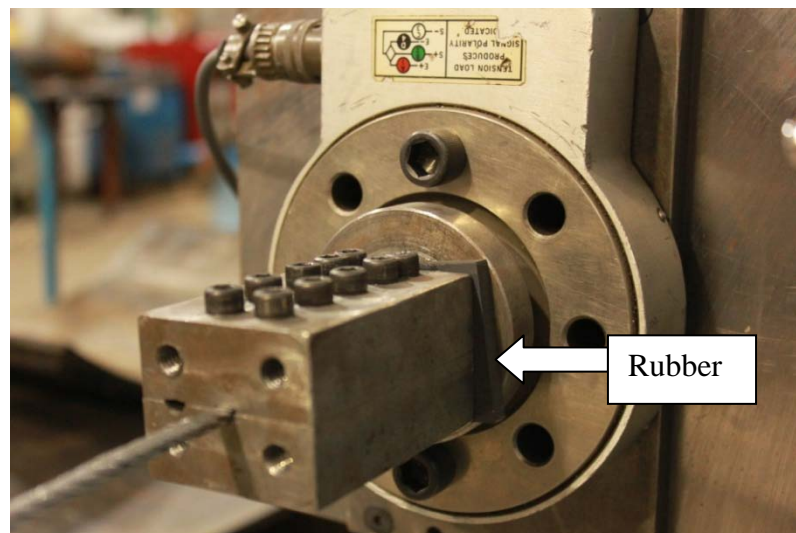


Figure 3-3(b) Universal Flat Load Cell Front View

4. Hydraulic hand pump

The hydraulic hand pump OTC 4017 (serial number HP061108) is shown in Figure 3- 4. It was used to apply tension to the model cable to simulate pretension in a real bridge stay cable. It has maximum pressure capacity of 10,000 psi.



Figure 3-4 Hydraulic hand pump

5. Accelerometer

An accelerometer from Dalimar Instruments Inc. (Model number 352A24) was used to capture acceleration of the cable motion. The applicable testing frequency range is 1 to 8000Hz, and the resolution is 9.95mV/g. It can record acceleration along a single direction. The accelerometer was glued exactly at the top of the cable to make sure that acceleration along vertical direction is measured. This is very important since the accelerometer is very sensitive to motion along any direction. The cable is pushed up and down during the tests to see if the accelerometer is moving vertically. In addition, the real-time collected data displayed by the Astrolink Xe controlling software was monitored to ensure the motion to be

symmetric about the centerline. Since the present study is focused on testing the first modal damping ratio of the cable, the accelerometer was placed in the middle of the cable, as shown in Figure 3-5.

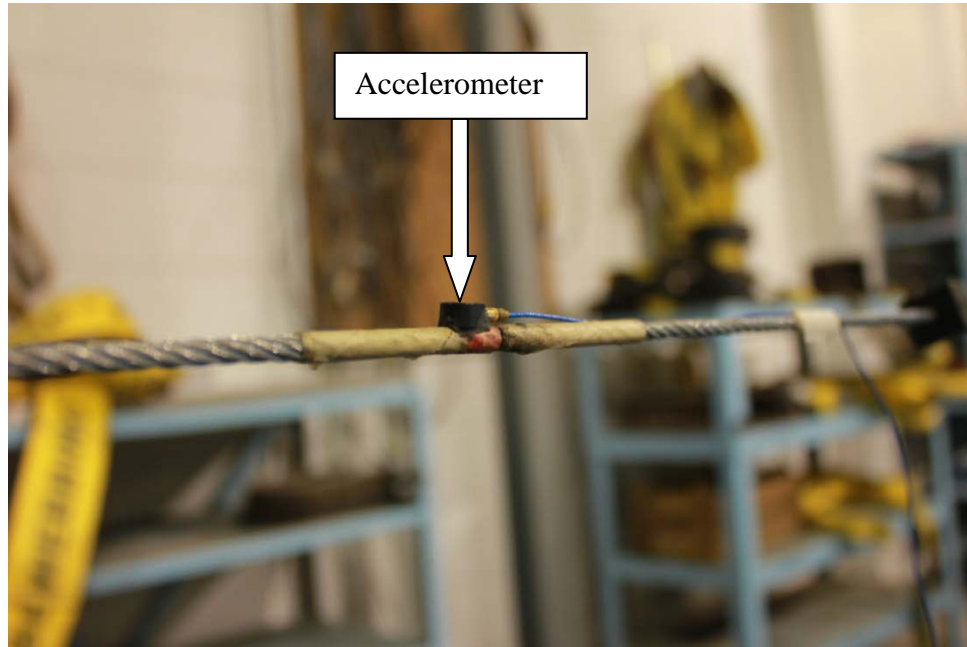


Figure 3-5 Accelerometer placed in the middle of the cable

6. Electronic dynamic smart shaker

An electronic dynamic smart shaker (Modal number K2007E01) from Modalshop Inc. is used in the current experimental study to excite the cable in the forced vibration tests. It can provide up to 7 pounds (31 N) peak sine force with a 1/2 inch (1.27 cm) stroke and its frequency range is from 1 to 9000Hz. And it has three vibration levels, 5db, 10db and 20db. The shaker is placed on a tripod and installed exactly to provide vertical excitation. Improper installation will result in looping motion, unsymmetrical motion etc. Level was used to make sure the shaker is installed exactly in the vertical plane of the cable. A load cell is also attached to the shaker to record loading history by the shaker at the mounting

point. Figure 3-6 shows when the shaker is installed at 5% of cable length away from one end of cable during the forced vibration test.

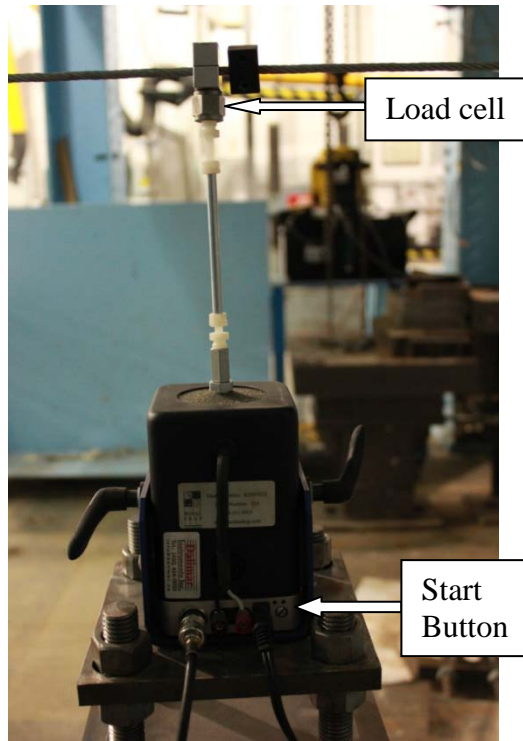


Figure 3-6 Back View of Shaker installed on cable

7. Signal generator

The HP signal generator (Modal 33120A), as shown in Figure 3-7, was used to generate signals of excitation force pattern for the shaker. It can simulate a dynamic force with frequency range of 1Hz to 15MHz. It was connected to the shaker by a cable to transfer the required signal to it. In the forced vibration test of this experimental study, the external excitation force was assumed to be a sinusoidal force with a frequency of 6 to 8 Hz.



Figure 3-7 HP 15MHz function/Arbitrary Waveform Generator

8. Data Acquisition system

The AstroDAQ Xe data acquisition system is shown in Figure 3-8. The accelerometer and the load cell were connected to it to record experimental data. The system had 8 channels of inputs and was connected to the computer using a USB 2.0 port. Channel 8 was used to capture load cell data which gave pretension in kN (after input 5.458 kN/mV in system). Channel 3 was used for capturing acceleration data. The accompanied data acquisition controlling software provided a real time monitoring of the recorded data and could perform preliminary analysis such as data filtering. The software contains Realtime mode and Review mode. The Realtime mode provides real-time waveform monitoring and data capture capabilities. The Review mode is used for reviewing and analyzing saved data in the data files. When cable is vibrating, blue lines will

show in Waveform 3 (corresponding to Channel 3), which is the acceleration data recorded by the accelerometer (Figure 3-9). To start a test, basic setups including file name, sampling frequency (ranging from 1 to 200,000 Hz) etc should be set in the controlling software. Figure 3-9 shows the interface of the software when collecting the acceleration data.



Figure 3-8 AstroDAQ Xe Data Acquisition System

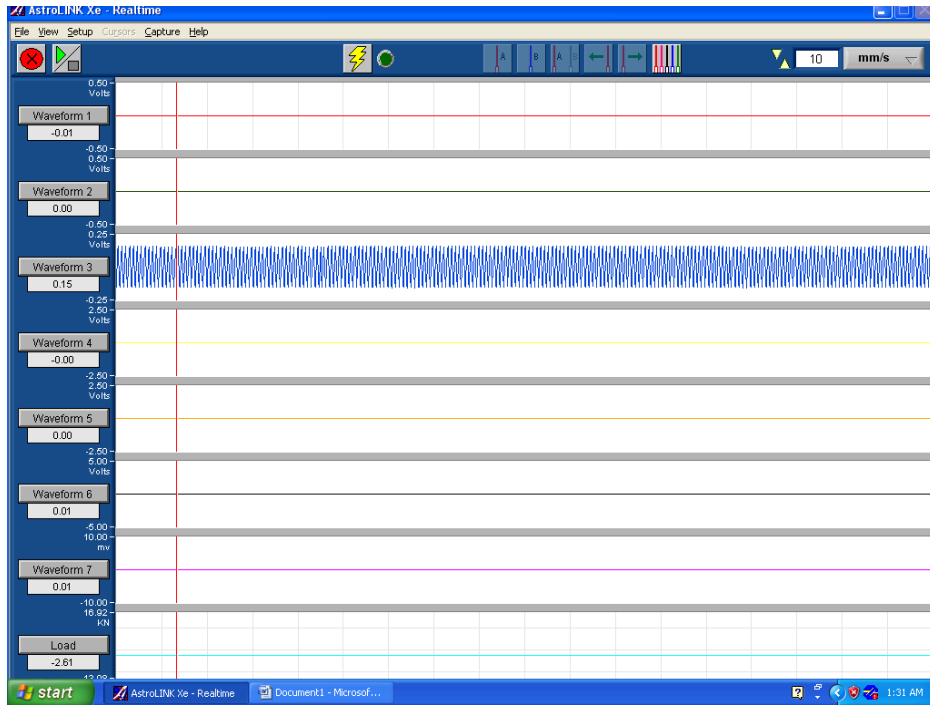


Figure 3-9 Realtime mode before testing

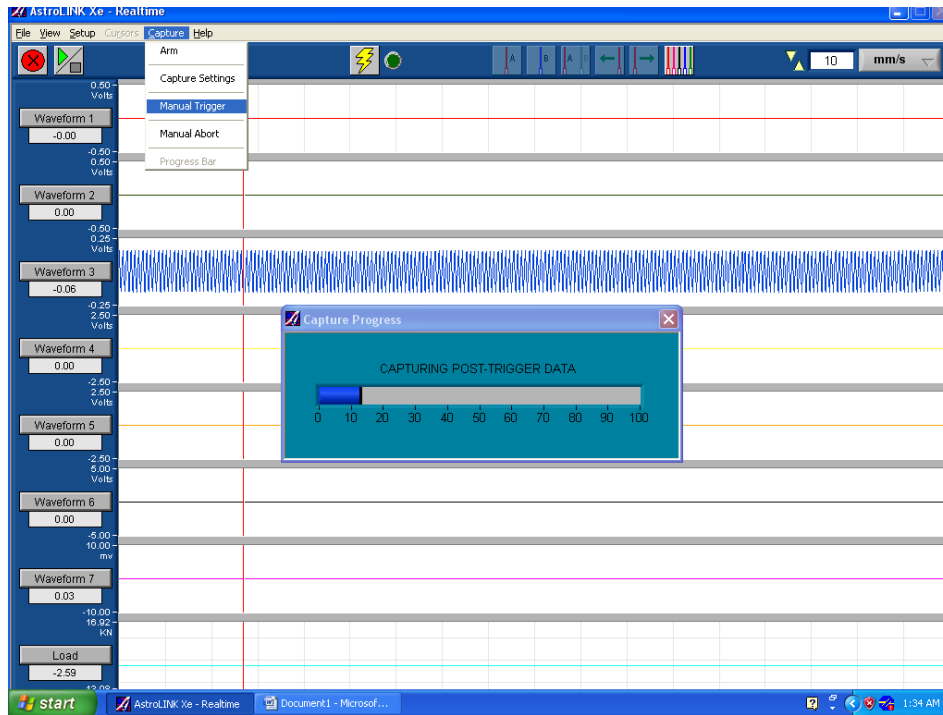


Figure 3-10 Capturing data in Realtime mode

3.2 Damper Design and Calibration

3.2.1 Damper Design

Different kinds of passive dampers are reviewed in section 2.2.2. A passive damper with adjustable damper size was required in this experimental study. In order to fulfill the requirement, a passive oil damper with adjustable damper size was designed and built. The mechanism of the oil damper is that the oil inside container can provide resistance to the plate merged in the oil while it is moving in it. The sketch of the damper design is depicted in Figure 3-11. The final finished damper is shown in Figure 3-12.

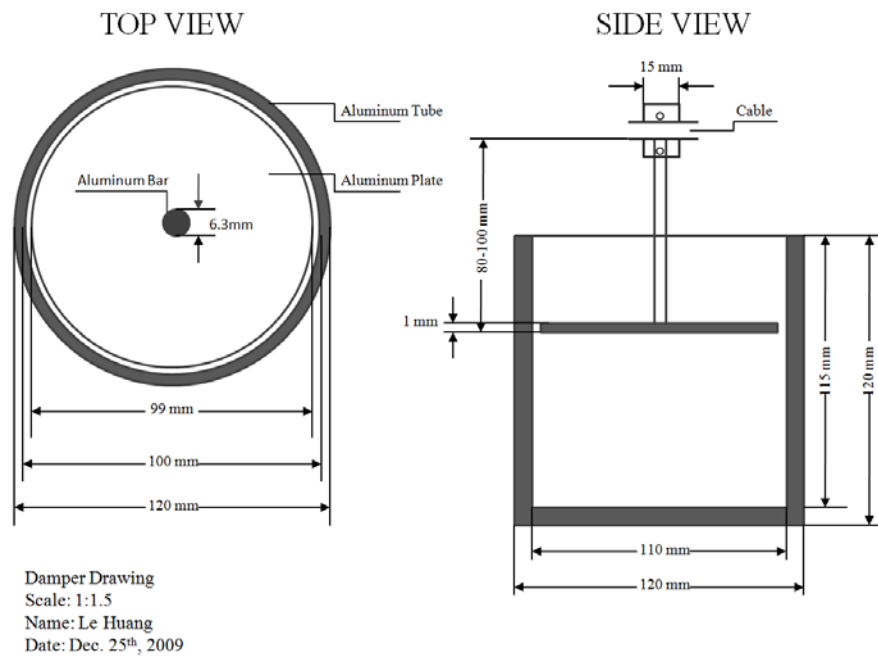
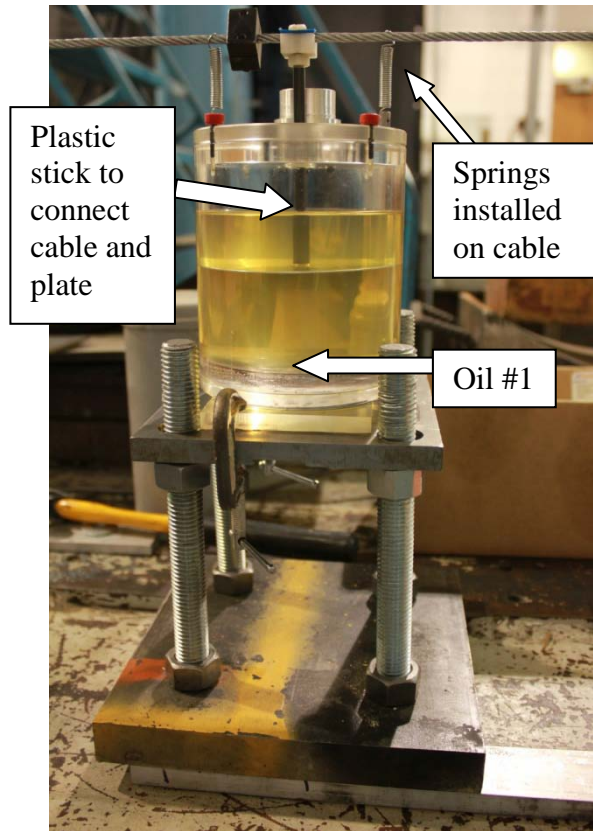
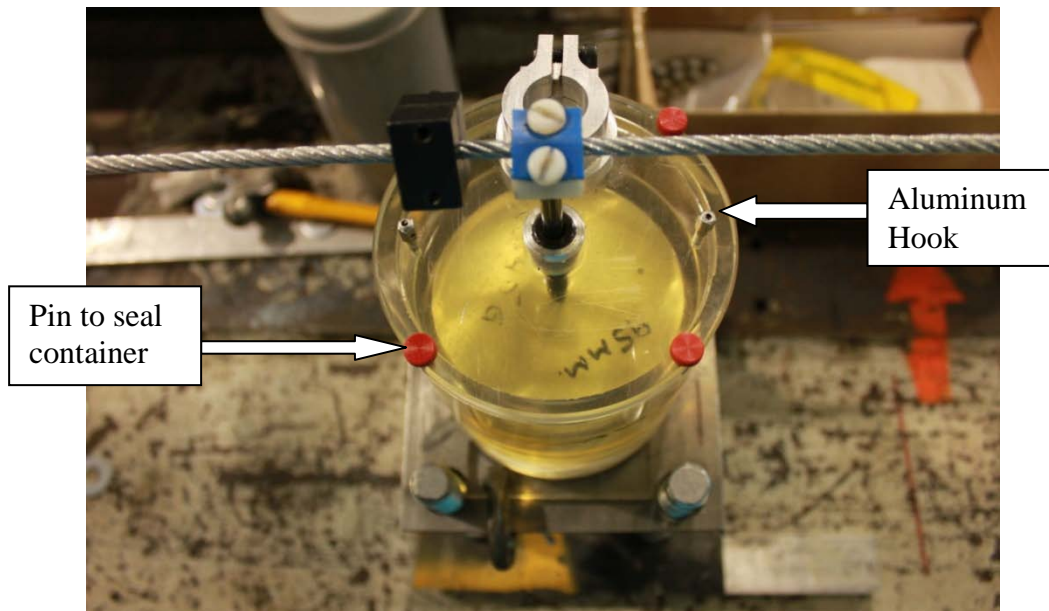


Figure 3-11 Damper design sketches



(a) Side View of Damper installed on cable



(b) Top view of Damper installed on cable

Figure 3-12 Oil damper designed in the current study

As shown in Figure 3-12, the designed damper consists of six parts:

1. A plastic container which has a lid on top with 4 pins equally spaced to seal the container. The container has a diameter of 100 mm.
2. An aluminum plate with thickness of 1mm. To simulate different damper size, a total number of four plates with different diameters were made, as presented in Table 3-1 and shown in Figure 3-13. There is a small hole on the plate which is used for damper calibration. Further illustration will be provided in the next section (3.2.2 Damper Calibration).

Table 3-1 Properties of Aluminum Plates

Plate No.	#1	#2	#3	#4
Diameter (mm)	99	95	90	80
Weight (g)	16.63	15.45	14.05	11.15



Figure 3-13 Four Solid Aluminum Plates

3. A plastic stick which is used to connect the model cable and the aluminum plate.
It has a mass of 11g.
4. Oil in the plastic container. Two types of oil of different viscosity and density were used in the test to simulate different damper resistance. Their physical properties are listed in Table 3-2.

Table 3-2 Oil Properties

Oil No.	#1	#2
Color	Yellow	White
Density @ 20°C, (kg/l)	0.8434	1.25
Viscosity @ 40 °C (mm ² s ⁻¹)	44.4	277.2

5. To study the damper stiffness effect, springs were installed in some cases which connected the cable and the damper container. Springs of three different stiffnesses were used, as shown in Figure 3-14. Their stiffness are listed in Table 3-3.

Table 3-3 Spring Properties

Spring Serial No.	9654K53	9654K812	9654K115
Stiffness k (N/cm)	0.77	1.47	2.15
Material	Steel	Steel	Zinc Steel



Figure 3-14 Three Springs from McMaster.com

6. Two aluminum hooks on top of the lid in order to hook the springs (simulate damper stiffness). Figure 3-12 shows the two aluminum hooks attached to the lid.

3.2.2 Damper Calibration

An LVDT was used for damper calibration. With four different size aluminum plates and two different types of oil, it yields a total of eight combinations for the damper capacity. Therefore, eight different damper sizes can be simulated. The weight of the LVDT stick is 15.18g. The whole calibration setup is shown in Figure 3-15. Before calibrating the damper, a linear relationship was found between the AstroDAQ Xe Data Acquisition system and the LVDT, i.e. 1 volt = 2.5mm. During calibration, a mass block was put on the top of the damper stick and subsequently released. The displacement of

the damper sticker was recorded by the data acquisition system. After the mass block stopped, the collected displacement data was reviewed and the slope of displacement time-history curve was computed for velocity. Repeat those steps by applying different mass blocks from 0g to 400g with 50g or 100g increment case by case. Since passive oil damper theoretically has a linear relationship between the applied force F and the velocity v , the damper coefficient c can thus be determined based on $c = F/v$. Note that, the applied force should include the weight of the plastic stick of the damper plate, the LVDT stick, the aluminum plate and the added mass. In Appendix A, all the data captured in damper calibration will be presented. The damping coefficients of these dampers are listed in Table 3-4.

Table 3-4 Damper properties

Combination	Oil #1+ Plate #3	Oil #1 +Plate #2	Oil #2 +Plate #3	Oil #1 +Plate #1	Oil #2 +Plate #2	Oil #2 +Plate #1
Damping Properties (N·s/m)	18.4	46.7	70.3	164.8	275.5	1463.8

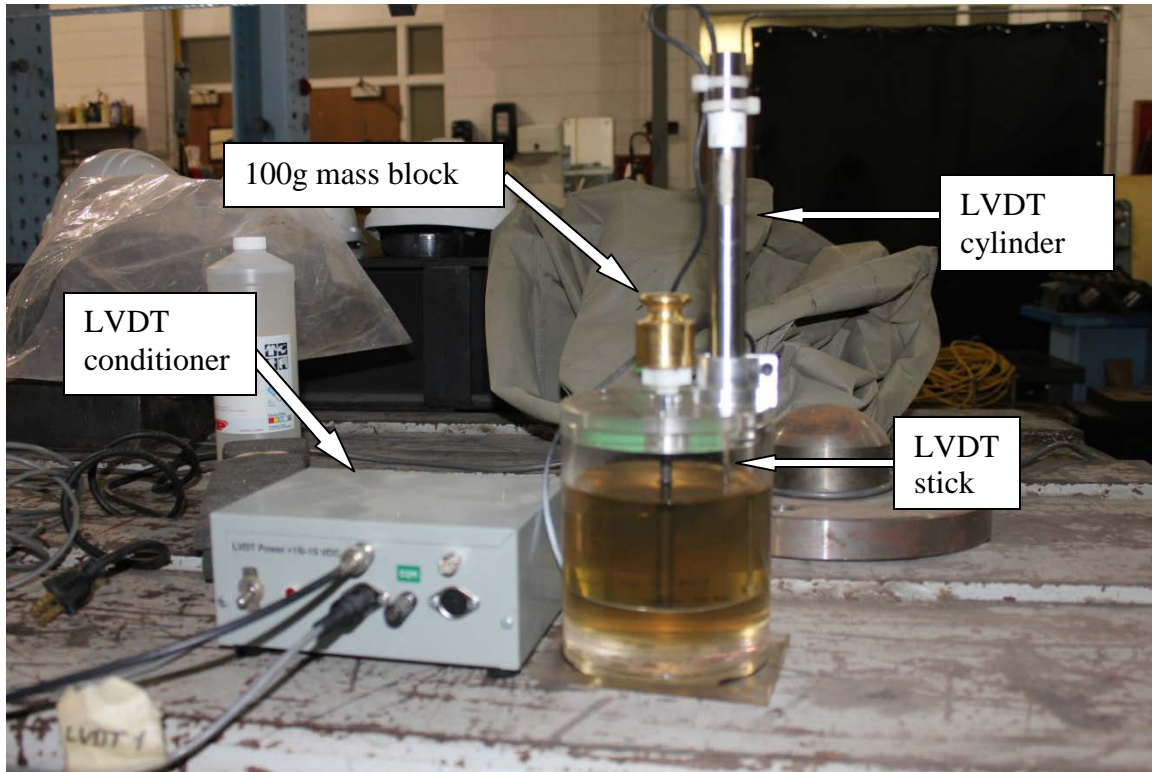


Figure 3-15 Damper Calibration Setup

3.3 Free Vibration Tests

As introduced in Chapter 2, the equivalent damping ratio of cable-damper system is a key parameter to describe the damper efficiency. In order to compute the damping ratio from the experimental raw data, different analysis methods have been used. The logarithmic decrement method used free vibration response data to determine the damping ratio of the system, whereas the half-power method used the forced vibration data instead. The theoretical background and testing procedures of free vibration test will be presented in this section. The potential problems of using this approach and the possible impact on the testing results will be discussed.

3.3.1 Testing procedures

In the preliminary testing stage, efforts were dedicated to use free vibration test and logarithmic decrement method to measure cable damping property. The test setup is shown in Figure 3-16.

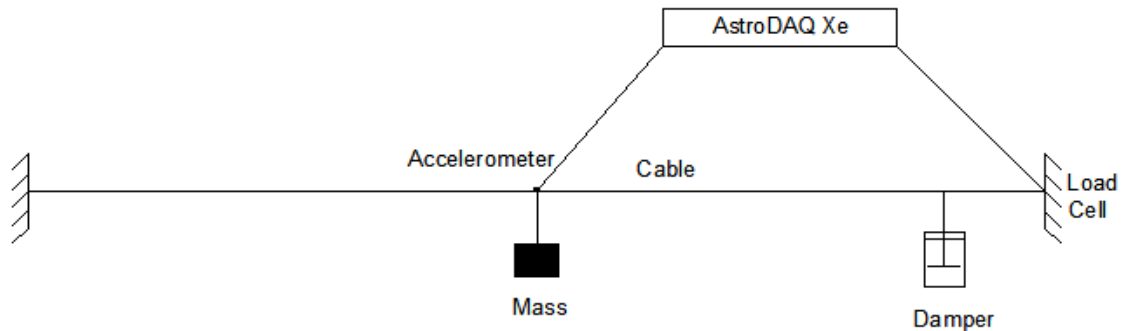


Figure 3-16 Free Vibration Test Setup

A mass block of 1kg shown in Figure 3-16 is used for exciting the model cable.

1. Set the input file name. In order to archive all the data files from the experimental work, file name was assigning using the following pattern: Cable_Tension_number and weight of supplementary mass _Shaker location_Damper location_Accelerometer location_Shaker excitation Frequency. For a file named as, B_3200_20050_S05_D06_A50_7Hz, it represents the Cable B with pretension of 3200N is tested. There are twenty of 50g iron masses added. For forced vibration tests, the shaker is installed at 5% L from left end of cable support. The damper is installed at 6% L from right end of cable support. The accelerometer is placed at the middle-span of the cable. The excitation frequency of the shaker is 7Hz.
2. Set the sampling frequency and the sampling time in the AstroDAQ Xe controlling software. The sampling frequency is normally set as 1000Hz, and the

sampling time is set as 30 seconds. The reason to set sampling frequency as 1000Hz is to guarantee each peak of the vibration cycles was captured.

3. Tie a wire on the mass block and then attach it to the cable, Figure 3-17 shows the mass block used in the free vibration tests.



Figure 3-17 Mass Block with wire tied on it

4. Burn wire to excite the cable and at the mean time start recording data in AstroDAQ Xe controlling software.
5. Review captured data in AstroDAQ Xe controlling software and save them in the excel format.

3.3.2 Theoretical background

Logarithmic decrement method is used to compute damping ratio of the damped cable using the displacement time-history data collected in free vibration tests. The captured data need to be pre-processed before applying logarithmic decrement method.

Pre-processing of experimental data will be described in Chapter 4. After pre-processing the data, only the 1st modal response is retained in the displacement time-history for determining 1st modal damping ratio. A sample of pre-processed free vibration displacement time-history is shown in Figure 3-18. Logarithmic decrement is the natural logarithmic value of the ratio of two adjacent peak values of displacement time-history in free decay vibration. The damping ratio is computed by

$$\delta = \frac{1}{n} \ln \left| \frac{Y_1}{Y_{n+1}} \right| \quad (3.1)$$

and
$$\xi = \frac{\delta}{\sqrt{4\pi^2 + \delta^2}} \quad (3.2)$$

where δ is logarithmic decay; ξ is the damping ratio of the modal cable; n is the number of cycle; Y_1 and Y_{n+1} are the displacement at the 1st and the $(n+1)^{th}$ peak of the displacement time-history curve.

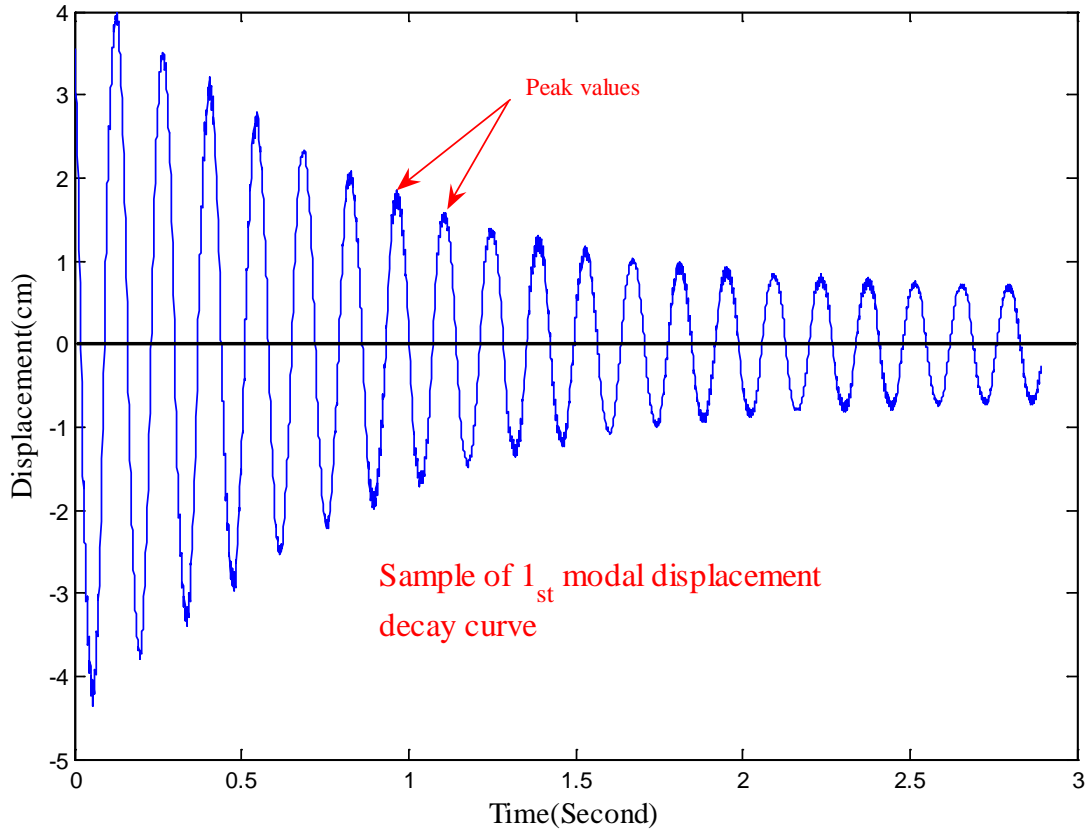


Figure 3-18 Sample of 1st modal displacement decay curve

3.3.3 Potential problem found in the free vibration tests

Although how to use free vibration test results to determine damping existed in the structure is mature in theories, after many times of trial tests, the following disadvantages are found, some of which could significantly affect the results.

1. Duration of cable vibration is very short. Due to the presence of damper, the cable vibration usually stops within 10 seconds. It is thus difficult to choose the useful part of data.

2. It is hard to control the cable to vibrate in the vertical direction. If the mass block was not tied to pass the mass center of the cable, tensional motion of the model cable will be excited.
3. Strange noise from damper was heard during early stages of testing. It was found to be induced by the friction between the plastic stick and the lid. To verify the significance of friction in contributing to suppress cable motion, a set of comparison test was done. The cable responses were measured when the damper was removed and when the damper was installed without the aluminum plate on the stick. Theoretically, these two sets of results should be very close. However, a considerable difference was detected as shown in Figure 3-19, where the grey line represents the former case and the black line represents the latter one. From the figure, it can be seen that the friction between the stick and the lid was acting like a damping force which helped to control cable vibration. Since the friction generated was not stable and could not be calibrated, in order to make sure the damper only have viscous damping by the oil, a thinner plastic stick replaced the previous one. Note that, The old plastic stick has a diameter of 9.5mm, and the new one has a diameter of 6.3mm.
4. Another problem associated with using free vibration tests is that the damping ratio determined by the logarithmic decrement method is amplitude dependent. For example, for the displacement time-history shown in Figure 3- 18, if different peaks are selected for Eq. (3.2), it will yield different damping ratios as:

$$\text{First and second Peak: } \xi = \ln(3.926/3.516)/(2*\pi*1) = 1.76\%;$$

$$\text{First and fourth Peak: } \xi = \ln(3.926/2.793)/(2*\pi*3) = 1.81\%;$$

$$\text{First and sixth Peak: } \xi = \ln(3.926/2.082)/(2*\pi*5) = 2.02\%;$$

First and ninth Peak: $\xi = \ln(3.926/1.388)/(2*\pi*8) = 2.07\%$.

Therefore, it will not be an appropriate index if comparisons with other studies needs to be made.

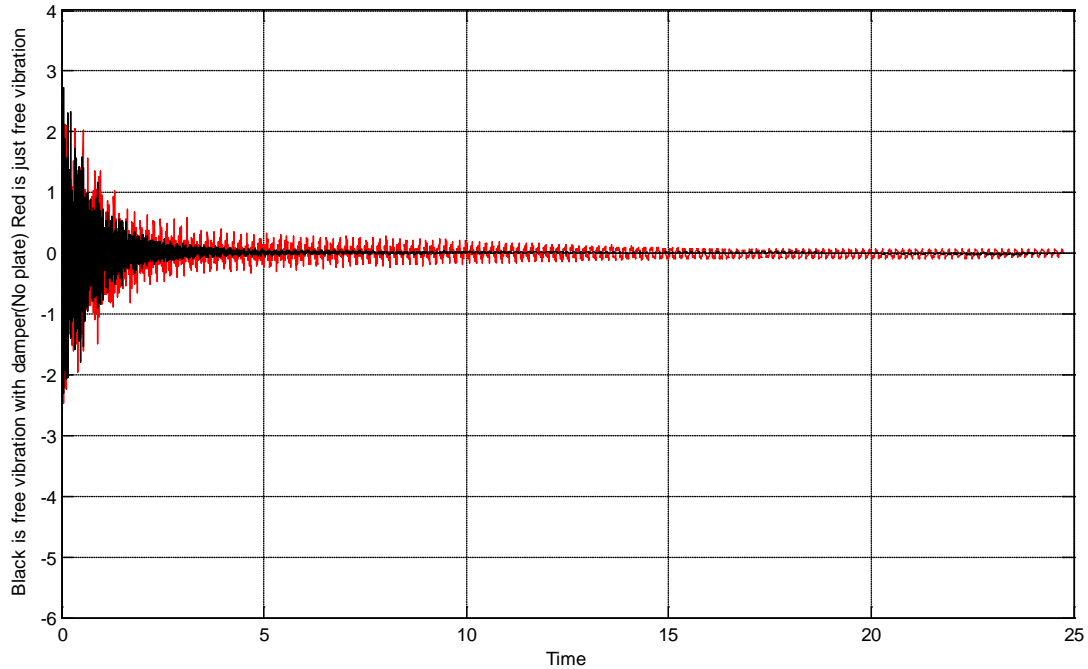


Figure 3-19 Free vibration responses to determine friction between the plastic stick and the lid

3.4 Forced Vibration Tests

Based on the above reasons, it was decided to use the forced vibration tests for the purpose of the current study. With everything remains the same as the free vibration tests, instead of a lumped mass block, a smart shaker was used to excite the cable continuously. The testing setup is illustrated in Figure 3-20. To investigate the effect of damper stiffness on damping ratio, springs were installed on model cable in some cases.

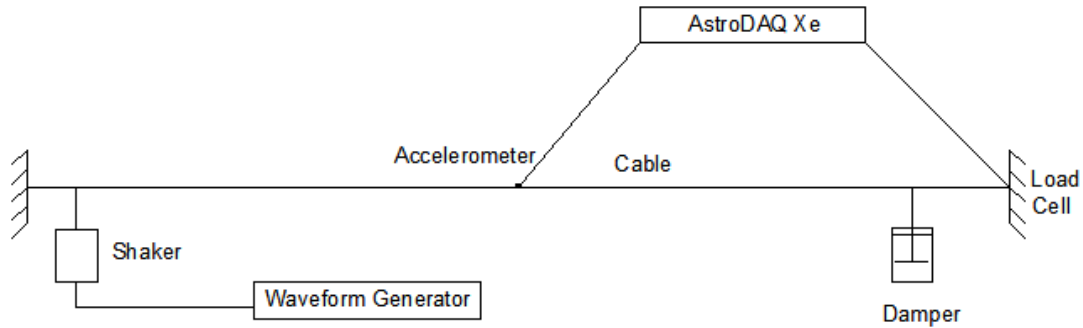


Figure 3-20 Forced Vibration Test Setup

3.4.1 Testing procedures

A. Tests not considering damper stiffness (springs are not installed)

1. Set up input file name. (Same as free vibration test).
2. Set sampling frequency and sampling time. (Same as free vibration test).
3. Connect the signal generator to the smart shaker.
4. Start the shaker and set the vibration amplitude to be 20db. Start the signal generator and adjust the excitation frequency to check the maximum displacement of the model cable and its corresponding excitation frequency. The maximum displacement of the modal cable can be observed when the excitation frequency by the signal generator equals to the natural frequency of the cable, i.e. when resonance occurs. The excitation frequency is normally around 7Hz based on the present condition.
5. Start the excitation frequency from (Natural frequency – 0.5 Hz). For example, if the natural frequency is 7Hz, the starting excitation frequency of the signal generator will be set at 6.5 Hz.

6. Review the recorded data in AstroDAQ Xe controlling software and save captured data in the excel format.
7. Increase the excitation frequency by 0.05 Hz, and then repeat steps 6 and 7. A total number of twenty runs should be done.

B. Tests considering damper stiffness (springs are installed)

1. Attach two springs on the lid of the damper and then mount them on the cable. (As shown in Figure 3.12)
2. Repeat steps 5 to 7 in part A.
3. Change a new pair of springs, and then repeat steps 1 and 2. Altogether 3 different types of springs (9654K53, 9654K812, 9654K115)

3.4.2 Theoretical background

Half-power method was used to find damping ratio from forced vibration response data. It is different from the logarithmic decrement method in that the former is a time domain analysis, where as this is a frequency domain analysis. The model cable vibration amplitude corresponding to each external excitation frequency was determined first based on the recorded displacement time-history at that particular excitation frequency. A frequency-response curve can be plotted, as shown in Figure 3-21, which describes the relation between the external excitation frequency and the maximum displacement response of the cable. The standard procedures of the half-power method are as follows:

1. Identify the peak response of the frequency-response curve. For example, point A in Figure 3-21, this has a maximum displacement D .

2. Obtain the displacement corresponding to half-power points by $D/\sqrt{2}$.
3. Draw a horizontal line at $D/\sqrt{2}$ and intersect with the frequency-response curve at two points (B and C). These two points are the half-power points in Figure 3-21.
4. Draw two vertical lines from the half-power points. The intersections with the horizontal axis (R_1 and R_2 in Figure 3-21) are the excitation frequency or frequency ratio (if the horizontal axis has a dimensionless form by normalizing with the cable natural frequency) corresponding to the half-power points.
5. Compute damping ratio of the cable-damper system using $\xi = \frac{R_2 - R_1}{R_2 + R_1}$.

3.4.3 Advantage of forced vibration tests

1. It is easy to capture model cable response at each excitation frequency.
2. The smart shaker can be installed in a way to guarantee the excitation of in-plane motion of the model cable.
3. The signal generator can control the vibration frequency. Repeatability of the testing conditions is good, which allows studying the damper stiffness effect under the same basic setup.
4. Damping ratio result obtained from the half-power method is less sensitive to the vibration amplitude.

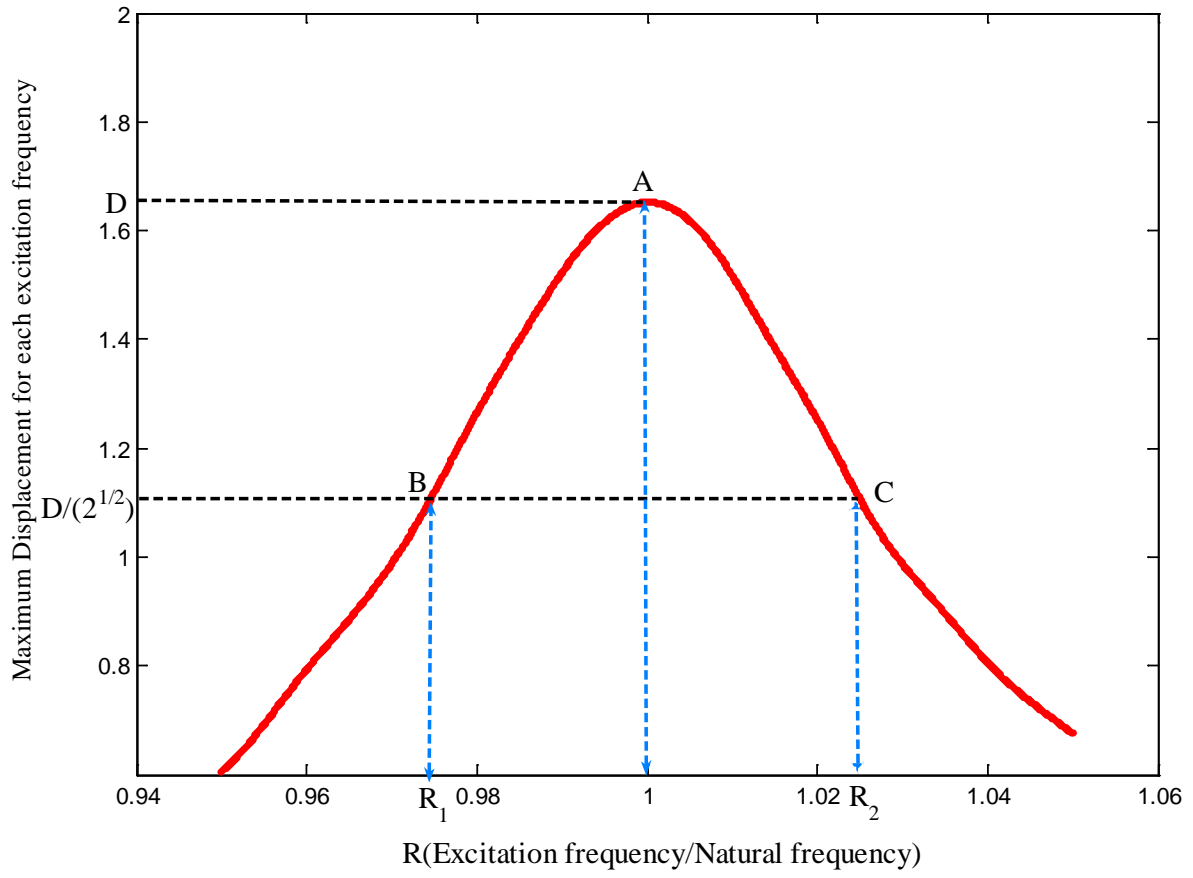


Figure 3-21 half power method illustration on frequency-response curve

Chapter 4 Results and Discussions

Based on the comparison between the free vibration and the forced vibration methods presented in the previous chapter, it was decided to use the latter to measure the cable damping ratio in the current study. Analysis results in terms of damping ratio of the damped cable corresponding to different damper sizes and damper locations, impact of damper stiffness on its suppression effect will be presented in this chapter. In addition, comparison of these results with the existing literature data will be made.

4.1 Pre-processing of Experimental Data

Data pre-processing consists of two steps: i) data filtering; 2) converting acceleration time-history to displacement time-history. When the cable was excited to vibrate, acceleration of cable motion at a specific point was recorded by an accelerometer. In general, the recorded data (raw data) contains contributions from different cable modes and noise from various environmental sources. Filter was applied to the raw data to extract the response of a certain mode of interest. For example, if it is aimed to determine the 2nd modal damping ratio of the damped cable, then the filter will be designed in a way which only allows the 2nd modal response (acceleration in this study) to be retained. In order to determine the damping ratio using either the logarithmic decrement method (free vibration) or the half-power method (forced vibration), displacement time history of cable response is required, which can be obtained by double integration or Fourier Transform of the filtered acceleration time history.

Step 1: Data filtering

Since the current study is focused on the 1st modal damping ratio of the damped cable, the Butterworth Filter is used to filter higher modes and extract the acceleration response associated with the first mode. The Butterworth filter is a type of signal processing filter designed to have as flat a frequency response as possible in the pass band so that it is also termed as a maximally flat magnitude filter (http://wikipedia.org/wiki/Butterworth_filter). The frequency pass band is set as [1st modal frequency – 0.6 Hz, 1st modal frequency + 0.6 Hz]. The order of the filter is normally set as 2.

Step 2: Compute displacement time-history

Two approaches of converting acceleration time-history to displacement time-history were used. The first one is the Double Integration method, and the second one is the Fourier Transform method.

The double integration method is based on the mathematical relation among displacement, velocity and acceleration. The acceleration time-history is integrated with respect to time to obtain the velocity time-history, and then integrate again to obtain the displacement time-history. A Matlab code was developed to perform the calculation by using trapezoidal rule. After a few sample calculations, it was found that there were some disadvantages of using the double integration method. First of all, although the trapezoidal rule is a well defined method to conduct integration “graphically”, it is still an approximation method which contains numerical error. In the dynamic analysis, especially for the current case, even the 4th digit after the decimal point is still important.

Therefore, the accumulated numerical error, which could be considerable, would lead to incorrect results. Secondly, the computation time is relatively long. One set of acceleration time-history contains more than 15,000 data, and based on double integration, it results in billions of operations to process one set of data.

The acceleration time-history obtained from experiment is the representation of modal cable vibration signal in the time domain, whereas Fourier transform is the representation of the modal cable vibration signal in the frequency domain. The definition of Fourier transform is an integral function shown below:

$$\hat{f}(f_n) = \int e^{-2\pi i f_n t} f(t) dt \quad (4.1)$$

where $f(t)$ represents the response time-history, t represents time (Second) and f_n is the natural frequency (Hz).

The inverse of Fourier transform is

$$f(t) = \int e^{2\pi i f_n t} \hat{f}(f_n) df_n \quad (4.2)$$

By applying Fourier transform and its inverse function, the time domain data and the corresponding frequency domain data could be transferred back and forth. In its application to the current study, the displacement time-history will be much easier to get if all the time domain data are transferred to the frequency domain. The detailed procedures are given as follows:

1. Apply Equations (4.1) and (4.2) to the current study. The circular frequency $\omega_n =$

$2\pi f_n$:

$$\hat{D}(\omega_n) = \int e^{-i\omega_n t} \ddot{D}(t) dt \quad (4.3)$$

$$\ddot{D}(t) = \int e^{i\omega_n t} \hat{D}(\omega_n) d\omega_n \quad (4.4)$$

where $\ddot{D}(t)$ represents the acceleration time-history (cm/s²), t represents the time (Second), and f_n is the natural frequency (Hz).

The same for the velocity time-history and the displacement time-history:

$$\hat{D}(\omega_n) = \int e^{(-i\omega_n t)} \dot{D}(t) dt \quad (4.5)$$

$$\dot{D}(t) = \int e^{i\omega_n t} \hat{D}(\omega_n) d\omega_n \quad (4.6)$$

where $\dot{D}(t)$ is velocity time-history, and

$$\hat{D}(\omega_n) = \int e^{(-i\omega_n t)} D(t) dt \quad (4.7)$$

$$D(t) = \int e^{i\omega_n t} \hat{D}(\omega_n) d\omega_n \quad (4.8)$$

where $D(t)$ is displacement time-history.

2. Since $\ddot{D}(t) = \frac{d}{dt} \dot{D}(t)$, by substituting equation (4.6) into it, yields:

$$\begin{aligned} \ddot{D}(t) &= \frac{d}{dt} [\int e^{i\omega_n t} \hat{D}(\omega_n) d\omega_n] \\ &= \int \left(\frac{d}{dt} e^{i\omega_n t} \right) \hat{D}(\omega_n) d\omega_n \\ &= \omega_n i \int e^{i\omega_n t} \hat{D}(\omega_n) d\omega_n \end{aligned} \quad (4.9)$$

Combining Equation (4.4) and (4.9), gives:

$$\hat{\ddot{D}}(\omega_n) = i\omega_n \hat{D}(\omega_n) \quad (4.10)$$

From Equation (4.10), it can be seen that in the frequency domain, the acceleration data could be easily converted to velocity data by dividing $\omega_n i$. The same procedure can be derived for converting velocity data to displacement data in the frequency domain, i.e.:

$$\hat{D}(\omega_n) = i \omega_n \hat{\dot{D}}(\omega_n) \quad (4.11)$$

Combining Equations (4.10) and (4.11), gives:

$$\hat{D}(\omega_n) = -\hat{\dot{D}}(\omega_n) / \omega_n^2 \quad (4.12)$$

Substitute Equation (4.12) into Equation (4.8), yields

$$D(t) = [\int e^{\omega_n t} \widehat{D}(\omega_n) d\omega_n] / (-\omega_n^2) \quad \text{or} \quad D(t) = \ddot{D}(t) / (-\omega_n^2) \quad (4.13)$$

It can be seen from Equation (4.13) that compared to the double integration method, it is more convenient to use Fourier transform to convert acceleration time-history to displacement time-history. In a sample run, by using Fourier transform, the computing time has been shortened to 10 seconds for processing one set of data. Therefore, it is decided to use Fourier transform to compute displacement time-history in the remaining analysis. The Matlab code for data processing is presented in Appendix B.

4.2 Experimental Results

4.2.1 Damping ratio of a damped cable

As illustrated in the previous sections, in order to obtain the first modal damping ratio of a damped cable, the recorded cable acceleration time-history raw data needs to be filtered first and then converted to the first modal displacement time-history. Next, the frequency-response curve is generated, based on which the damping ratio of a cable-damper system can be determined by applying the half-power method.

A sample analysis of a testing case is presented as follows:

In this testing case, twenty of 50g supplementary mass blocks were attached to the model cable. The damper was installed at 6% of cable length away from the right support of the modal cable. The smart shaker was installed at 5% of cable length away from the left support of the modal cable. The accelerometer was placed in the middle of the cable to capture acceleration data. As described in Section 3.3.1, based on these testing conditions,

the data file was named as B_3200_20050_S05_D06_A50_XXHz, where XX represents the excitation frequency from the signal generator which was adjustable. The test started by setting the initial excitation frequency at 7.00 Hz, with the increment of 0.05Hz, and finished at 7.90Hz. At each excitation frequency, the sampling rate was 1000Hz, and the sampling time was 15 seconds. The acceleration time-histories corresponding to each excitation frequencies were saved as excel files. The first modal displacement time-histories corresponding to each excitation frequencies were computed by applying the Butterworth filter to extract the response of the first mode and then converted to displacement time-history using Fourier transform analysis. For example, Figure 4-1 shows the filtered first modal displacement time-history of the studied cable at excitation frequency of 7.40Hz.

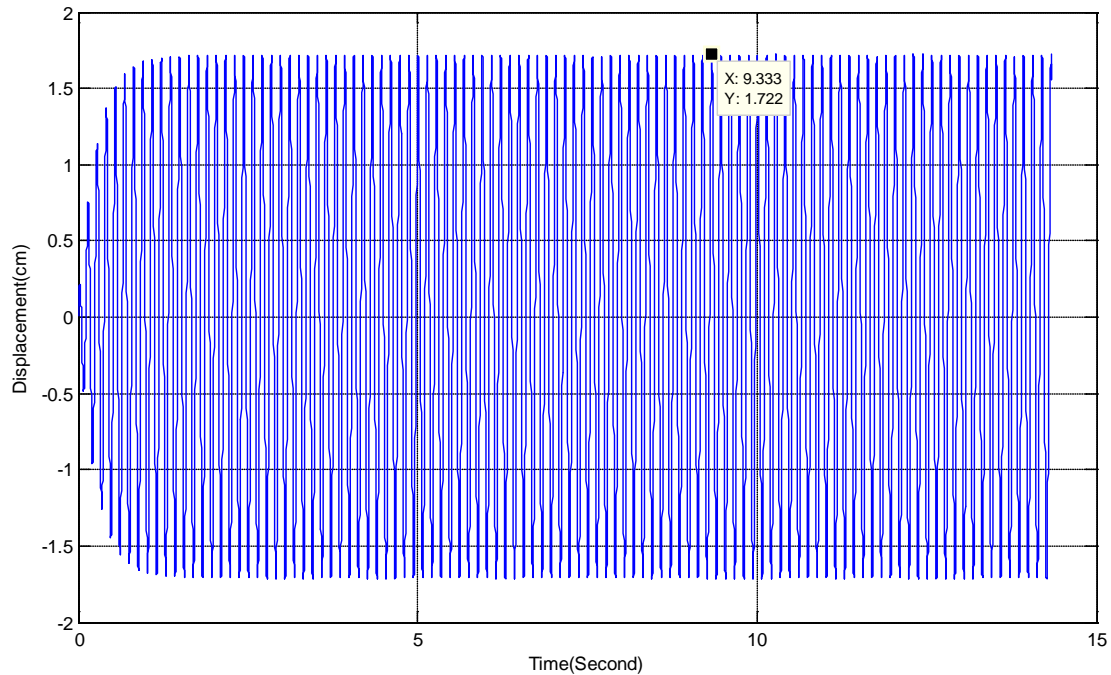


Figure 4-1 First modal displacement time-history of case

B_3200_20050_S05_D06_A50_7.40Hz

The complete set of displacement time-histories corresponding to each excitation frequency in this testing case is included in Appendix C. The maximum cable displacements at each excitation frequency are summarized in Table 4-1.

Table 4-1 Summary of maximum displacements in case B_3200_20050_S05_D06_A50

Excitation Frequency (Hz)	*Frequency Ratio R	Maximum Displacement (cm)
7.00	0.946	0.5871
7.05	0.953	0.6798
7.10	0.959	0.7916
7.15	0.966	0.9228
7.20	0.973	1.0780
7.25	0.980	1.2530
7.30	0.986	1.4440
7.35	0.993	1.6240
7.40	1.000	1.7220
7.45	1.007	1.7110
7.50	1.014	1.5860
7.55	1.020	1.4120
7.60	1.027	1.2350
7.65	1.034	1.0790
7.70	1.041	0.9433
7.75	1.047	0.8322
7.80	1.054	0.7380
7.85	1.061	0.6566
7.90	1.068	0.5890

*R = excitation frequency/natural frequency.

Figure 4-2 shows the frequency response curve plotted based on data in Table 4-1. The cubic spline function was applied for curve fitting. Following the procedures of the half-power method illustrated in Section 3.4.2, in Figure 4-2, the peak displacement of the frequency response curve is 1.722 cm, so the corresponding to half power points is $1.722 \times \frac{1}{\sqrt{2}} = 1.218$ cm. The frequencies corresponding to the two half power points can thus be found from the figure, which are $R_1 = 0.97875$ and $R_2 = 1.02770$, respectively.

Thus the damping ratio of the damped cable can be determined as $\xi = \frac{R_2 - R_1}{R_2 + R_1} = 0.0244 = 2.44\%$.

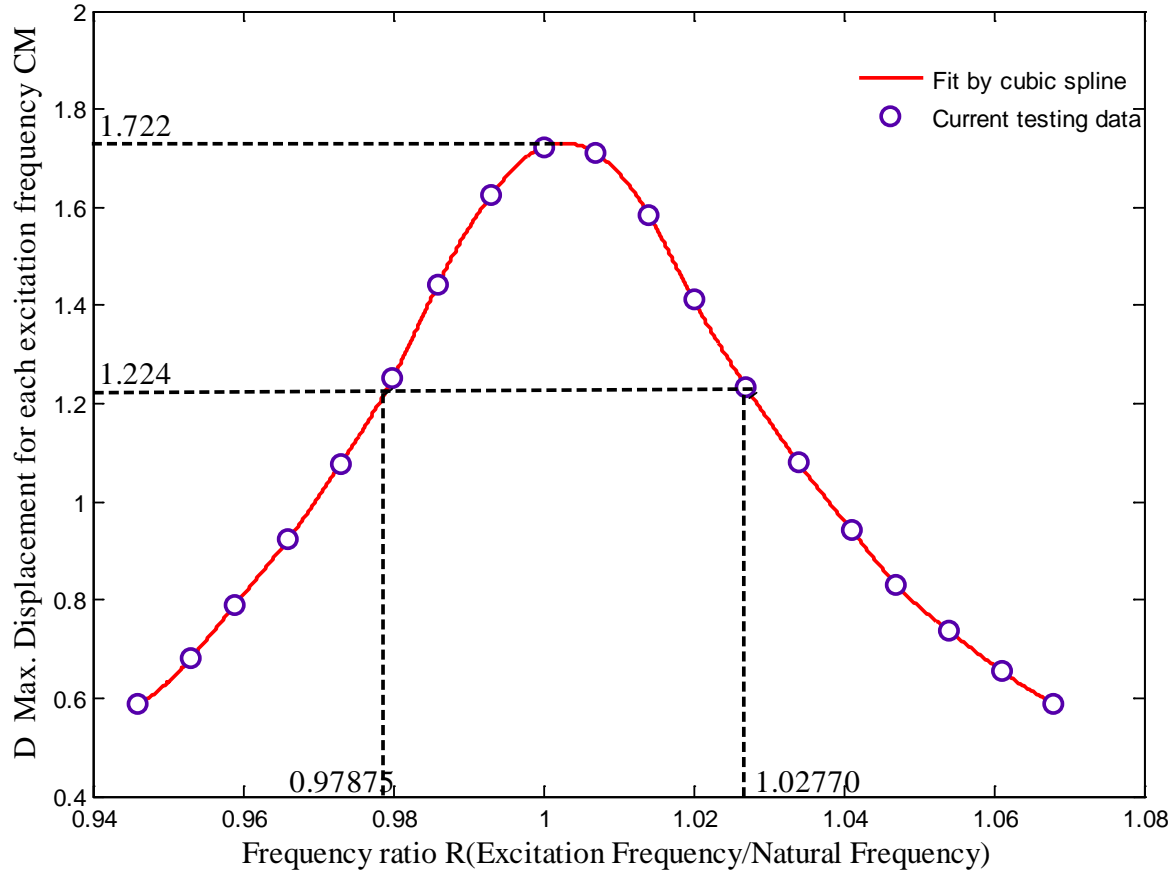


Figure 4-2 Frequency-response curve for case B_3200_20050_S05_D06_A50

Following the same procedure, the equivalent damping ratio of a cable attached to damper of different sizes and installed at different locations are listed in Table 4-2 with the following testing conditions:

- Cable tension $T = 3200 \text{ N}$
- Length of cable $L = 9.33 \text{ m}$
- Unit mass of cable $= 0.2 \text{ kg/m}$

Table 4-2 Equivalent cable damping ratio for different damper sizes and locations

Cases	Oil #1+ Plate #3	Oil #1 +Plate #2	Oil #2 +Plate #3	Oil #1 +Plate #1	Oil #2 +Plate #2	Oil #2 +Plate #1
Damping Properties (N·s/m)	18.4	46.7	70.3	164.8	275.5	1463.8
Damper location 4% L	1.53	2.49	2.80	2.31	2.08	1.15
Damper location 6% L	2.38	3.80	4.27	2.44	2.29	1.12
Damper location 10% L	2.46	5.73	5.40	2.82	2.33	1.24

Damper design curve plotted for different damper locations based on the current testing results are shown in Figures 4-3 to 4-5. Two facts can be observed from the figures:

- 1) As the damper moves away from the cable end, the optimum damper size decreases and the corresponding maximum damping ratio increases. When the damper installed at 4%L, the optimum damper size is 75 N·s/m and the maximum damping ratio is 2.73%. When the damper is installed at 6%L, the optimum damper size is 66 N·s/m and the maximum damping ratio is 4.20%. When the damper moves to 10%L, the optimum damper size is 55 N·s/m and the maximum damping ratio is 5.85%.

2) As the damper moves away from the cable end, the damper size has a greater effect on the equivalent cable damping ratio. For the three studied damper location 4%L, 6%L, and 10%L, if double the optimum damper size, and compare the associated equivalent 1st modal cable damping ratio with that corresponding to the optimum damper size, it is found that the equivalent 1st modal cable damping ratio is reduced by 8.4%, 28.6%, and 34.2%, respectively. For instance, when the damper is installed at 6%L, the equivalent 1st modal cable damping ratio corresponding to the optimum damper size of 66 N·s/m is 4.27%, whereas by doubling the damper size to 132 N·s/m, it decreases to 3.00%. The reduction is 28.6%.

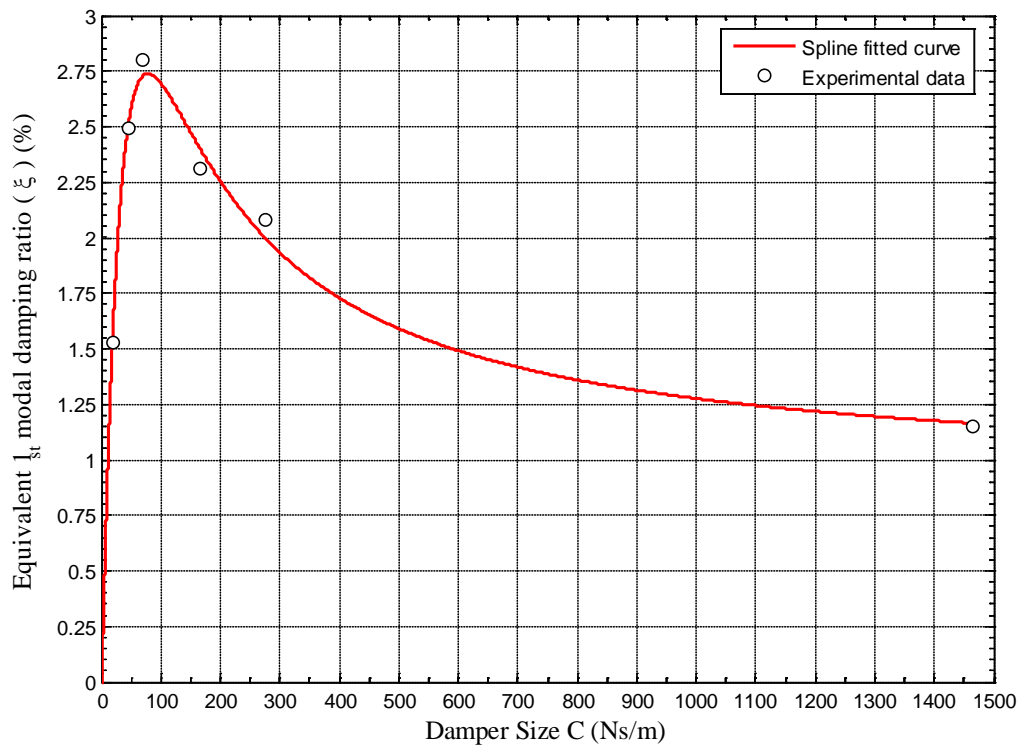


Figure 4-3 Equivalent first modal damping ratio with damper installed at 4%L

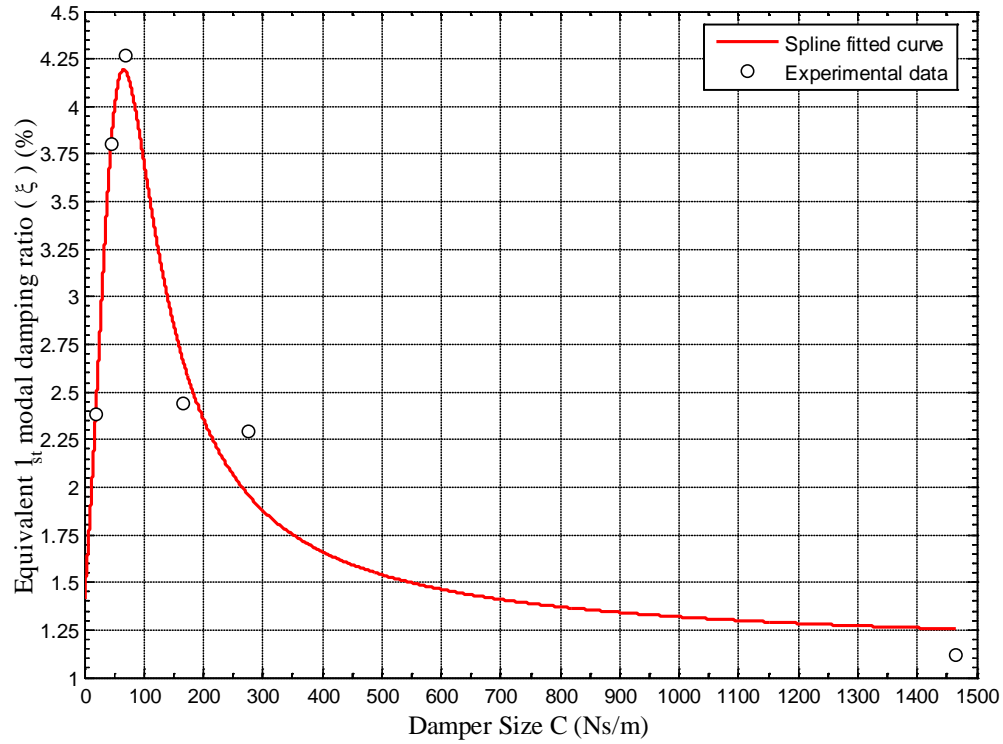


Figure 4-4 Equivalent first modal damping ratio with damper installed at 6%L

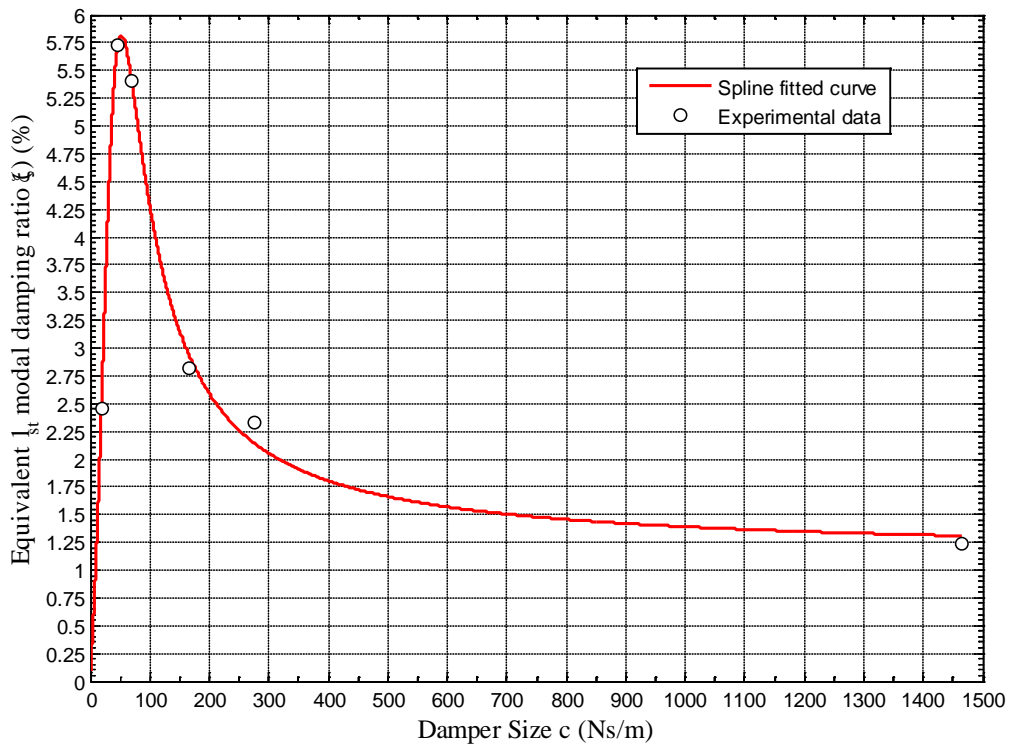


Figure 4-5 Equivalent first modal damping ratio with damper installed at 10%L

4.3 Comparison with Other Studies

4.3.1 Universal damper design curve (Pacheco et al, 1993)

As reviewed in Chapter 2, install external damper to suppress stay cable vibrations is one of the most commonly used methods on bridge site. In designing the viscous damper, an estimation of the additional damping offered by the damper for the various natural modes of the cable is usually obtained by eigenvalue analysis. Such an analysis is usually very time consuming. Pacheco et al. (1993) proposed a universal damper design curve which is very useful for selecting damper size and installation location during the preliminary design stage. Without large amount of numerical simulation effort, the universal damper design curve could be used to find the proper damper size and location for the required amount of damping ratio of a particular stay cable or estimate the equivalent damping ratio of a particular stay cable for a given damper size and location. This universal curve was developed by performing eigenvalue analysis of a taut cable attached with a linear viscous damper. In the analysis, the cable sag and bending stiffness were neglected. The cable structural inherent damping was assumed to be zero. The universal damper design curve proposed by Pacheco et al. (1993) is shown in Figure 4-6. The plot is produced by using two non-dimensional parameters, i.e. $\xi_i/(x_c/L)$ in the vertical axis, and $c/(mL\omega_{01})ix_c/L$ in the horizontal axis, where “m” is the mass per unit length, “L” is the total length of cable, “ ω_{01} ” is the first mode angular natural frequency of cable, “i” is the mode number which is 1 for our case. “ x_c/L ” is the location damper installed.

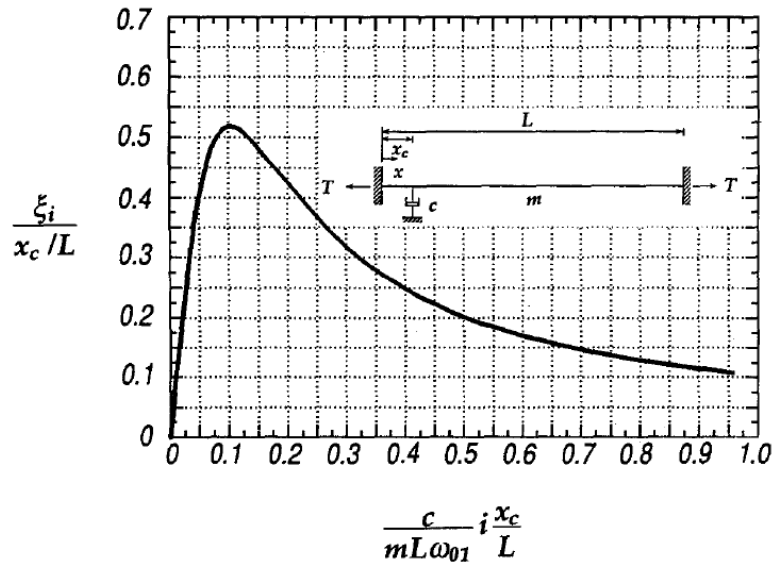


Figure 4-6 Universal damper design curve proposed by Pacheco et al. (1993)

Figure 4-7 shows the comparison between the current results and the universal damper design curve by plotting them in the same figure. It can be seen from the figure that although the pattern of the current results seem to be lifted and shifted towards left, the overall pattern of the current set agrees with the universal curve. During the tests, it was observed from time to time that if the cable vibration amplitude was relatively large, the contact between the plastic stick of the damper and the lid would occur, particularly when the excitation frequency of the signal generator approaches to the natural frequency of the cable. This type of contact would induce friction force, which would directly contribute to the total damping force offered by the damper. Therefore, the actual damping provided by the damper is larger than its calibrated value shown in Table 3-4. Considering this fact, if the damping ratio results are plotted using the “real” damping value, the present set of results would be shifted toward right, i.e. has a better agreement with the universal curve. In addition, the derivation of the universal curve is based on an

idealized taut cable, i.e. the bending stiffness and sag of the cable are neglected, which are in presence in the physical tests and would have an impact on the experimental results.

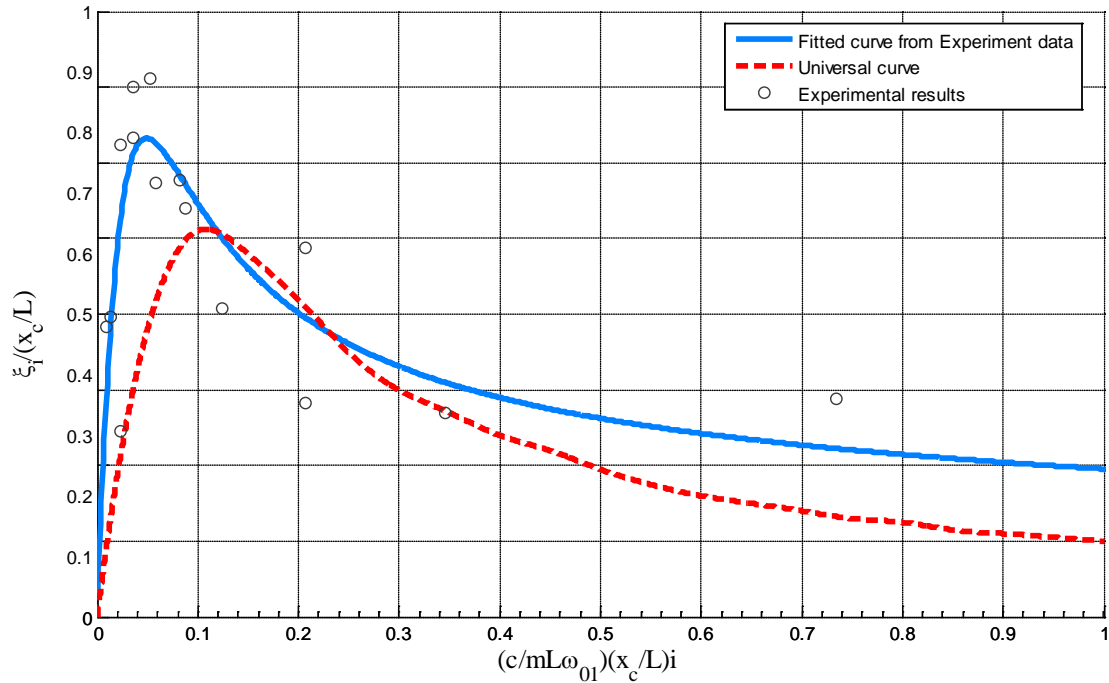


Figure 4-7 Comparison between the current results and the universal damper design curve proposed by Pacheco et al. (1993)

It can be seen from the figure 4-7 that test on the present study, the point corresponding to the optimum damper design has coordinates of (0.05, 0.63). It's a very useful reference for damper design. For example, if we have a cable has unit weight “m” of 98 kg/m and 215 meters in length “L”. The tension “T” applied on cable is 3000kN, so

that its first modal circular natural frequency is $\omega_{01} = \frac{\pi}{L} \sqrt{\frac{T}{m}} = 2.557 \text{ rad/s}$, if the required

damper should be installed at 5% of cable length towards cable-deck anchorage, then the required damper size for the 1st cable mode should equal to $c = 0.05 \text{ mL}\omega_{01}/5\% = 53876$

N·s/m and its corresponding damping ratio is $\xi_1 = 0.63 \cdot 0.05 = 0.0315 = 3.15\%$. For the model cable tested in the current study, which has cable tension “T” of 3200N, unit mass

“ m ” of 0.2kg/m, length “ L ” equal 9.33m and its first modal circular frequency “ ω_{01} ” is 42.59 rad/s. If the damper installs at 5% of cable length, the optimal damper size “ c ” is 79.5 N·s/m.

4.3.2 Damper design curves (Cheng et al, 2010)

In an independent study, Cheng et al (2010) developed a group of damper design curves using energy-based approach. In the derivation, both the bending stiffness and sagging effect were taken into account. The cable-damper system studied by Cheng et al (2010) is shown in Figure 4-8.

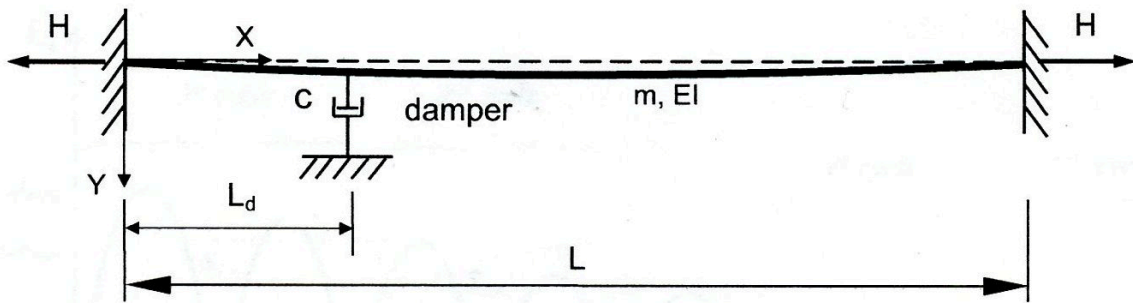


Figure 4-8 Layout of a cable-damper system studied by Cheng et al (2010)

The cable with length L is laid out in the horizontal direction with a pretension H , a mass per units span m , finite flexural rigidity EI , and a damper with damping coefficient c attached transversely a distance L_d from one cable end. All those parameters were combined into non-dimensional forms as:

- Damper location parameter $\Gamma_d = L_d/L$.
- Bending stiffness parameter $\zeta = L/(H/EI)^{1/2} = 297$
- Nondimensional Damping parameter $\psi = (\pi c)/(mL\omega_{1s})$.

where the 1st mode frequency $\omega_{1s} = (\pi/L)(H/m)^{1/2}$. In the current study, $\omega_{1s} = 42.59$ rad/s.

The free vibration response of a cable-damper system is obtained from finite element simulation using ABAQUS, and the kinetic energy decay ratio and the corresponding structural equivalent damping ratio of the damped cable was determined. The kinetic energy decay ratio d_n was defined as follow (Cheng et al, 2010):

$$d_n = \frac{1}{j} \sum_{i=1}^j \frac{(E_{ki,n})_{max} - (E_{k(i+1),n})_{max}}{(E_{ki,n})_{max}} \quad (4.14)$$

where $(E_{ki,n})$ is the kinetic energy of the cable in the i^{th} cycle of the n^{th} mode, which is shown in Figure 4-9. The equivalent damping ratio of the cable was derived as $\xi_n = -\ln(1 - d_n)/(4\pi)$. Design curves were produced by varying the three non-dimensional parameters in the practical length, tension, bending stiffness of real bridge stay cables. They are attached in Appendix C.

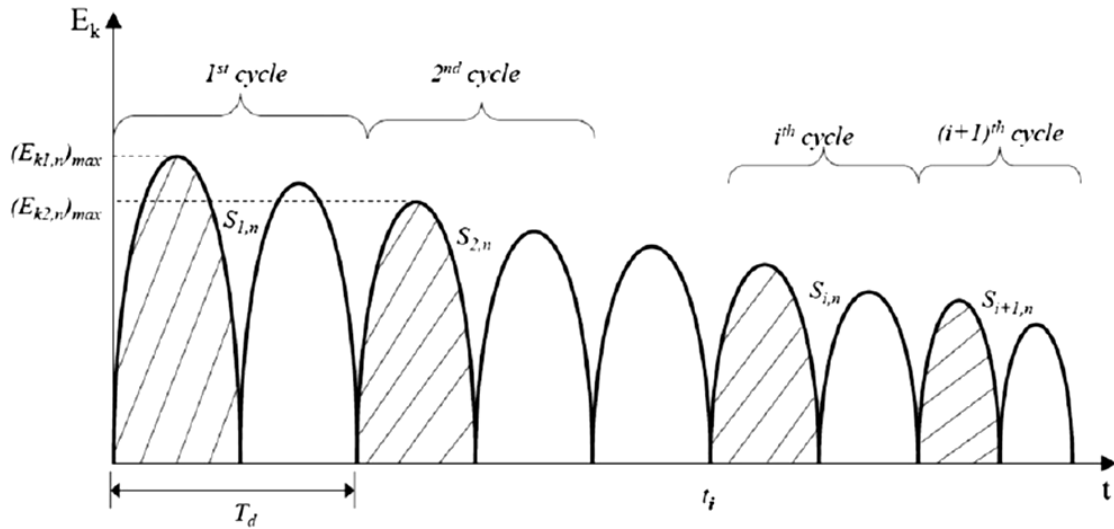


Figure 4-9 Schematic illustration of kinetic energy time history of the n^{th} mode of a damped cable (Cheng et al., 2010)

Figures 4-10, 4-11, and 4-12 show the comparison between the current experimental results and those by Cheng et al (2010). The X-axis represents the nondimensional damping parameter ψ , and Y-axis represents the equivalent first modal

damping ratio ξ (%). The nondimensional damping parameter ψ corresponding to the six damper sizes used in the current study are listed in Table 4-3.

Table 4-3 Different damper size and its corresponding nondimensional damping parameter ψ

Combination	Oil #1+ Plate #3	Oil #1 +Plate #2	Oil #2 +Plate #3	Oil #1 +Plate #1	Oil #2 +Plate #2	Oil #2 +Plate #1
Damping Properties (N·s/m)	18.4	46.7	70.3	164.8	275.5	1463.8
Nondimensional damping parameter ψ	0.7	1.9	2.8	6.5	10.9	57.8

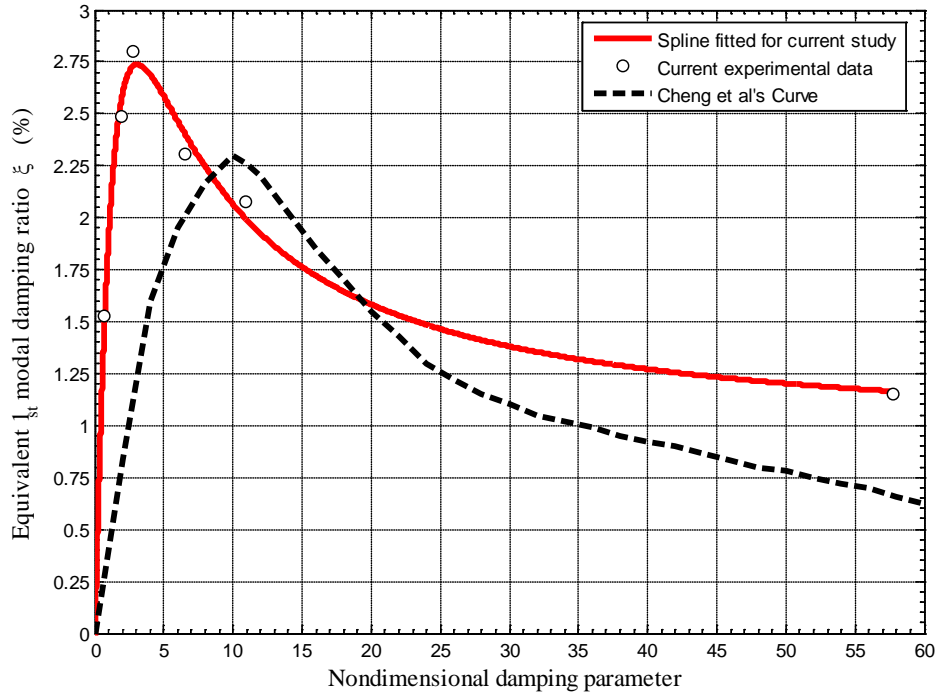


Figure 4-10 Comparison between the current study and Cheng et al (2010)'s design curve

at 4%L

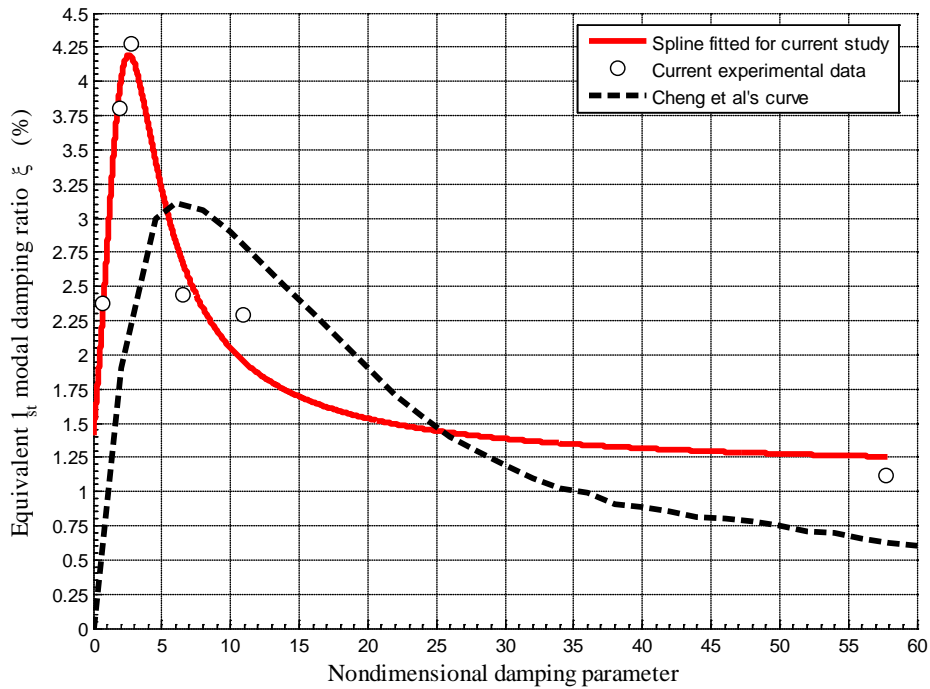


Figure 4-11 Comparison between the current study and Cheng et al (2010)'s design curve

at 6%L

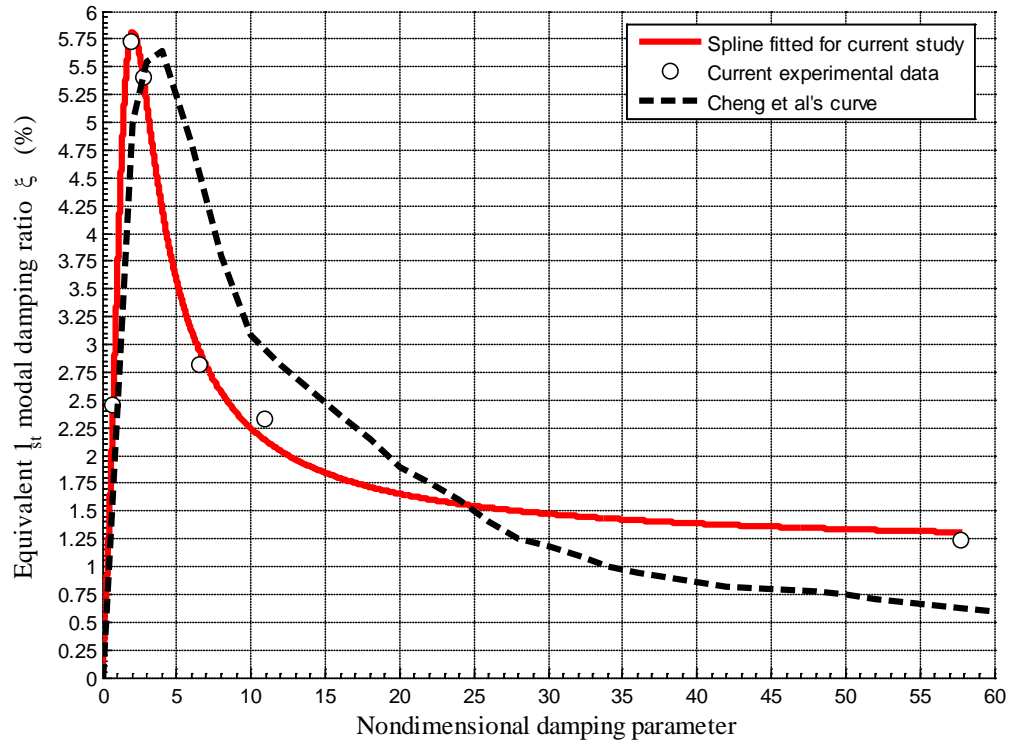


Figure 4-12 Comparison between the current study and Cheng et al (2010)'s design curve at 10%L

Figures 4-10 to 4-12 are shown that the current experimental curves are lifted and shifted to the left from those by Cheng et al (2010). As explained in Section 4.3.1, this could be resulted from the friction generated between the lid and the damper stick which contribute additional damping to the damper. It is worth mentioning that when the damper is installed closer to the cable anchorage, the cable attachment point to the damper has smaller vibration amplitude. Therefore, the damping force provided by the damper, which is proportional to the response of the cable at the attachment point, is lower. Since in the experiment, the actual damping provided by the damper includes that due to oil viscosity (which we designed for) and that due to friction between the damper lid and the piston (observed during tests), therefore, the latter has more weight when

damper location is closer to the cable end. This could be the reason why in Figure 4-10 (damper location 4%L), the current damper design curve shifts more towards the left of the one proposed by Cheng et al (2010), and Figure 4-12 (damper location 10%L) shows better agreement.

In general, the optimal damper sizes from the current experimental results are smaller than those predicted by Cheng et al (2010). The efficiency of the damper in terms of damping ratio corresponding to the optimal damper size at 4%, 6% and 10% L are higher than Cheng et al's predicted results. There are a number of reasons which could cause this discrepancy. First of all, it could be resulted from the non-linearity of the damper property due to additional friction between the lid and the damper stick near resonance response of the cable. Since the half-power method used in the current study for determining the damping ratio of the damped cable utilizes the cable response data in the neighborhood of the resonance point, this friction-related nonlinearity which is not included in the formulation by Cheng et al (2010), could lead to a lower damping ratio, as compared to the current set. Secondly, it could be related to the supplementary mass cell added on the cable model. There are twenty 50g mass cells installed evenly on the cable to simulate the behavior of a real stay cable. These supplementary mass might not only increase the mass property of the cable, but also have some contributions to the bending stiffness of the cable. Previous studies (eg. Cheng et al. 2010, Hoang et al, 2007) showed that cable bending stiffness is an important parameter in determining equivalent damping ratio of a damped cable. The current design curve, which is plotted based on the bending stiffness of the cable itself, could deviate from the actual one which considers the stiffness contribution from the supplementary mass.

The results from the current experimental tests show reasonable trend of viscous damper performance at different locations with different sizes. The fact that the optimal damper size is existed and attainable for the damper design of cable-stayed bridge has been confirmed.

4.4 Effect of Damper Stiffness

Possible impact of damper stiffness on its effectiveness to control cable vibrations was noticed by Zhou (2005) and Krenk and Hogsberg (2005). However, no extensive study on this issue is available in the literature. To understand the effect of damper stiffness on the performance of a damper, a set of experimental tests have been designed. Two parallel springs with the same spring constant connecting the damper lid and the cable are used to simulate the damper stiffness effect (Figure 3-12). Since the two springs are parallel to each other, the equivalent spring constant $k_{eq} = 2k$, where k is the stiffness constant of each spring. As described in Chapter 3, three types of spring with different spring constants were used in the current tests. For example, if two 9654K53 springs with spring constant $k = 0.77$ N/cm were attached to the cable, k_{eq} would be 1.54 N/cm. Experimental results of the 1st modal damping ratio of the modal cable with dampers installed at 4%L, 6%L and 10%L with different springs are summarized in Table 4-4.

From Table 4-4, it can be seen that for the same damper installed at the same location, if the damper stiffness increases, the equivalent cable damping ratio will decrease. From Figures 4-13 to 4-15, it clearly shows that damper stiffness have greater effect on the equivalent cable damping ratio when the damper is installed closer to the cable end. For instance, when the damper is installed at 4%L, the equivalent cable damping ratio ignoring damper stiffness ($k = 0$) is equal to 2.8%; whereas the equivalent

cable damping ratio considering damper stiffness ($k = 4.3 \text{ N/cm}$) is equal to 2.17%, reduced by 22.5%.

It can be seen from Figures 4-13 to 4-15 that the existence of damper stiffness will have a negative impact on damper efficiency. Compared to the damping force generated by the damper itself, the elastic force resulted from the damper stiffness has a much smaller magnitude. Compared to a damper location more towards the cable midpoint, when the damper is installed closer to the cable end, it is less effective in controlling cable vibration, i.e. the damping force contributed by the damper is smaller when the damper location is closer to the cable anchorage. Therefore, the reduction effect induced by the damper stiffness will decrease when moving the damper away from the cable end.

Table 4-4 Damper stiffness effect on cable damping ratio (%)

Damper Size	Oil #1 Plate #3 (18.4 N·s/m)			Oil #1 Plate #2 (46.7 N·s/m)			Oil #2 Plate #3 (70.3 (N·s/m)			Oil #1 Plate #1 (164.8 (N·s/m)			Oil #2 Plate #2 (275.5 N·s/m)			Oil #2 Plate #1 (1463.8 N·s/m)		
	4	6	10	4	6	10	4	6	10	4	6	10	4	6	10	4	6	10
Without spring	1.53	2.38	2.46	2.49	3.80	5.73	2.80	4.27	5.40	2.31	2.44	2.82	2.08	2.29	2.33	1.15	1.12	1.24
With 9654k53 ($k_{eq}=1.54$ N/cm)	1.43	2.35	2.40	2.31	3.58	5.56	2.60	4.12	5.37	2.32	2.34	2.80	1.78	2.17	2.24	1.12	1.05	1.24
With 9654k812 ($k_{eq} = 2.94$ N/cm)	1.36	2.30	2.36	2.19	3.42	5.36	2.36	3.99	5.29	2.27	2.29	2.73	1.32	2.06	2.10	1.06	1.02	1.16
With 9654k115 ($k_{eq} = 4.30$ N/cm)	1.26	2.25	2.29	2.13	3.21	4.88	2.17	3.70	5.17	2.20	2.26	2.70	1.12	2.01	2.03	1.05	0.99	1.15

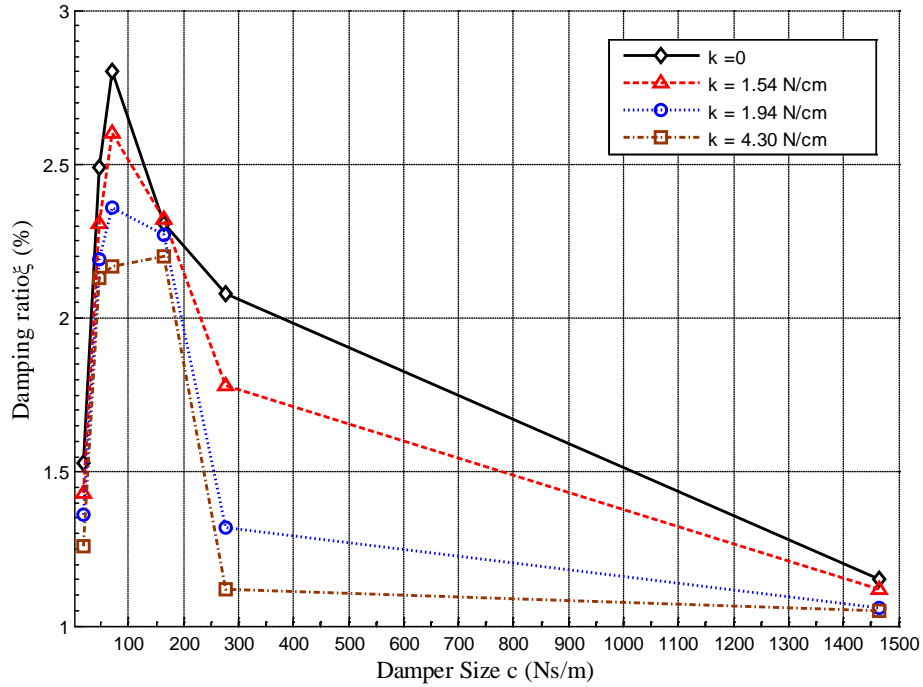


Figure 4-13 Impact of damper stiffness on equivalent 1st modal cable damping ratio
(damper location 4%L)

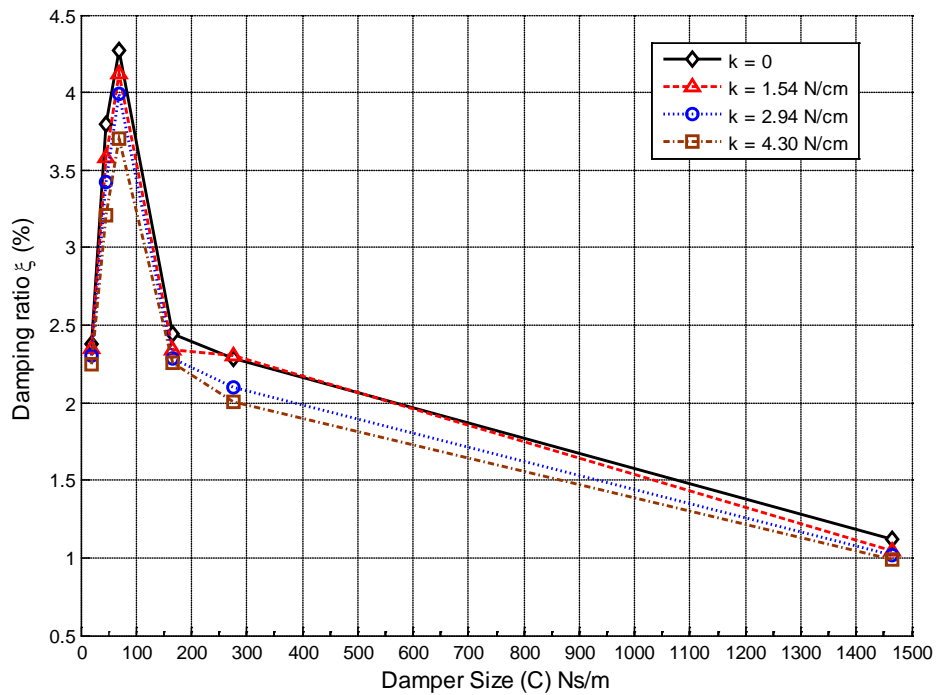


Figure 4-14 Impact of damper stiffness on equivalent 1st modal cable damping ratio
(damper location 6%L)

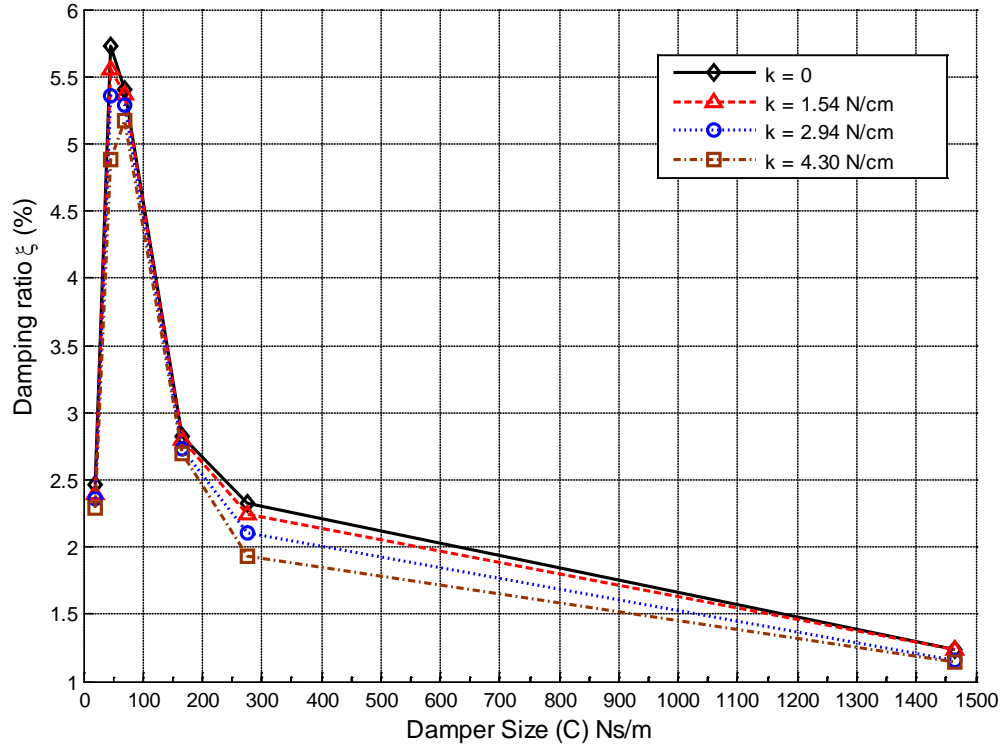


Figure 4-15 Impact of damper stiffness on equivalent 1st modal cable damping ratio
(damper location 10%L)

In Figures 4-16 to 4-21, the impact of damper stiffness on the same damper installed at different locations are shown more clearly. It can be observed that an approximately linear relationship exists between the damper stiffness and the damping ratio. When the damper size is smaller than twice of the optimum value. When the damper size is larger than twice of the optimum one, the stiffness effect becomes unstable. In these cases, since the damper is very strong, it will actually act more like an additional support at that location.

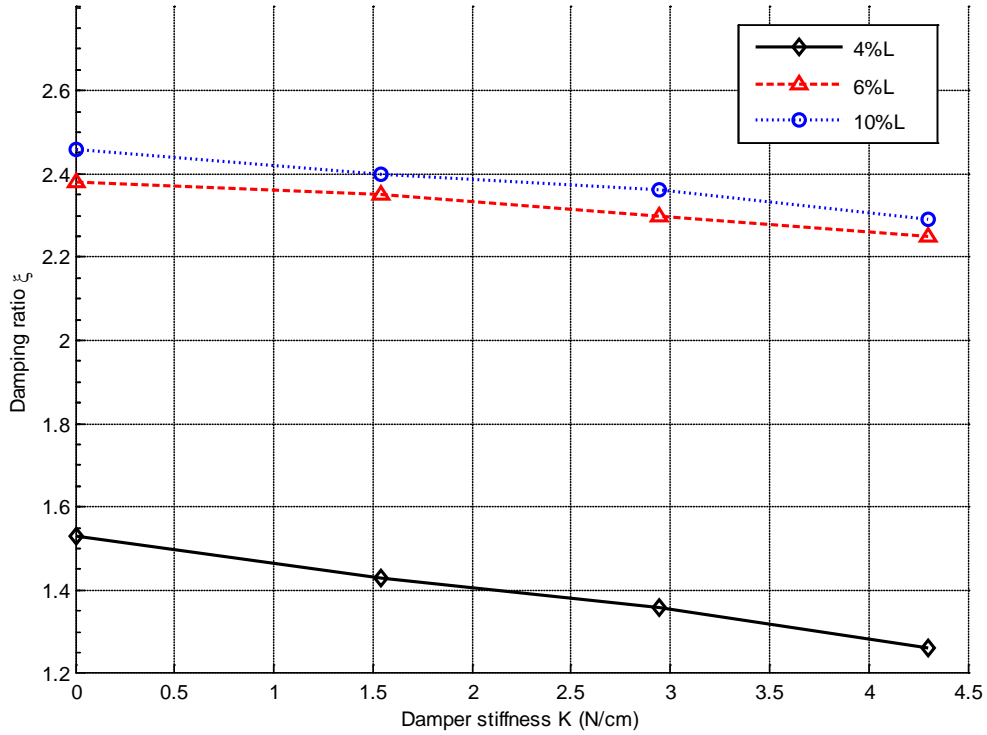


Figure 4-16 Damping ratio vs Damper stiffness (C = 18.4 N·s/m)

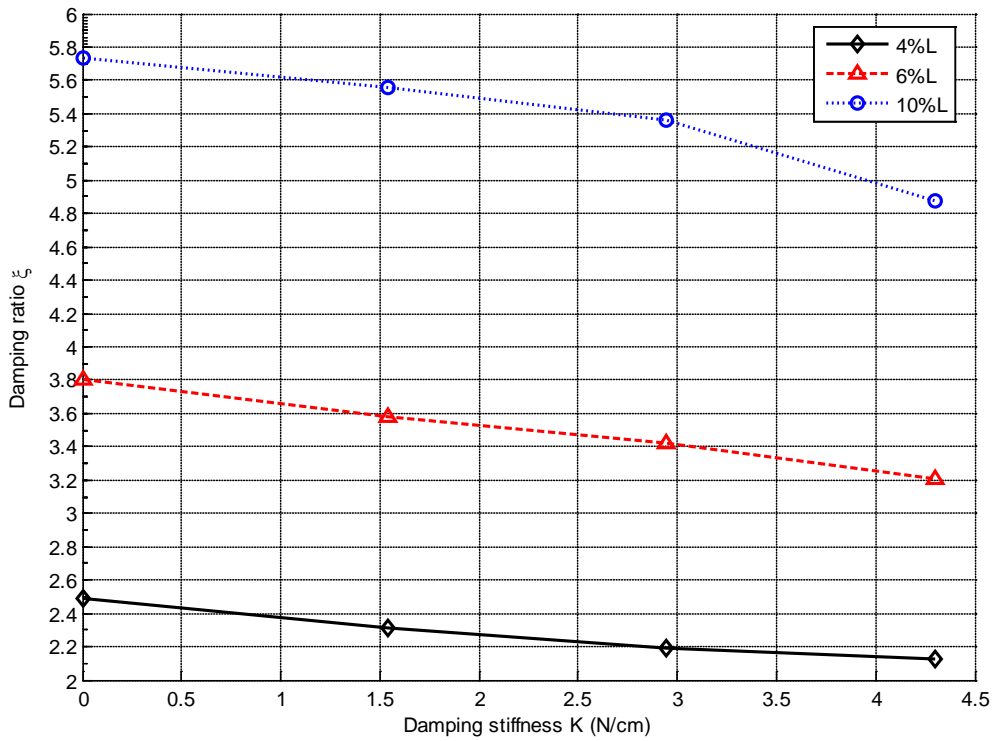


Figure 4-17 Damping ratio vs Damper stiffness (C = 46.7 N·s/m)

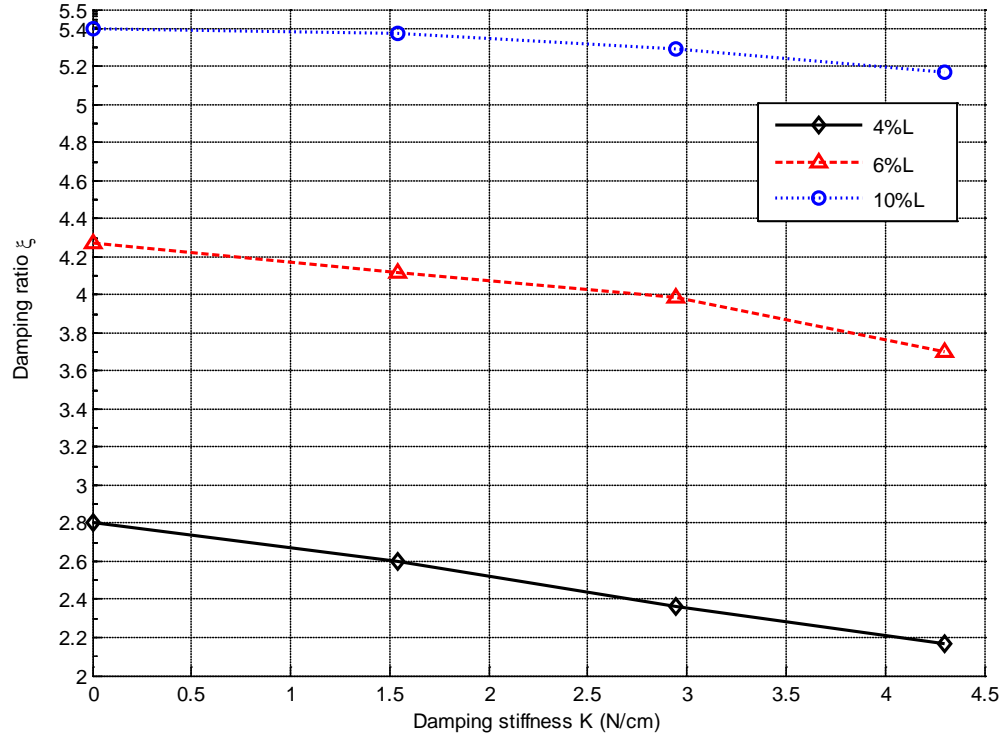


Figure 4-18 Damping ratio vs Damper stiffness ($C = 70.3 \text{ N}\cdot\text{s/m}$)

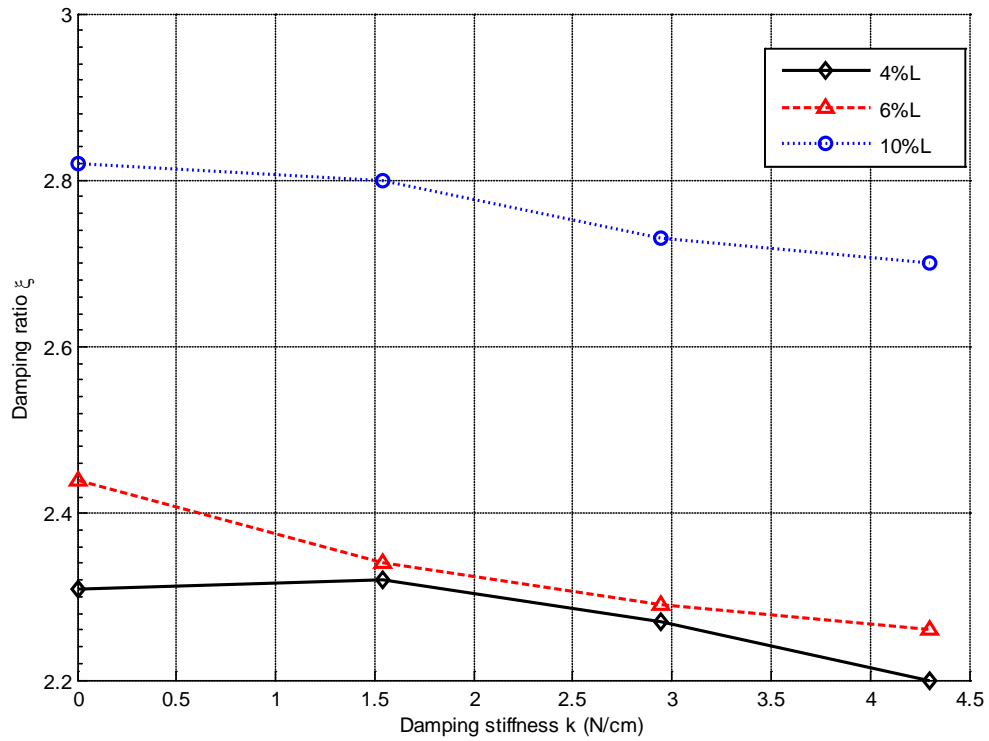


Figure 4-19 Damping ratio vs Damper stiffness ($C = 164.8 \text{ N}\cdot\text{s/m}$)

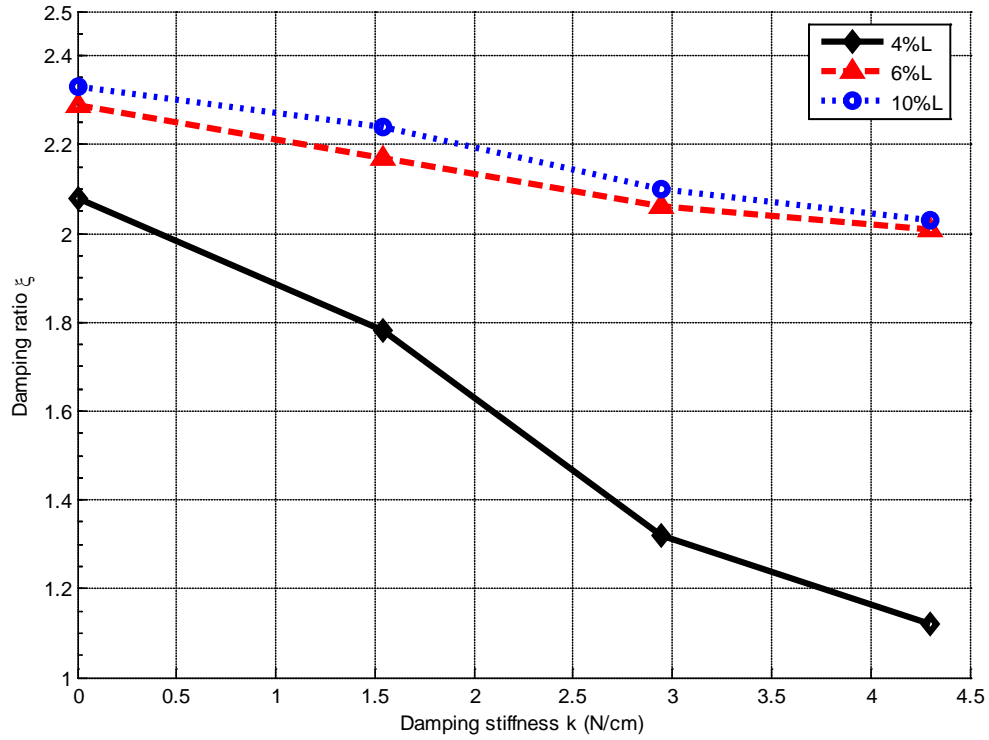


Figure 4-20 Damping ratio vs Damper stiffness ($C = 275.5 \text{ N}\cdot\text{s/m}$)

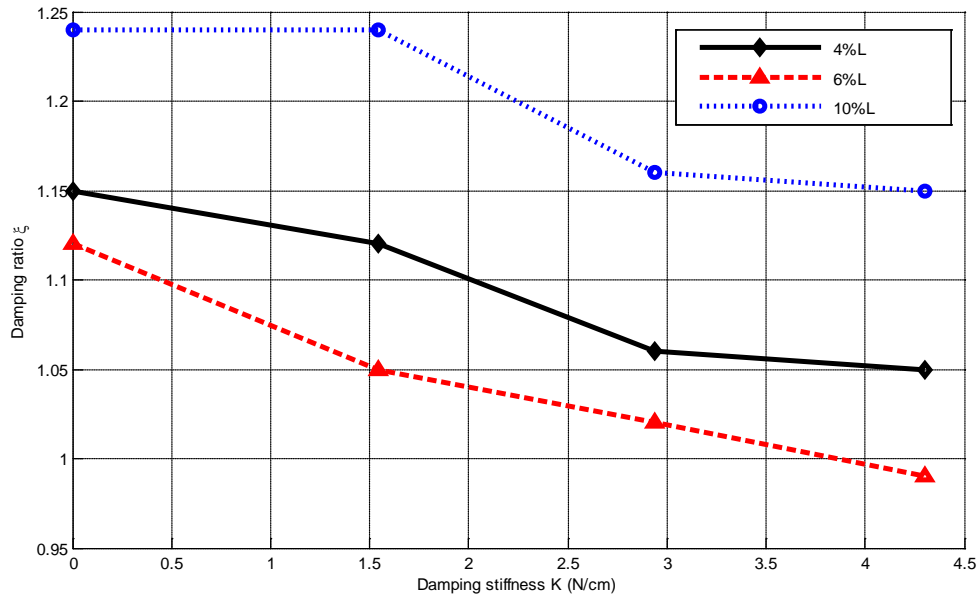


Figure 4-21 Damping ratio vs Damper stiffness ($C = 1463.8 \text{ N}\cdot\text{s/m}$)

Zhou (2005) studied the damper stiffness effect by proposing a nondimensional parameter, the maximum modal damping ratio decay rate $R_{\max} = 1/(1 + \gamma)$, where γ is the non-dimensional damper stiffness. $\gamma = kx_c/H$. k is stiffness of damper (N/m); x_c is damper location from near end of anchor (m); and H is the tension of Cable (N). This parameter is defined as the difference between the modal damping ratio with and without considering damper stiffness normalized by the modal damping ratio without considering damper stiffness. It clearly indicates the impact of damper stiffness on the modal damping ratio of a damped cable.

Tables 4-5 to 4-10 present a comparison of damping ratio decay rate between the current set and Zhou's work. The two sets of results are found to agree well with each other with error to be less than 5% when the damper size is not closed to the optimum one. Damper stiffness obviously has a greater effect on the damping ratio when the damper size is closed to optimum value. Thus maximum modal damping ratio decay rate R_{\max} becomes smaller near that range. This set of comparison is also portrayed in Figures 4-21 to 4-27 for a more convenient comparison. It can be observed from the figures that in terms of the reduction rate of maximum modal damping in the cable due to the existence of damper stiffness, the two sets of results agree well. However, the current set is more sensitive to the damper location. It is worth noting that the maximum modal damping ratio decay rate $R_{\max} = 1/(1 + \gamma) = H/(H + kx_c)$. Compared to cable pretension H , the product of damper stiffness k and damper location x_c is very small. Thus, either varying k or x_c will slight affect the magnitude of R_{\max} . This could be the reason why the damper stiffness effect derived from Zhou's formula for different damper locations all collapse on one curve.

Table 4-5 Damping ratio decay rate of experimental results and Zhou's formula with damper size 18.4 N·s/m

Spring No.	Equivalent stiffness k_{eq} (N/cm)	Damper location								
		4% L			6%L			10%L		
		γ	R_{max}		γ	R_{max}		γ	R_{max}	
			Current	Zhou(2005)		Current	Zhou(2005)		Current	Zhou(2005)
9654K53	1.54	0.018	93.5%	98.2%	0.026	98.7%	97.7%	0.046	97.6%	95.6%
9654K812	2.94	0.034	88.9%	96.7%	0.051	96.6%	95.2%	0.086	95.9%	92.1%
9654K115	4.3	0.050	82.4%	95.2%	0.075	94.5%	93.0%	0.126	93.1%	88.8%

Table 4-6 Damping ratio decay rate of experimental results and Zhou's formula with damper size 46.7 N·s/m

Spring No.	Equivalent stiffness k_{eq} (N/cm)	Damper location								
		4% L			6%L			10%L		
		γ	R_{max}		γ	R_{max}		γ	R_{max}	
			Current	Zhou(2005)		Current	Zhou(2005)		Current	Zhou(2005)
9654K53	1.54	0.018	92.8%	98.2%	0.026	94.2%	97.7%	0.046	97.0%	95.6%
9654K812	2.94	0.034	88.0%	96.7%	0.051	90.0%	95.2%	0.086	93.5%	92.1%
9654K115	4.3	0.050	85.5%	95.2%	0.075	84.5%	93.0%	0.126	85.2%	88.8%

Table 4-7 Damping ratio decay rate of experimental results and Zhou's formula with damper size 70.3 N·s/m

Spring No.	Equivalent stiffness k_{eq} (N/cm)	Damper location								
		4% L			6%L			10%L		
		γ	R_{max}		γ	R_{max}		γ	R_{max}	
			Current	Zhou(2005)		Current	Zhou(2005)		Current	Zhou(2005)
9654K53	1.54	0.018	92.9%	98.2%	0.026	96.5%	97.7%	0.046	99.4%	95.6%
9654K812	2.94	0.034	84.3%	96.7%	0.051	93.4%	95.2%	0.086	98.0%	92.1%
9654K115	4.3	0.050	77.5%	95.2%	0.075	86.7%	93.0%	0.126	95.7%	88.8%

Table 4-8 Damping ratio decay rate of experimental results and Zhou's formula with damper size 164.8 N·s/m

Spring No.	Equivalent stiffness k_{eq} (N/cm)	Damper location								
		4% L			6%L			10%L		
		γ	R_{max}		γ	R_{max}		γ	R_{max}	
			Current	Zhou(2005)		Current	Zhou(2005)		Current	Zhou(2005)
9654K53	1.54	0.018	92.8%	98.2%	0.026	94.2%	97.7%	0.046	97.0%	95.6%
9654K812	2.94	0.034	88.0%	96.7%	0.051	90.0%	95.2%	0.086	93.5%	92.1%
9654K115	4.3	0.050	85.5%	95.2%	0.075	84.5%	93.0%	0.126	85.2%	88.8%

Table 4-9 Damping ratio decay rate of experimental results and Zhou's formula with damper size 275.5 N·s/m

Spring No.	Equivalent stiffness k_{eq} (N/cm)	Damper location								
		4% L			6%L			10%L		
		γ	R_{max}		γ	R_{max}		γ	R_{max}	
			Current	Zhou(2005)		Current	Zhou(2005)		Current	Zhou(2005)
9654K53	1.54	0.018	85.6%	98.2%	0.026	94.8%	97.7%	0.046	96.1%	95.6%
9654K812	2.94	0.034	63.5%	96.7%	0.051	90.0%	95.2%	0.086	90.1%	92.1%
9654K115	4.3	0.050	53.8%	95.2%	0.075	87.8%	93.0%	0.126	87.1%	88.8%

Table 4-10 Damping ratio decay rate of experimental results and Zhou's formula with damper size 1463.8 Ns/m

Spring No.	Equivalent stiffness k_{eq} (N/cm)	Damper location								
		4% L			6%L			10%L		
		γ	R_{max}		γ	R_{max}		γ	R_{max}	
			Current	Zhou(2005)		Current	Zhou(2005)		Current	Zhou(2005)
9654K53	1.54	0.018	97.4%	98.2%	0.026	93.8%	97.7%	0.046	100%	95.6%
9654K812	2.94	0.034	92.2%	96.7%	0.051	91.1%	95.2%	0.086	93.5%	92.1%
9654K115	4.3	0.050	91.3%	95.2%	0.075	88.4%	93.0%	0.126	92.7%	88.8%

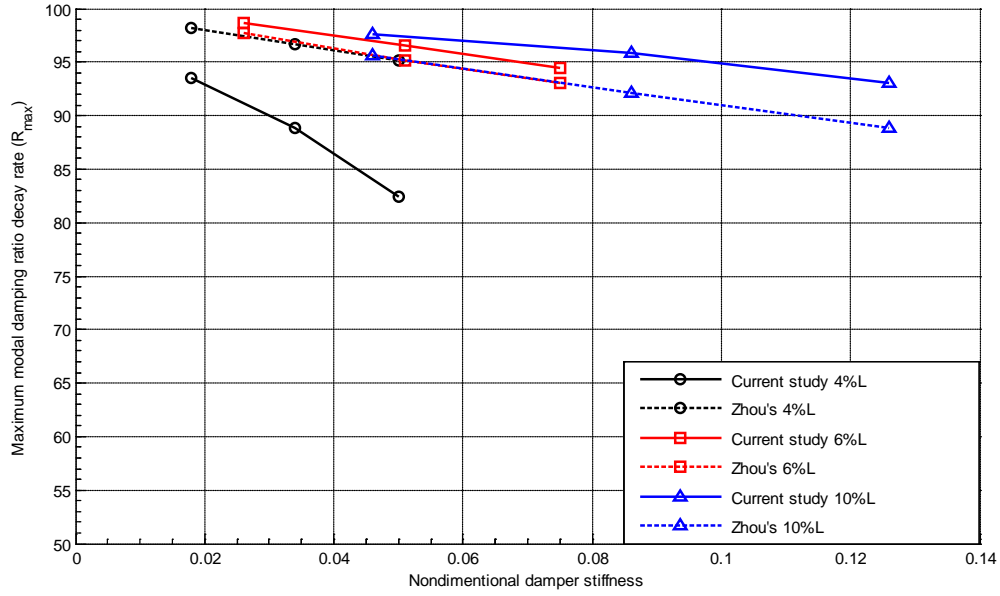


Figure 4-22 Damping ratio decay rate of experimental results and Zhou's formula with damper size 18.4 N·s/m

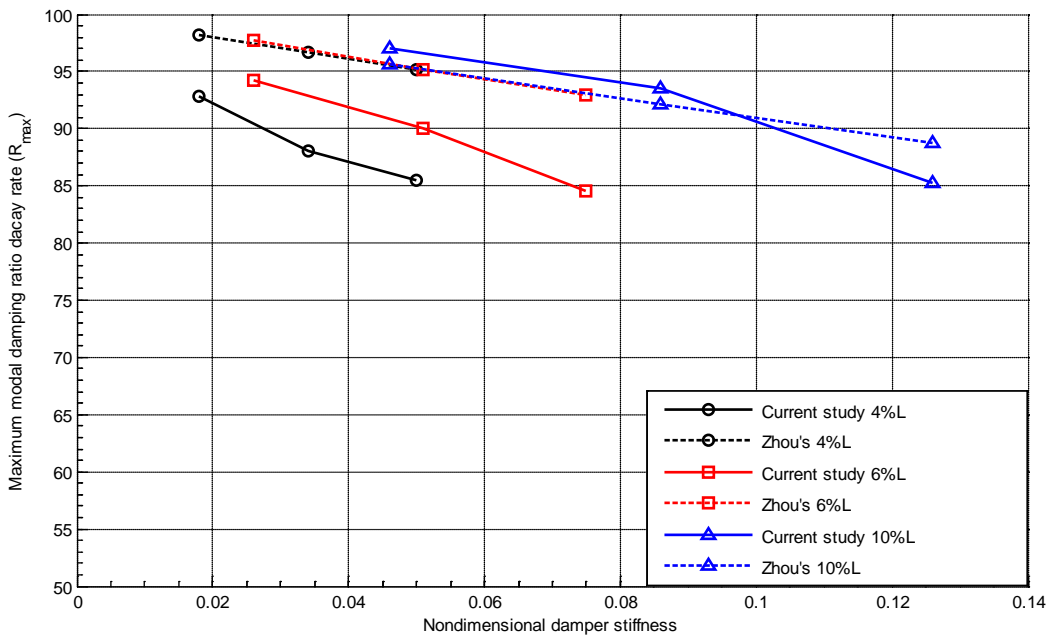


Figure 4-23 Damping ratio decay rate of experimental results and Zhou's formula with damper size 46.7 N·s/m

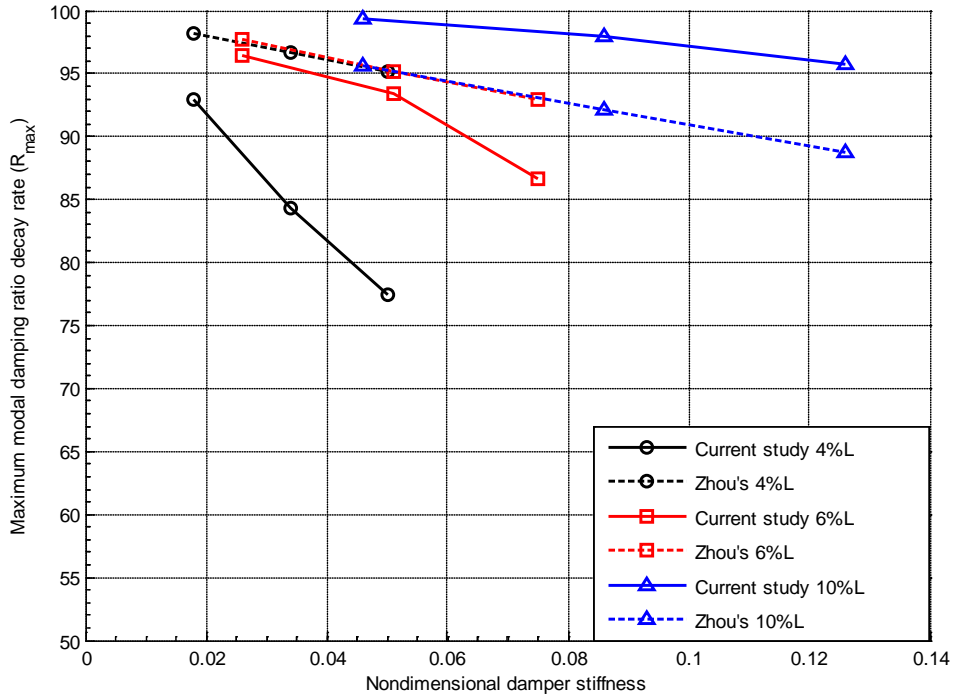


Figure 4-24 Damping ratio decay rate of experimental results and Zhou's formula with damper size 70.3 N·s/m

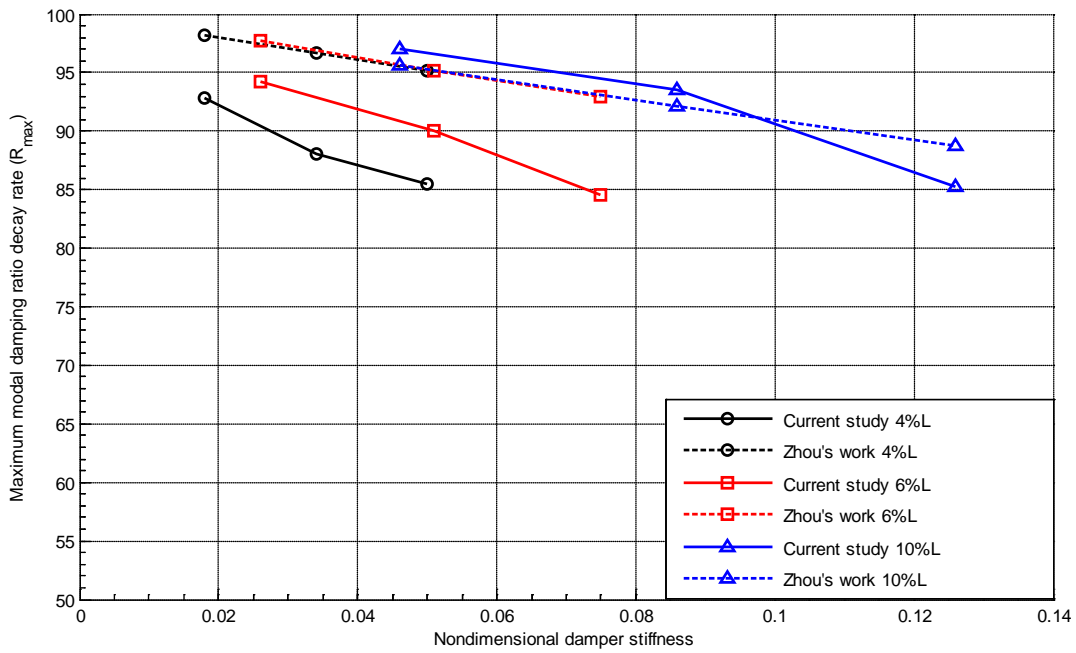


Figure 4-25 Damping ratio decay rate of experimental results and Zhou's formula with damper size 164.8 N·s/m

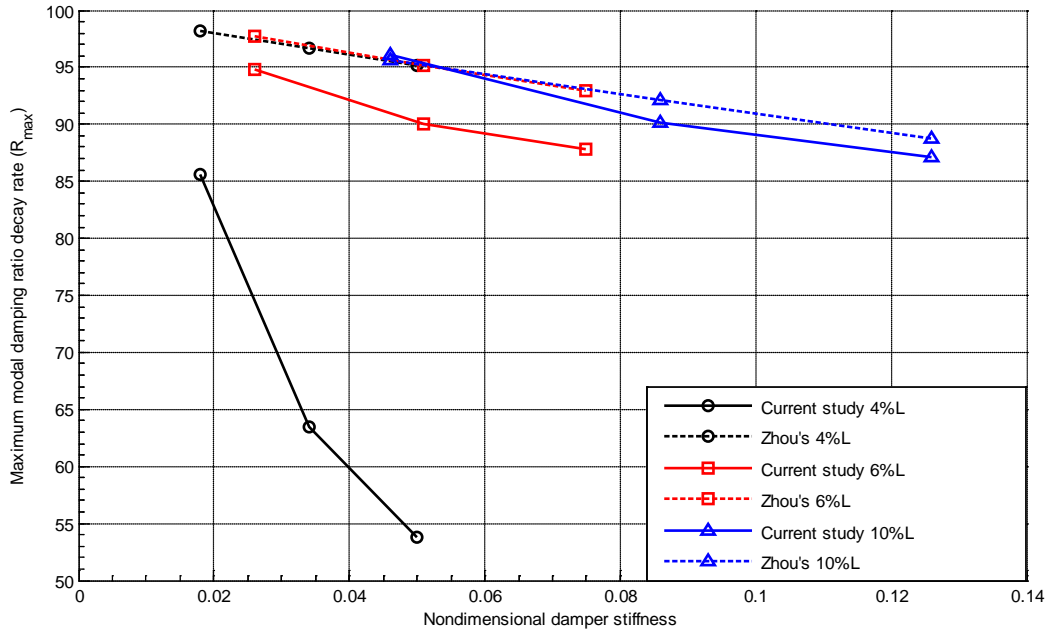


Figure 4-26 Damping ratio decay rate of experimental results and Zhou's formula with damper size 275.5 N·s/m

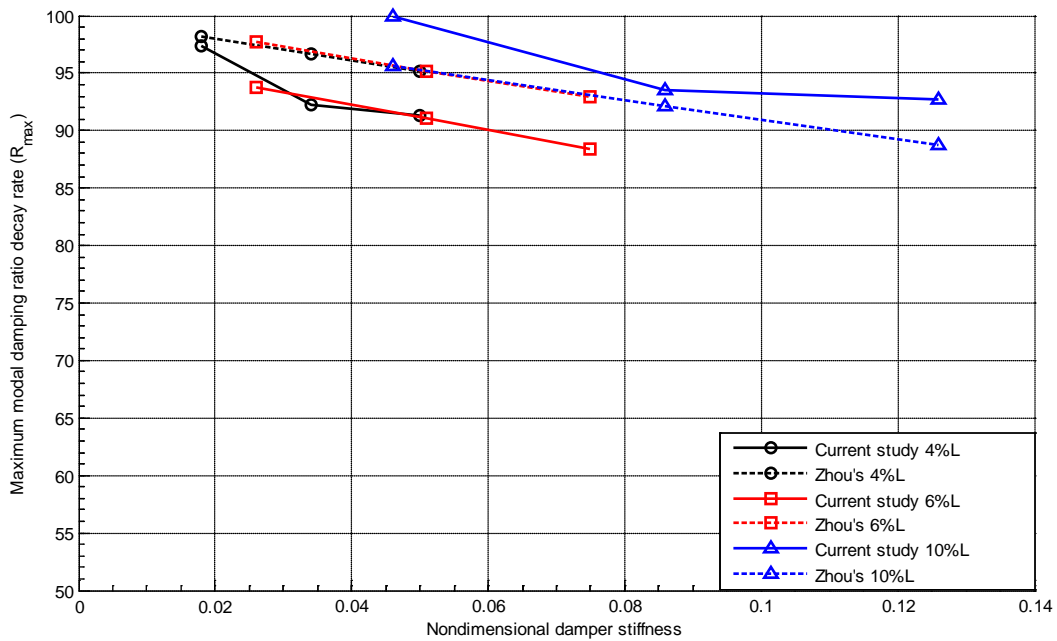


Figure 4-27 Damping ratio decay rate of experimental results and Zhou's formula with damper size 1463.8 N·s/m

Chapter 5 CONCLUSIONS AND RECOMMENDATIONS

5.1 Conclusions for Current Study

In the current research, an experimental study was performed to investigate the effectiveness of a linear viscous oil damper in controlling bridge stay cable vibration. A series of experimental tests have been conducted, which include free vibration tests with and without damper, forced vibration tests with damper considering or not considering damper stiffness. The half-power method was utilized for analyzing all forced vibration tests data. General damper design curves have been proposed based on experimental results. The damper stiffness effect on efficiency of a damper, which is rarely reported in the literature, has been extensively examined in the current study. The main conclusions are summarized as follows:

1. A linear viscous damper which has six adjustable damper sizes have been designed and built.
2. A procedure to preprocess the experimental raw data has been developed. The Butterworth filter was used for filtering the experimental raw data and the Fourier transform theorem was applied to convert acceleration time-history to displacement time-history.
3. Free vibration tests have been performed to study dynamic properties of the model cable and justify the reliability of the model system such as natural frequencies, vibration modes etc.
4. Forced vibration tests have been conducted to produce general damper design curves. Comparisons with the existing literature show that the general pattern of

the proposed damper design curves agreed well with other studies. The existence of the optimum damper size has been confirmed.

5. Damper stiffness effect has been extensively studied. An approximately linear relationship is found to exist between the damper stiffness and the damping ratio. As the damper stiffness increases, damping ratio will decrease. The damping ratio decay rate is highly dependent on the damper installation location.

The main contributions of this study are that general damper design curves based on the experimental study have been developed. To the knowledge of the author, this is the first time that such curves are developed based on pure experimental study. In addition, the damper stiffness effect, which is usually ignored in the past studies, has been investigated in details.

5.2 Recommendations for Future Work

Based on the experience gained from the present study, some recommendations are made below to be considered for future research on this topic:

1. Refinement of damper design could be done since it will justify the difference between previous researches and current study. The friction force generated in a viscous damper will always exist. From the current study, it was observed that friction could stop the damper at small vibration amplitude. The friction is not only generated from the contact between the lid and the stick, but also between the oil and the plate when the plate is intended to start moving from the still position. This non-linear behavior should be considered for future study.

2. Study the effect of damper support stiffness on the damper efficiency. From the current study, it can be seen that as damper moves away from the cable end, a better damping ratio will yield. However, on real bridges, the damper could not reach too far away from the cable end due to size limitation. If it requires installing damper beyond its conventional location, a support will be needed to connect the damper and the bridge deck. The stiffness of the support could also have an impact on the damper efficiency.

Reference

1. Astrolink Xe Data Acquisition and Control Software Operational Manual, Astro-Med Inc.
2. Bosdogianni, A., Olivari, D. (1996). "Wind and Rain Induced Oscillations of Cables of Stayed Bridges", *Journal of Wind Engineering and Industrial Aerodynamics*.
3. Cheng, S. (2010). Lecture of Wind-induced Response of Structures, Wind Engineering.
4. Cheng, S., Darivandi, N., & Ghrib, F. (2010). "The design of an optimal viscous damper for a bridge stay cable using energy-based approach", *Journal of Sound and Vibration*.
5. Cheng, S., Irwin, P. A., Tanaka, H. (2008a). "Experimental study on the wind-induced vibration of a dry inclined cable—Part II: proposed mechanism", *J. Wind Eng. Ind. Aerodyn.*, 96, pp. 2254-2272.
6. Cheng, S., Larose, G. L., Savage, M. G., Tanaka, H., Irwin, P. A. (2008b). "Experimental study on the wind-induced vibration of a dry inclined cable—Part I: Phenomena", *J. Wind Eng. Ind. Aerodyn.* 96, pp. 2231-2253.
7. Cheng, S., Larose, G.L., Savage, M.G., Tanaka, H. (2003). "Aerodynamic behaviour of an inclined circular cylinder", *Wind and Structures*, Vol. 6, No. 3, pp. 197-208..
8. Cheng, S., Tanaka, H. (2005). "Correlation of aerodynamic forces on an inclined circular cylinder", *Wind and Structures an Int. J.* 8(2), pp. 135-146.
9. Cremona, C. (1997). "Courbe Universelle pour le Dimensionnement d, Amortisseurs en Pied de Haubans", *Revue Francaise de Genie Civil* (in German).
10. Davenport, A. (1994). "A Simple Representation of the Dynamics of a Massive Stay Cable in Wind", *Proceedings of the IABSE/FIP International Conference on Cable-Stayed and Suspension Bridges*.
11. Den Hartog, J.P. (1932). "Transmission-line vibration due to sleet", *Quarterly Transactions of the American Institute of Electrical Engineers*.
12. Den Hartog, J.P. (1956). *Mechanical Vibrations (fourth Ed.)*, McGraw-Hill, New York.

13. Elsa, C de Sá. (2007). Structural Engineering Documents - Cable Vibrations in Cable-Stayed Bridges (SED 9), IABSE
14. Flamand, O. (1994). "Rain-Wind Induced Vibration of Cables", *Proceeding of International Conference on Cable-Stayed and Suspension Bridges (AFPC)*.
15. Hikami, Y., Shiraisi, N. (1988). "Rain-Wind Induced Vibrations of Cables in Cable-Stayed Bridges", *Journal of Wind Engineering and Industrial Aerodynamics*.
16. Hoang, N., Fujino, Y. (2007). "Analytical study on bending effects in a stay cable with a damper", *Journal of Engineering Mechanics, ASCE* 133(11), pp. 1241-1246
17. Honda, A., Yamanaka, T., Fujiwara, T., Saito, T. (1995). "Wind tunnel test on rain-induced vibration of the stay cable", *Proceedings of International Symposium on Cable Dynamics, Lie`ge, Belgium*, pp. 255–262.
18. Irvine, H.M., Caughey, T.K. (1974). "The Linear Theory of Free Vibrations of a Suspended Cable", *Proceedings of the Royal Society of London Series A*, Vol. 341, pp.299-315.
19. Irwin, P.A., Nedim, A., Telang, N., (1999). "Wind induced stay cable vibrations—a case study", *Proceeding of the Third International Symposium on Cable Aerodynamics, Trondheim*, pp. 171–176.
20. Jiang, X. (2006). "A New Energy-based Method for Evaluating the Damping Properties of Cable-Damper Systems".
21. Jung, H., Spencer, B., and Lee, I. (2005). "Benchmark Control Problem of a Seismically Excited Cable-Stayed Bridge Using MR Dampers".
22. Kleissl, K. (2009). "Master Thesis of Vibration Control of Bridge cables", Technical University of Denmark.
23. Kovács, I. (1982). "Zur Frage der Seilschwingungen und der Seidämpfung (In German)".
24. Krenk, S. (2000). "Vibrations of a Taut Cable with an External Damper", *Transactions of the ASME*.
25. Krenk, S., Hogsberg, J. (2005). "Damping of Cables by a Transverse Force", *Journal of Engineering Mechanics*.

26. Kumarasena, S., Jones, N.P., Irwin, P., Taylor, P. (2007). "Wind-induced Vibration of Stay Cables".
27. Lopez, I., Busturia, J.M. and Nijmeijer, H. (2004). "Energy dissipation of a friction damper", *Journal of Sound and Vibration*, pp. 539-561.
28. Matsumoto, M., Ishizki, H., Kitazawa, M., Aoki, J., Fujii, D. (1995). "Cable Aerodynamics and its Stabilization", *Proceeding of the International Symposium on Cable Dynamics*, Liege, Belgium.
29. Matsumoto, M., Yamagishi, M., Aoki, J., Shiraishi, N. (1995). "Various Mechanism of Inclined Cable Aerodynamics", Ninth International Conference on Wind Engineering.
30. Miyata, T., Yamada, H., Hojo, T. (1994). "Aerodynamic response of PE stay cables with pattern-indented surface", *Proceedings of International Conference on Cable-Stayed and Suspension Bridges (AFPC)*, Deauville, France, Vol. 2, pp. 515–522.
31. Pacheco, B. M., Fujino, Y., & Sulkh, A. (1993). "Estimation curve for modal damping in stay cable with viscous damper for modal damping in stay cables", *ASCE Journal of Structure Engineering*.
32. PTI Guide Specification. (2000) "Recommendations for stay cable design, Testing and Installation"; PTI, USA.
33. Saito, T., Matsumoto, M., Kitazawa, M. (1994). "Rain-wind excitation of cables of cable-stayed Higashi-Kobe Bridge and cable vibration control", *Proceedings of International Conference on Cable-Stayed and Suspension Bridges (AFPC)*, Deauville, France, 2, pp. 507–514.
34. Simiu, E., Robert H. (1986). *Wind Effects on Structures*, 2nd edition, John Wiley & Sons.
35. Simiu, E., Scanlan, R. (1996). *Wind Effects on Structures: Fundamentals and Applications to Design*, 3rd Edition, John Wiley & Sons, ISBN 0-471-12157-6.
36. Sulekh, A., Pacheco, B. M. (1990). "Non-dimensional curves for modal damping in stay cables with viscous dampers", MS thesis, Dept. of Civil Eng., University of Tokyo, Tokyo, Japan.

37. Sun, L., Huang, H., & Liang, D. (2010). "Studies on Effecting Factors of Damper Efficiency for Long Stay Cables".
38. Tabatabai, H., Mehrabi, A. (2000). "Evaluation of Various Damping Treatments for Stay Cables", Proceedings of the International Modal Analysis Conference – IMAC.
39. Tanaka, H. (2003). "Aerodynamics of Cables", in Fifth International Symposium on Cable Dynamics.
40. Uno, K., Kitagawa, S., Tsutsumi, H., Inoue, A., Nakaya, S. (1991). "A Simple Method of Designing Cable Vibration Dampers of Cable-stayed Bridges", *Journal of Structural Engineering*.
41. Verwiebe, C. (1998). "Rain-Wind-Induced Vibrations of Cables and Bars", *Bridge Aerodynamics*.
42. Virlogeux, M. (1998). "Cable vibrations in cable-stayed bridges", *Bridge Aerodynamics*, Balkema, pp. 213–233.
43. VSL. (2008). SSI 2000 Stay cables system
44. Wagner, P., Fuzier, J-P. (2003). "Health Monitoring of Structures with Cables-Which Solutions. Dissemination of the Results of the IMAC European Project" in Fifth International Symposium on Cable Dynamics, "Tutorial on Health Monitoring of Structures with Cables".
45. Wikipedia.org, http://en.wikipedia.org/wiki/Butterworth_filter#A_simple_example.
46. Xu, Y.L., Zhan, S., Ko, J.M., Yu, Z. (1999). "Experimental study of vibration mitigation of bridge stay cables", *Journal of structural engineering*, Vol. 125, No. 9, pp. 977-986.
47. Yamaguchi, H. (1995). "Control of Cable Vibrations with Secondary Cables", Proceedings International Symposium on Cable Dynamics.
48. Yamaguchi, H., Fujino, Y. (1998) "Stayed cable dynamics and its vibration control", *Bridge Aerodynamics*. 235-253.
49. Yoneda, M., Maeda, K. (1989). "A Study on Practical Estimation Method for Structural Damping of Stay Cable with Damper", *Canada-Japan Workshop on Bridge Aerodynamics*.
50. Zhou, H., (2005). "Analytical and Experimental Studies on Vibration Control of Stay

Appendix A Damper Properties

With Oil #1 calibration results are shown below:

Plate #1 first calibration:

Mass (kg)	Force(N)	velocity (volts/s)	Velocity(m/s)
0	0	0	0
0.04281	0.4199661	0.36282	0.00091
0.04281	0.4199661	0.340306	0.00085
0.09281	0.9104661	1.86334	0.00466
0.09281	0.9104661	1.82184	0.00455
0.14281	1.4009661	3.18011	0.00795
0.14281	1.4009661	3.20155	0.00800
0.19281	1.8914661	4.33894	0.01085
0.19281	1.8914661	4.5418	0.01135
0.24281	2.3819661	5.48554	0.01371
0.24281	2.3819661	5.52327	0.01381
0.34281	3.3629661	7.68069	0.01920
0.34281	3.3629661	7.71736	0.01929

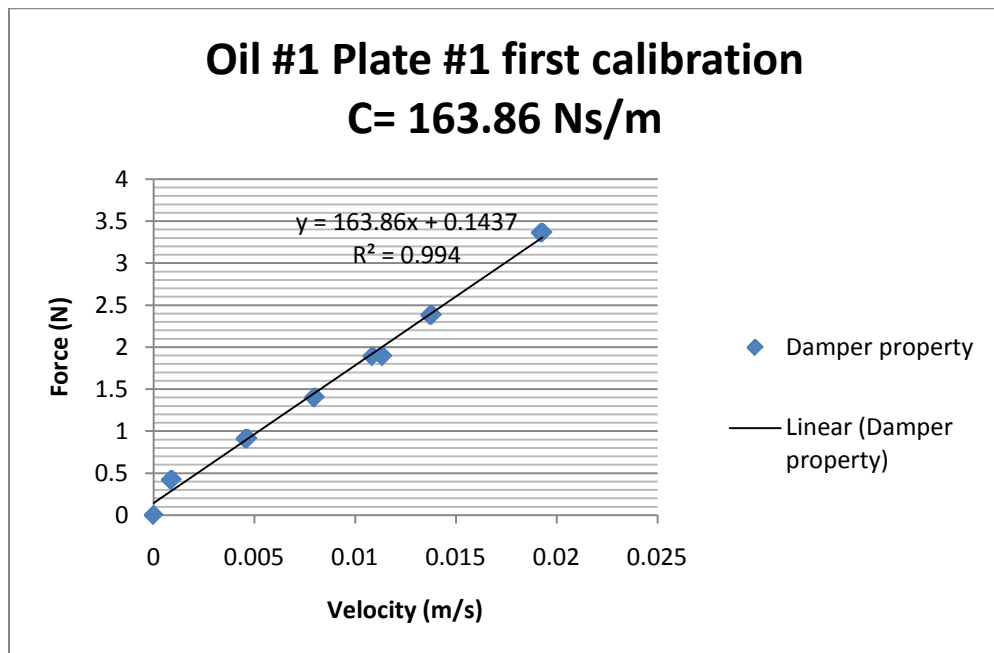
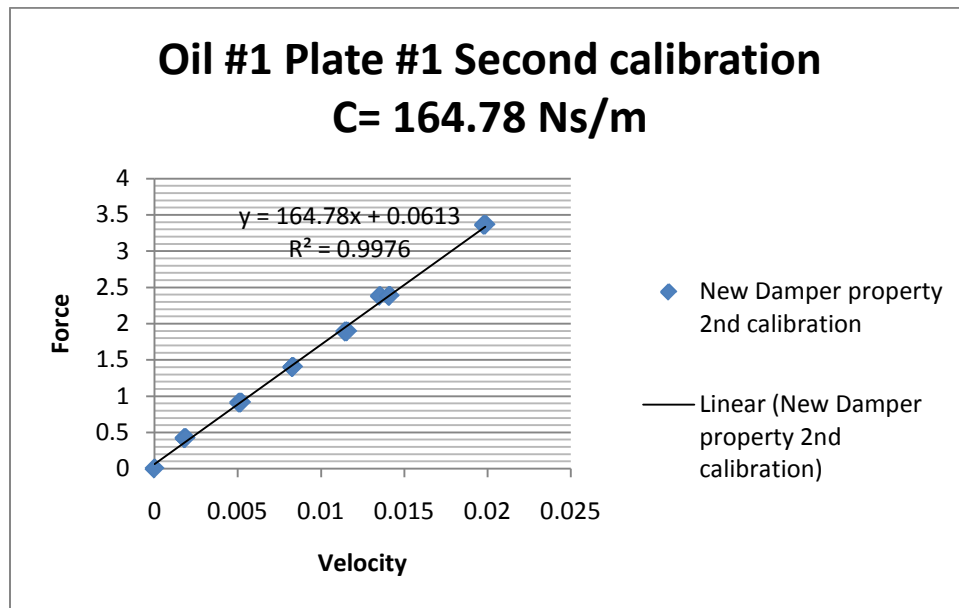


Plate #1 Second Calibration:

Mass (kg)	Force(N)	velocity (volts/s)	Velocity(m/s)
0	0	0	0
0.04281	0.4199661	0.725	0.00181
0.04281	0.4199661	0.72	0.00180
0.04281	0.4199661	0.747	0.00187
0.09281	0.9104661	2.03	0.00508
0.09281	0.9104661	2.06	0.00515
0.09281	0.9104661	2.08	0.00520
0.14281	1.4009661	3.31	0.00828
0.14281	1.4009661	3.33	0.00833
0.14281	1.4009661	3.31	0.00828
0.19281	1.8914661	4.63	0.01158
0.19281	1.8914661	4.59	0.01148
0.19281	1.8914661	4.58	0.01145
0.24281	2.3819661	5.41	0.01353
0.24281	2.3819661	5.65	0.01413
0.24281	2.3819661	5.63	0.01408
0.34281	3.3629661	7.95	0.01988
0.34281	3.3629661	7.91	0.01978



Average of two calibration C= 164.3 N·s/m

Plate #2 Calibration:

Mass (kg)	Force(N)	velocity (volts/s)	Velocity(m/s)
0	0	0	0
0.04163	0.4083903	3.69	0.00923
0.04163	0.4083903	3.69	0.00923
0.09163	0.8988903	9.35	0.02338
0.09163	0.8988903	9.36	0.02340
0.14163	1.3893903	13.78	0.03445
0.14163	1.3893903	13.45	0.03363
0.19163	1.8798903	17.41	0.04353
0.19163	1.8798903	16.49	0.04123
0.24163	2.3703903	19.42	0.04855
0.24163	2.3703903	20.33	0.05083

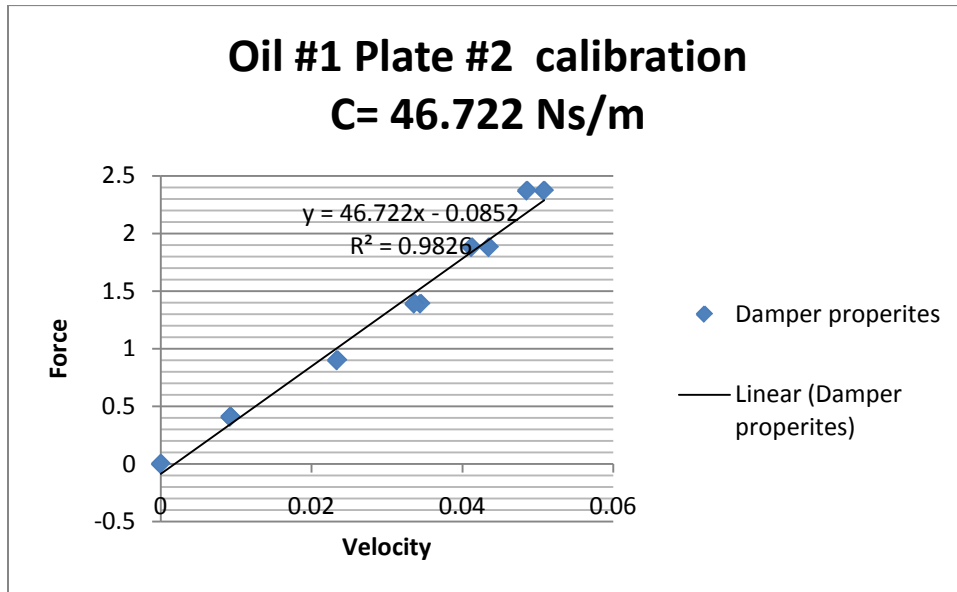
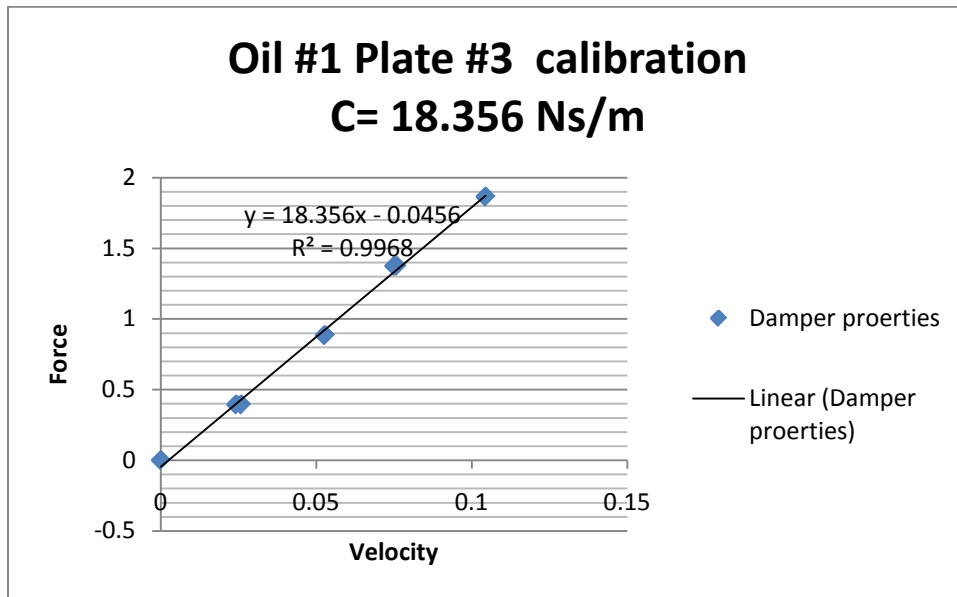


Plate #3 Calibration:

Mass (kg)	Force(N)	velocity (volts/s)	Velocity(m/s)
0	0	0	0
0.04023	0.3946563	10.34	0.02585
0.04023	0.3946563	9.69	0.02423
0.09023	0.8851563	21.09	0.05273
0.09023	0.8851563	21.09	0.05273
0.14023	1.3756563	30.33	0.07583
0.14023	1.3756563	30.03	0.07508
0.19023	1.8661563	41.78	0.10445
0.19023	1.8661563	36.77	0.09193
0.24023	2.3566563	42.72	0.10680



With Oil #2 calibration results are shown below:

Plate #1 calibration:

Mass (kg)	Force(N)	velocity (volts/s)	Velocity(m/s)
0	0	0	0
0.04281	0.4199661	0.0529171	0.00013
0.04281	0.4199661	0.0536366	0.00013
0.09281	0.9104661	0.1873	0.00047
0.09281	0.9104661	0.181515	0.00045
0.14281	1.4009661	0.341727	0.00085
0.14281	1.4009661	0.338904	0.00085
0.19281	1.8914661	0.51657	0.00129
0.19281	1.8914661	0.504878	0.00126
0.24281	2.3819661	0.59101	0.00148
0.24281	2.3819661	0.589863	0.00147
0.29281	2.8724661	0.726229	0.00182
0.29281	2.8724661	0.741984	0.00185
0.34281	3.3629661	0.873696	0.00218
0.34281	3.3629661	0.874107	0.00219

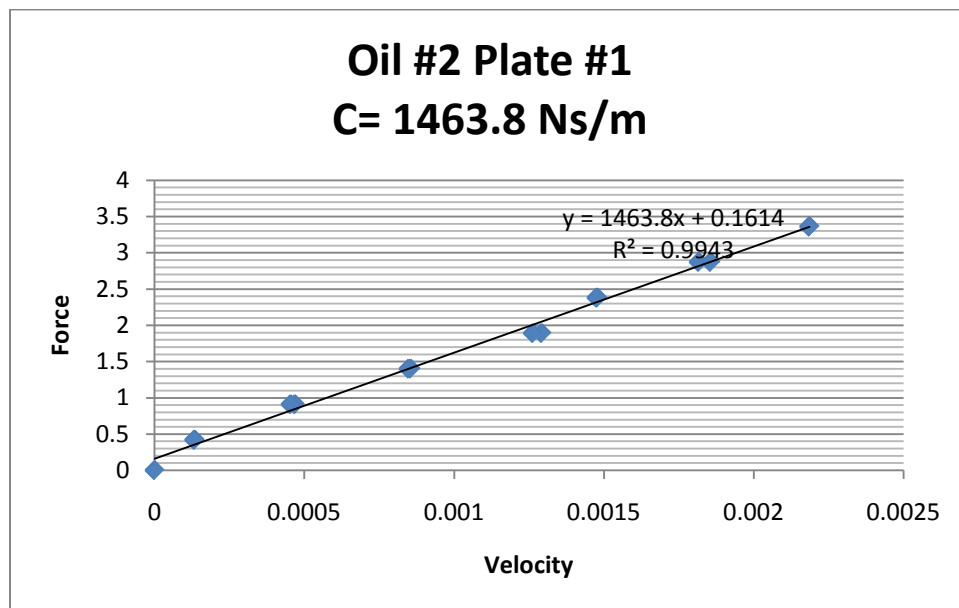


Plate #2 calibration:

Mass (kg)	Force(N)	velocity (volts/s)	Velocity(m/s)
0	0		0
0.04163	0.4083903	0.447455	0.00112
0.04163	0.4083903	0.422917	0.00106
0.09163	0.8988903	1.22646	0.00307
0.09163	0.8988903	1.22476	0.00306
0.14163	1.3893903	1.95663	0.00489
0.14163	1.3893903	1.99883	0.00500
0.19163	1.8798903	2.76645	0.00692
0.19163	1.8798903	2.759	0.00690
0.24163	2.3703903	3.3376	0.00834
0.24163	2.3703903	3.31824	0.00830
0.29163	2.8608903	4.1325	0.01033
0.29163	2.8608903	4.1925	0.01048
0.34163	3.3513903	4.67651	0.01169
0.34163	3.3513903	4.71936	0.01180

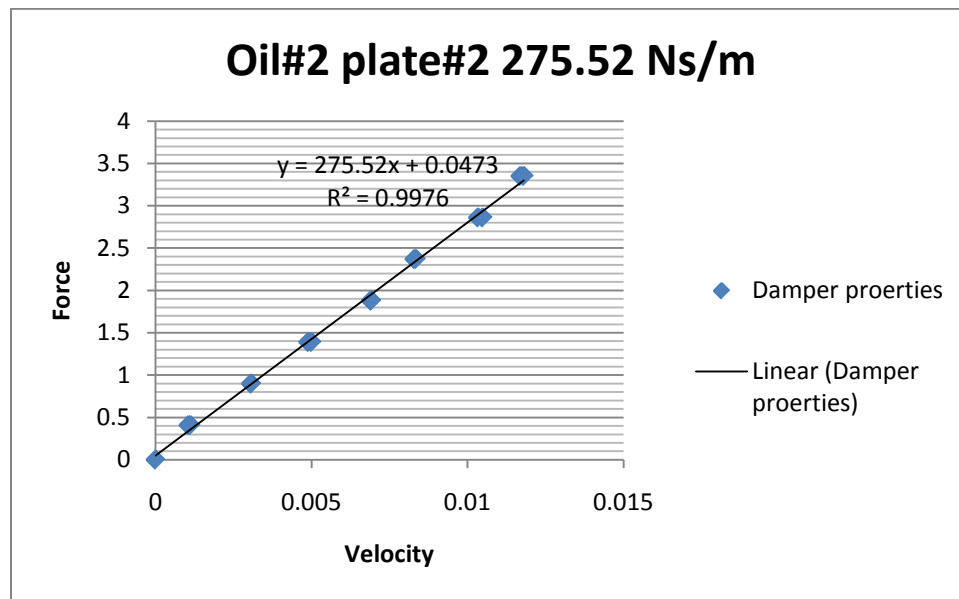
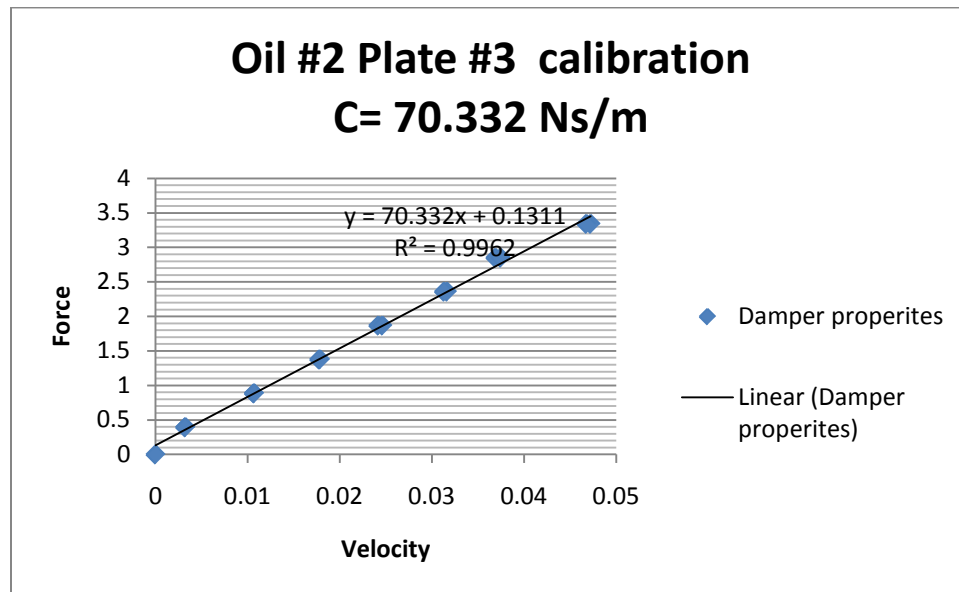


Plate #3 calibration:

Mass (kg)	Force(N)	velocity (volts/s)	Velocity(m/s)
0	0		0
0.04023	0.3946563	1.29429	0.00324
0.04023	0.3946563	1.28662	0.00322
0.09023	0.8851563	4.28083	0.01070
0.09023	0.8851563	4.2681	0.01067
0.14023	1.3756563	7.14481	0.01786
0.14023	1.3756563	7.1028	0.01776
0.19023	1.8661563	9.67055	0.02418
0.19023	1.8661563	9.85063	0.02463
0.24023	2.3566563	12.6537	0.03163
0.24023	2.3566563	12.522	0.03131
0.29023	2.8471563	14.754	0.03689
0.29023	2.8471563	14.9834	0.03746
0.34023	3.3376563	18.8875	0.04722
0.34023	3.3376563	18.7	0.04675



Appendix B Matlab code for data processing

Filter design

It could be set up in filter design and analysis tool by type in “fdatool” or by follow code

```
function Hd = filter %FILTER Returns a discrete-time filter object
```

```
% M-File generated for filtering instead of filter design and analysis tool
```

```
% Butterworth Bandpass filter designed using FDESIGN.BANDPASS.
```

```
% All frequency values are in Hz.
```

```
Fs = 1000; % Sampling Frequency is 1000 Hz
```

```
N = 2; % Order
```

```
% Fc1 and Fc2 need to change case by case. I normally set Fc1 as natural frequency + 0.6  
Hz and Fc2 as natural frequency – 0.6 Hz.
```

```
Fc1 = 4; % First Cutoff Frequency
```

```
Fc2 = 5.5; % Second Cutoff Frequency
```

```
% Construct an FDESIGN object and call its BUTTER method.
```

```
h = fdesign.bandpass('N,Fc1,Fc2', N, Fc1, Fc2, Fs);
```

```
Hd = butter(h);
```

```
% End of program and please look at workspace and filter object “Hd” was generated.
```

Natural frequency analysis

```
pwelch(b,[],[],2048,1000,'one sided') % find out fundamental frequency
```

```
%pwelch is defined as the best power spectrum analysis tool in Matlab, and Psd is no  
longer recommended.
```

Transfer from acceleration data to displacement data (Fourier transform)

```
%Signal processing using Fourier Transform(Time domain to Frequency domain)
a=b*100.513 % convert data units to m/s^2, 100.513 is conversion factor which
calibrated in advance.

Af = filter(Hd,a) % apply designed filter "Hd" generated from previous code.

F = fft (Af) %convert all filtered data set from time domain to frequency domain by
fourier transform

Df = F/(2*pi*7.30)^2 % convert acceleration to displacement, 7.30 is the fundamental
frequency

D=ifft (Df)*100 % convert displacement data from frequency to time domain by inverse
fourier transform; and 100 is convert meter to CM

T=0:1/1000:length(Af)/1000-1/1000 % Create time increment

plot(T,D)

xlabel('Time(Second)')

ylabel('Displacement(cm)')

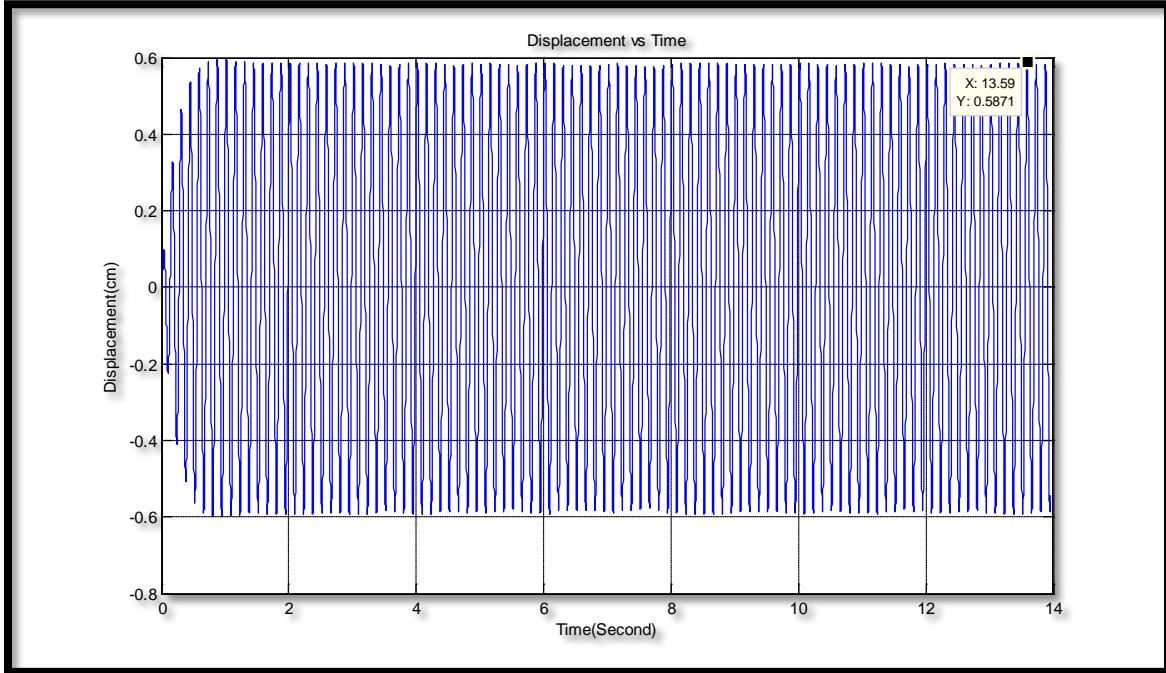
title('Displacement vs Time')

grid on
```

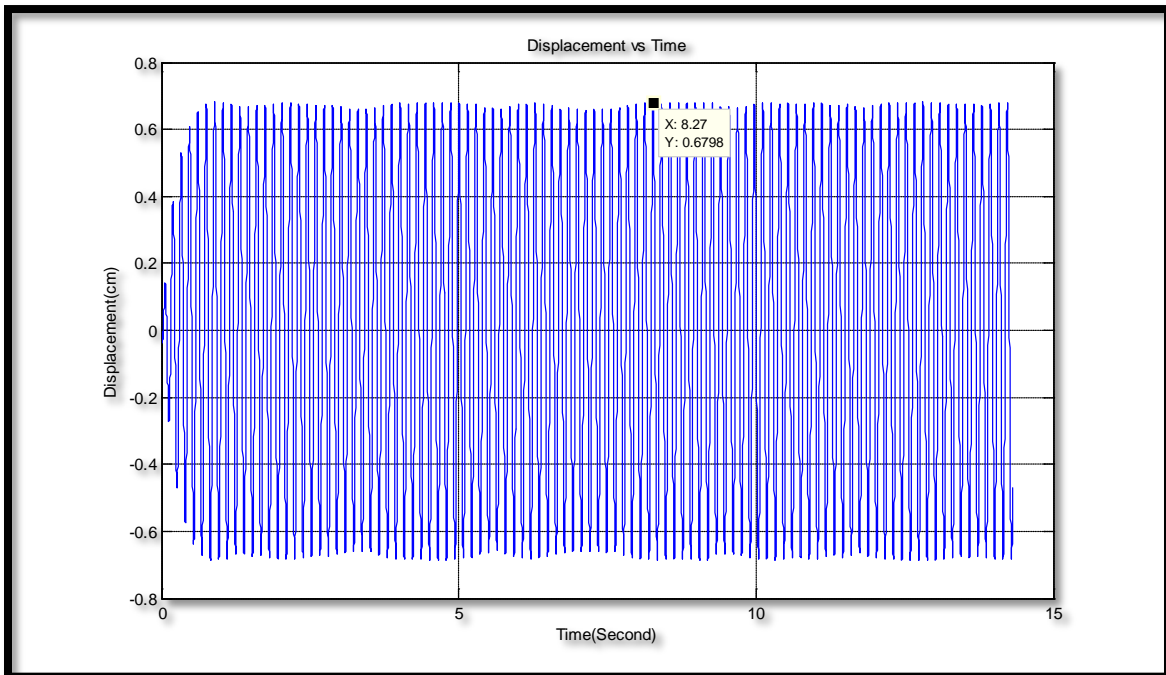
Appendix C filtered and converted data

3200_20500_S05_D06_A50 without spring

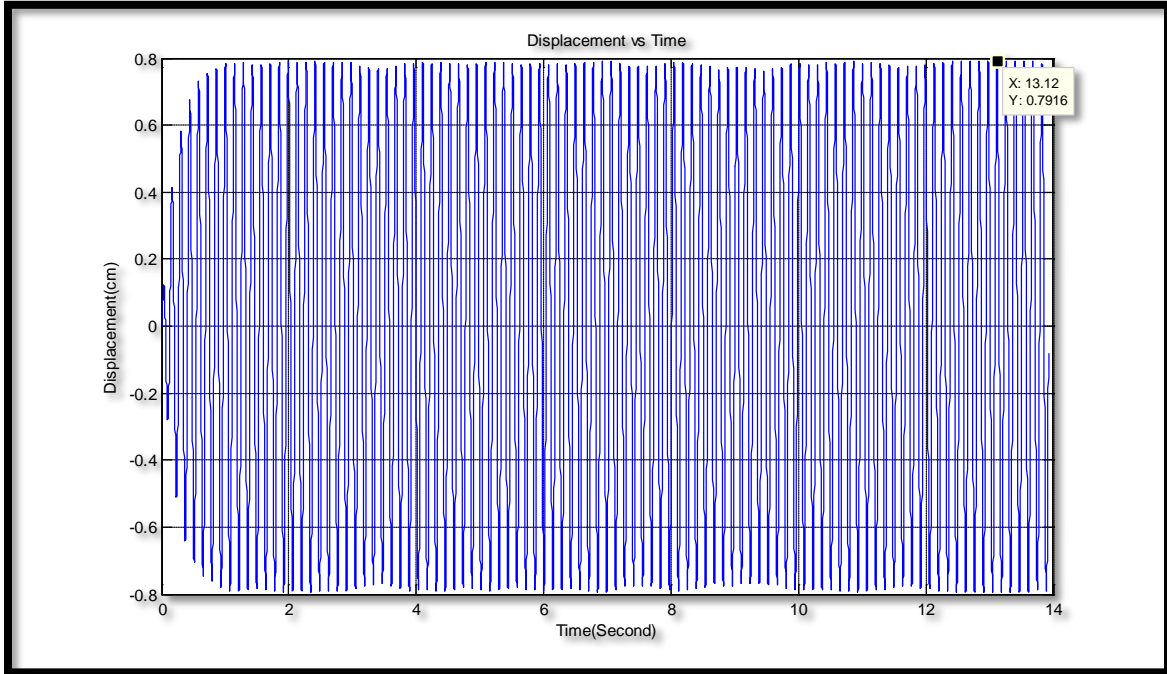
B_3200_20050_S05_D06_A50_7.00 Hz



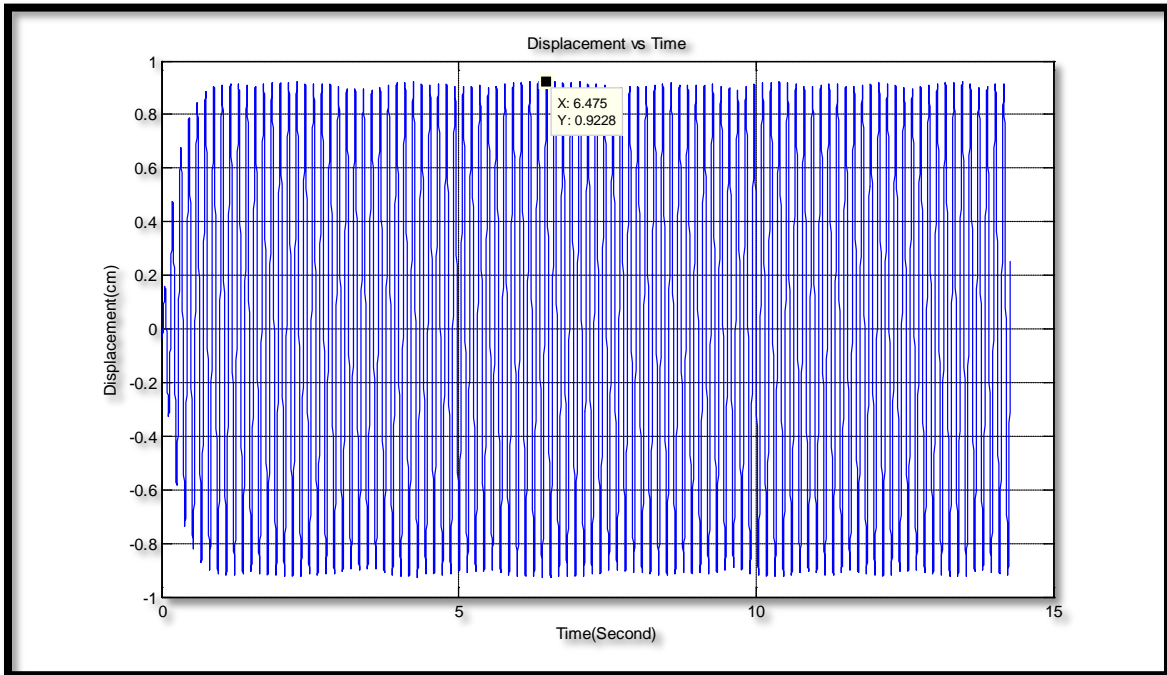
B_3200_20050_S05_D06_A50_7.05 Hz



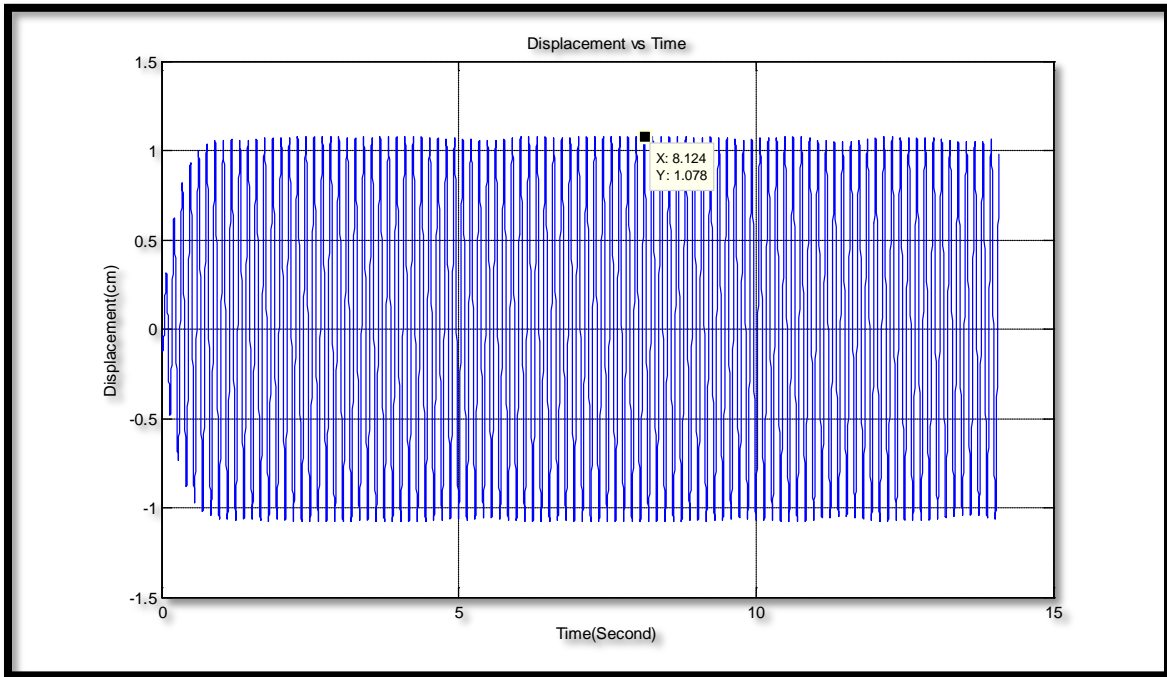
B_3200_20050_S05_D06_A50_7.10 Hz



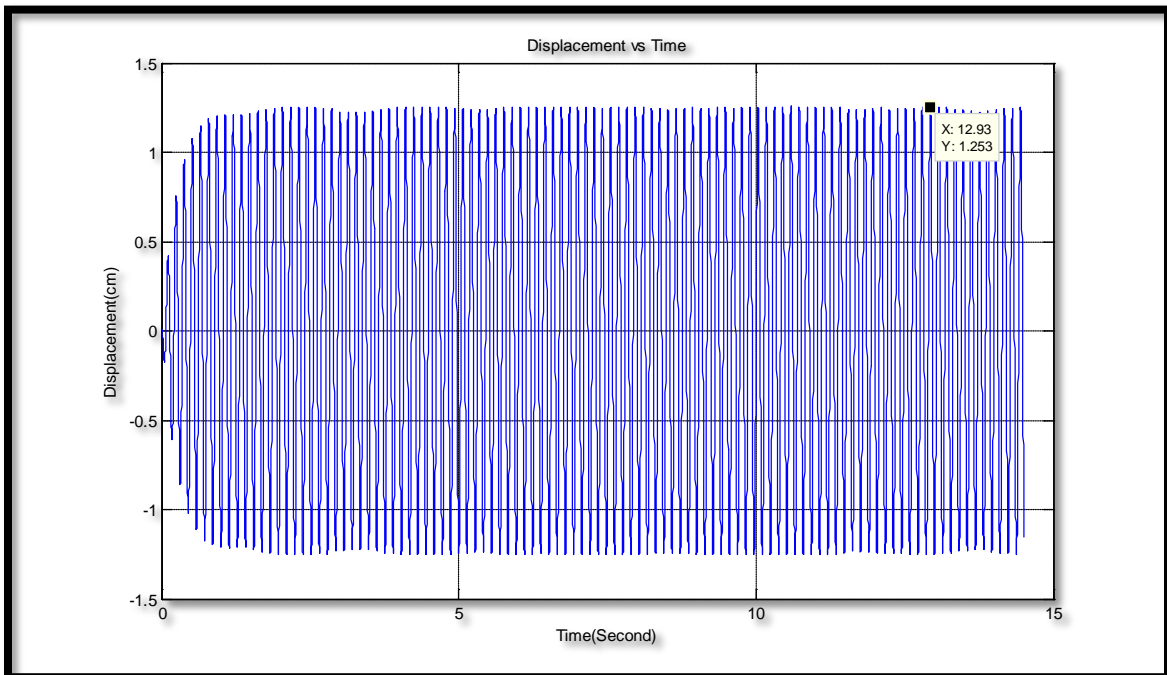
B_3200_20050_S05_D06_A50_7.15 Hz



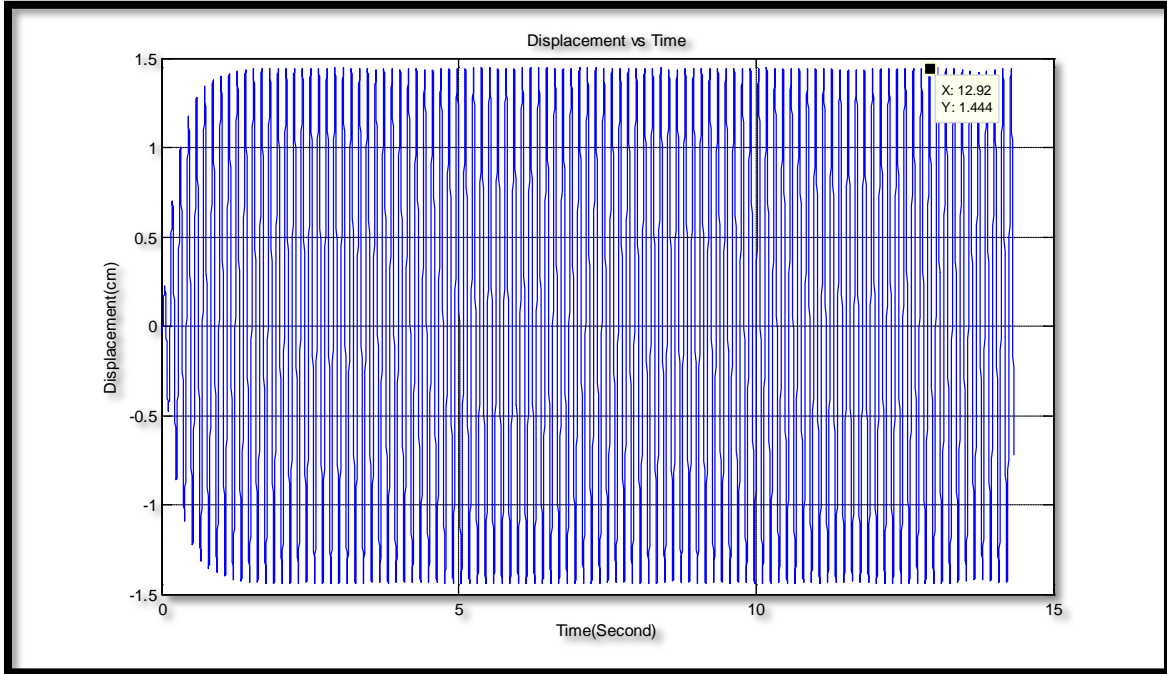
B_3200_20050_S05_D06_A50_7.20 Hz



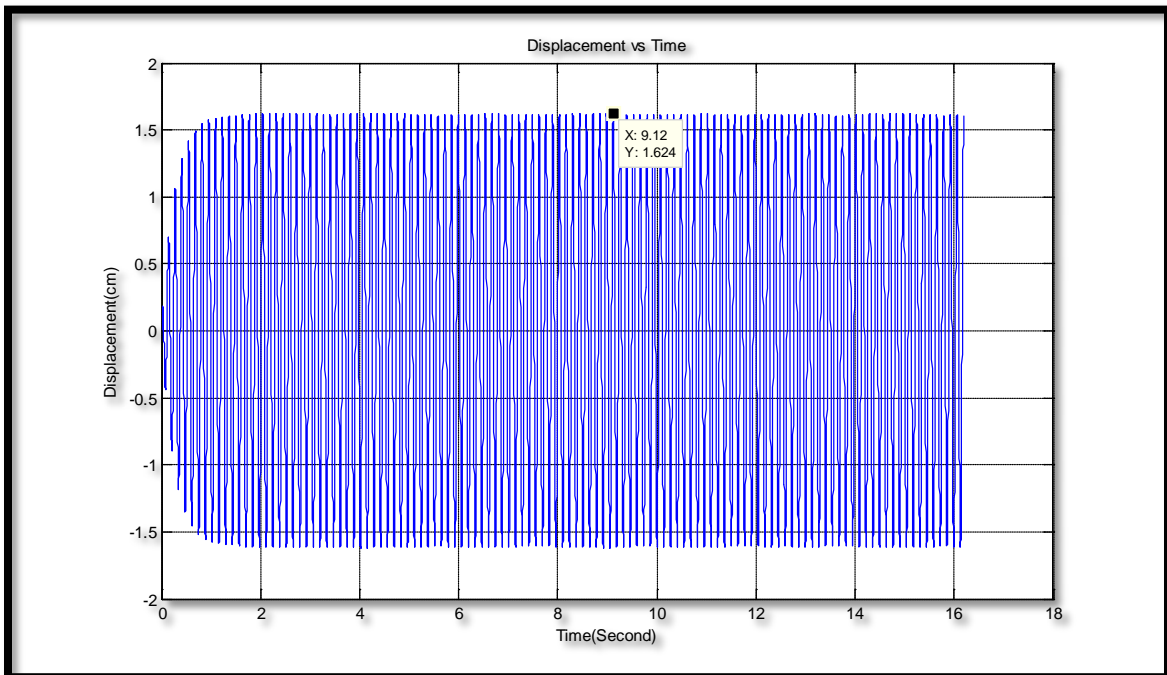
B_3200_20050_S05_D06_A50_7.25 Hz



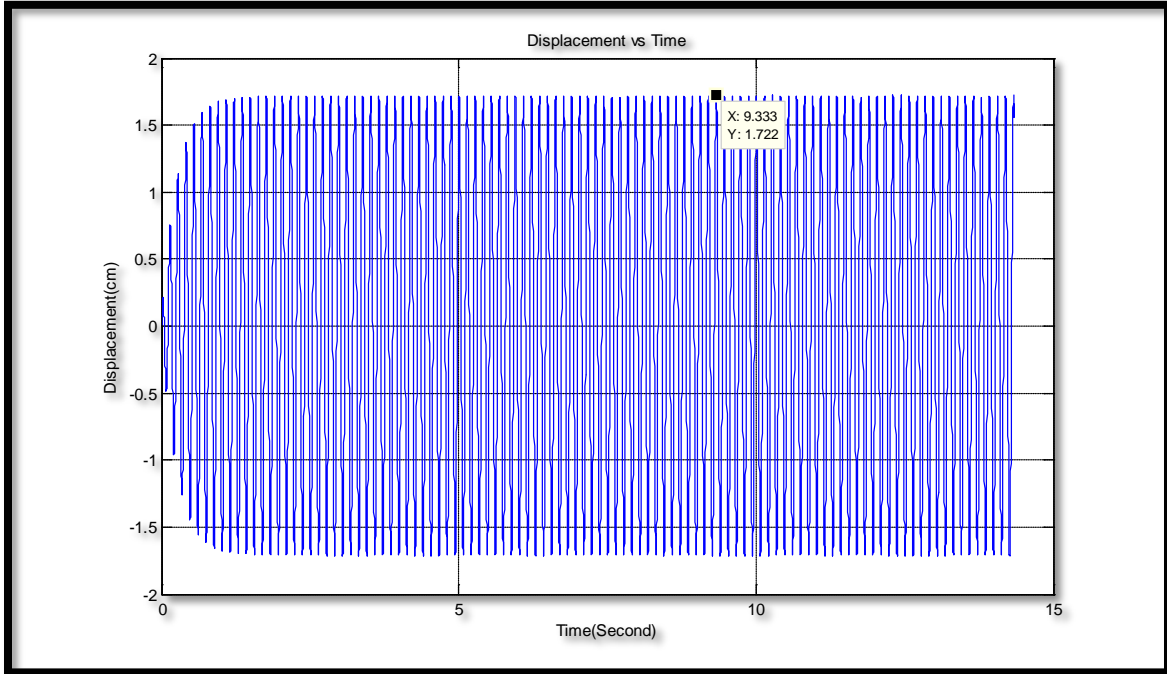
B_3200_20050_S05_D06_A50_7.30 Hz



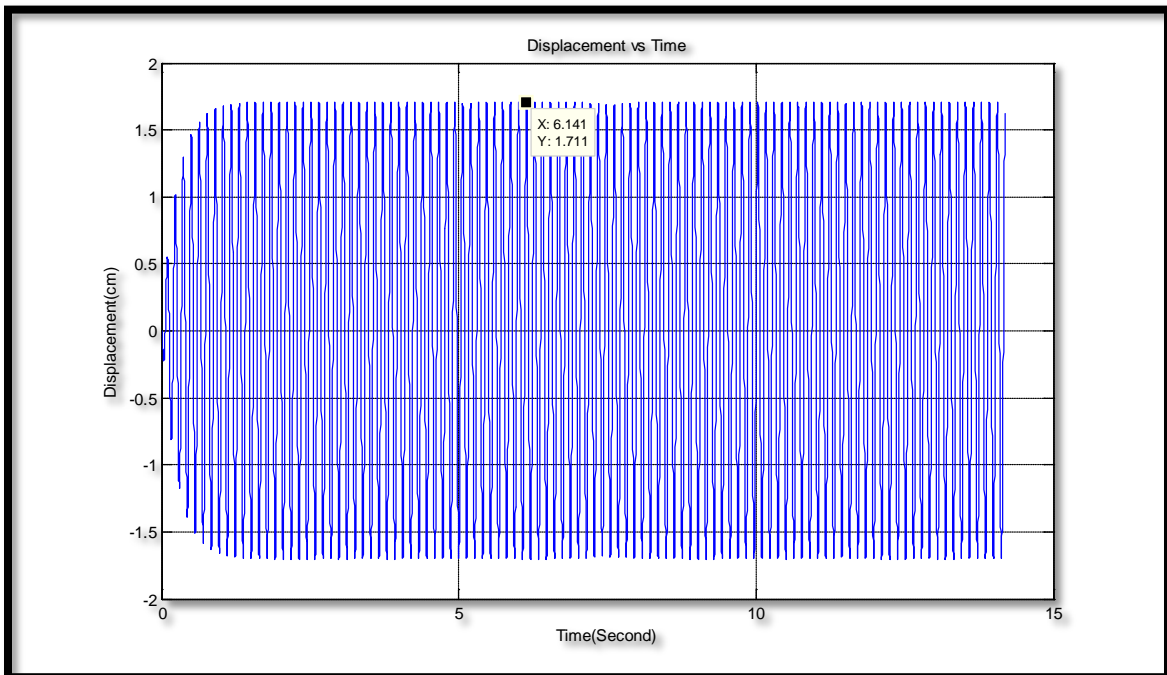
B_3200_20050_S05_D06_A50_7.35 Hz



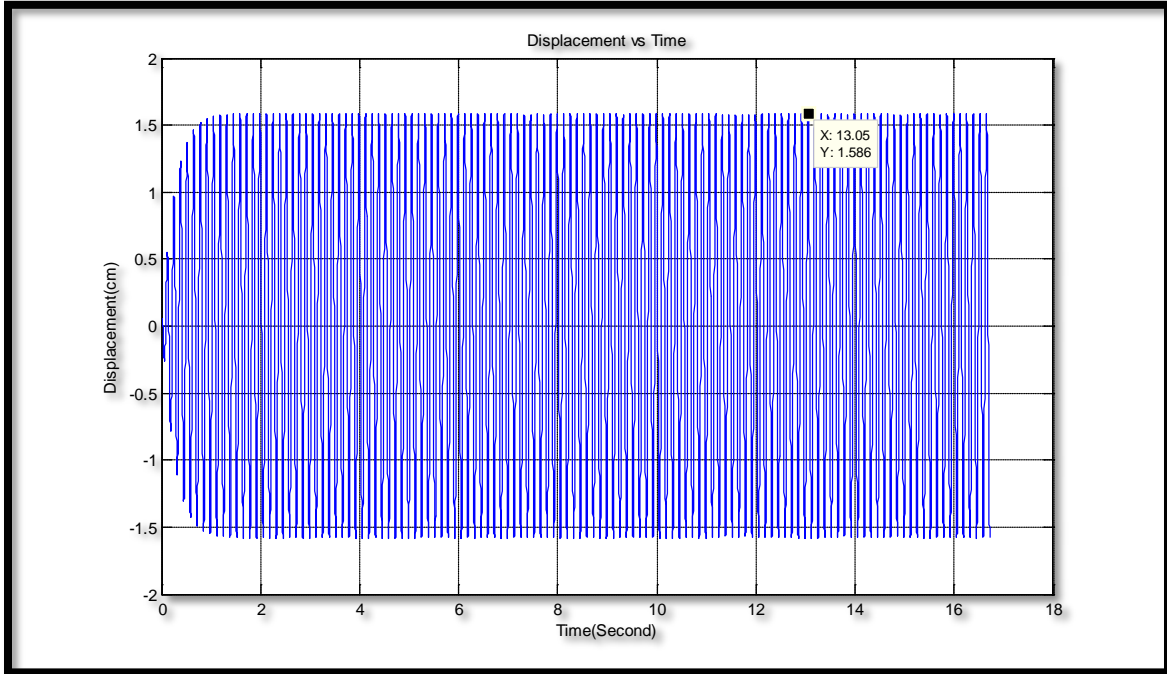
B_3200_20050_S05_D06_A50_7.40 Hz



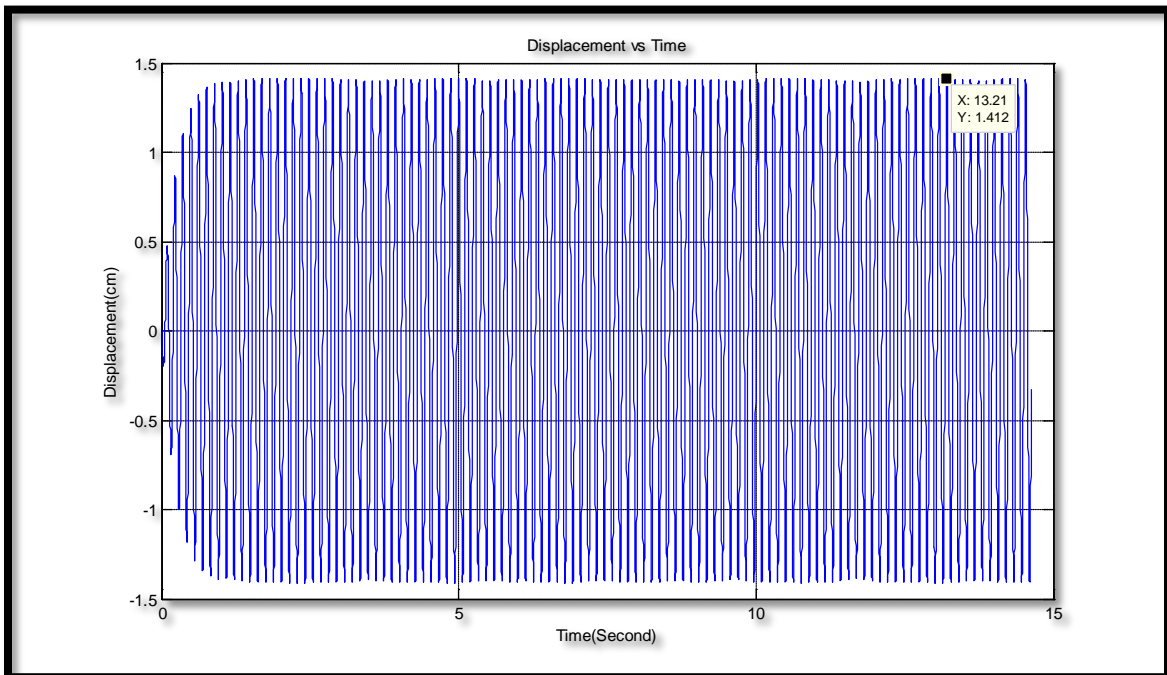
B_3200_20050_S05_D06_A50_7.45 Hz



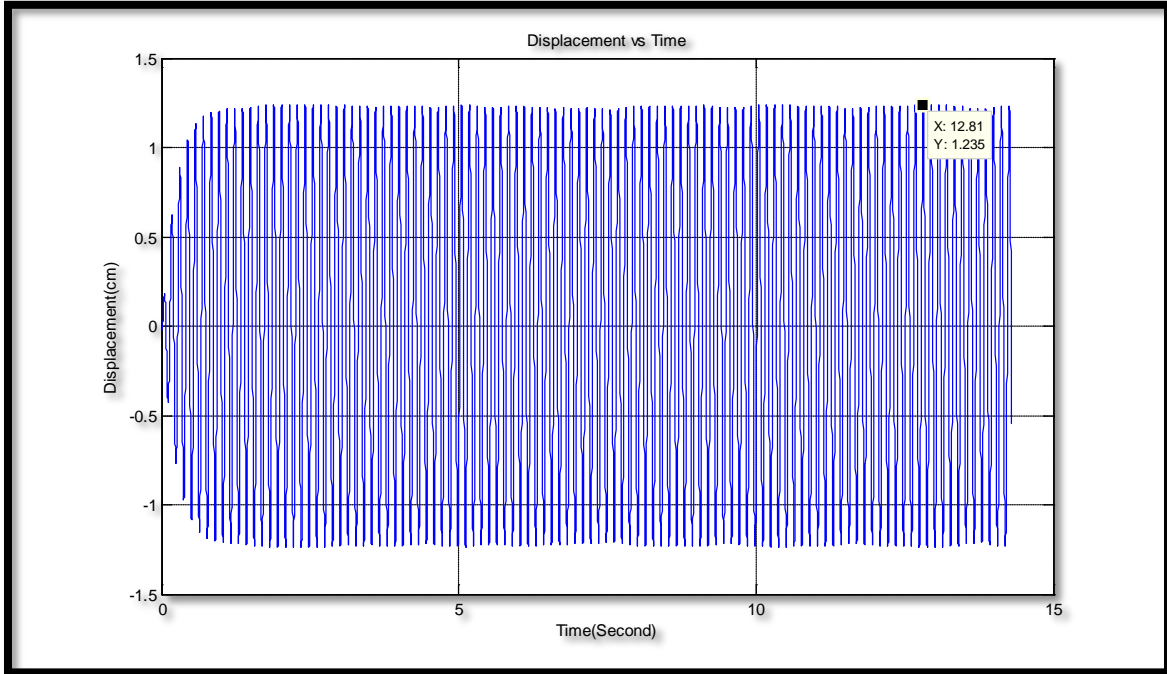
B_3200_20050_S05_D06_A50_7.50 Hz



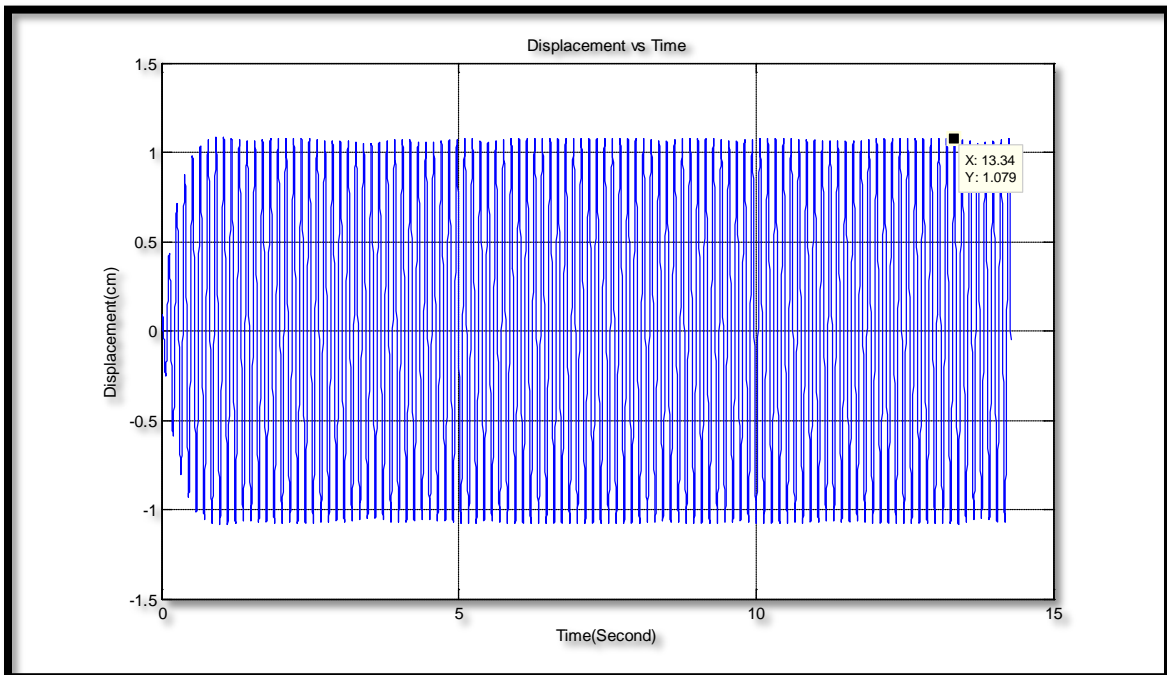
B_3200_20050_S05_D06_A50_7.55 Hz



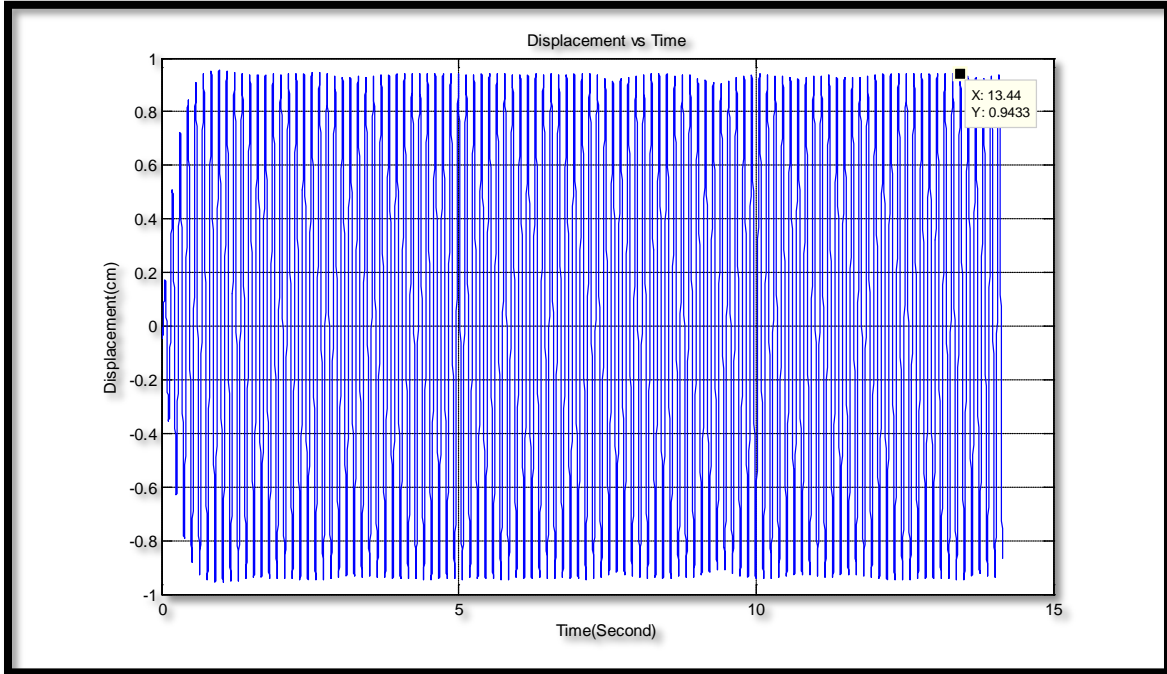
B_3200_20050_S05_D06_A50_7.60 Hz



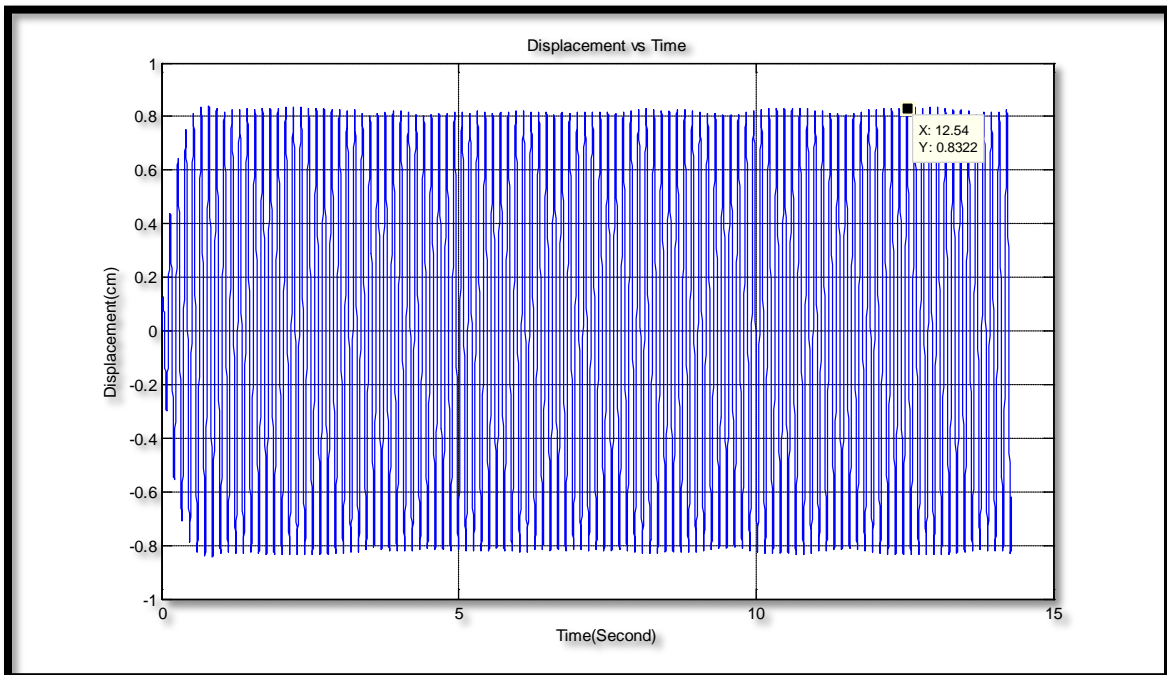
B_3200_20050_S05_D06_A50_7.65 Hz



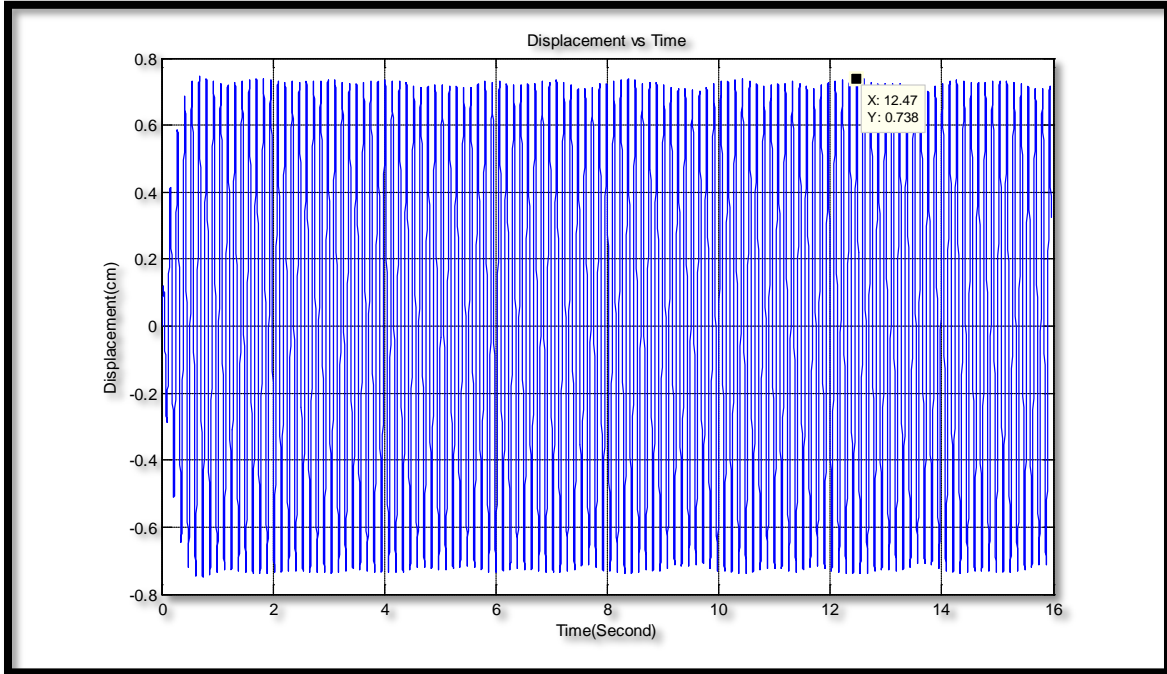
B_3200_20050_S05_D06_A50_7.70 Hz



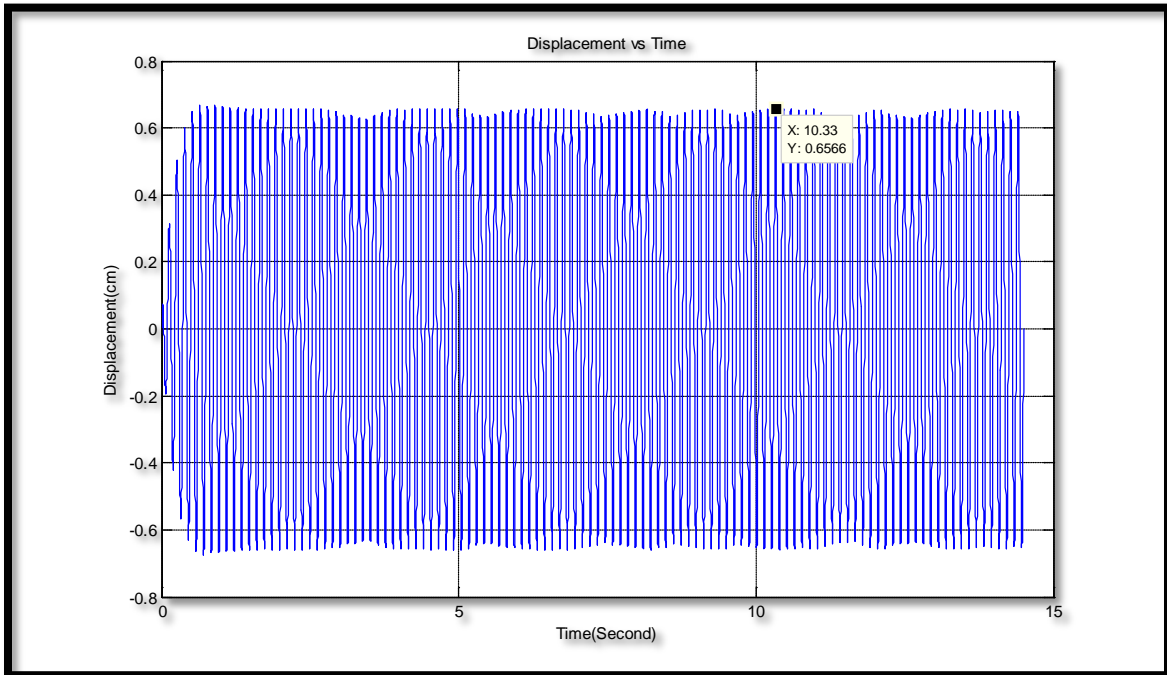
B_3200_20050_S05_D06_A50_7.75 Hz



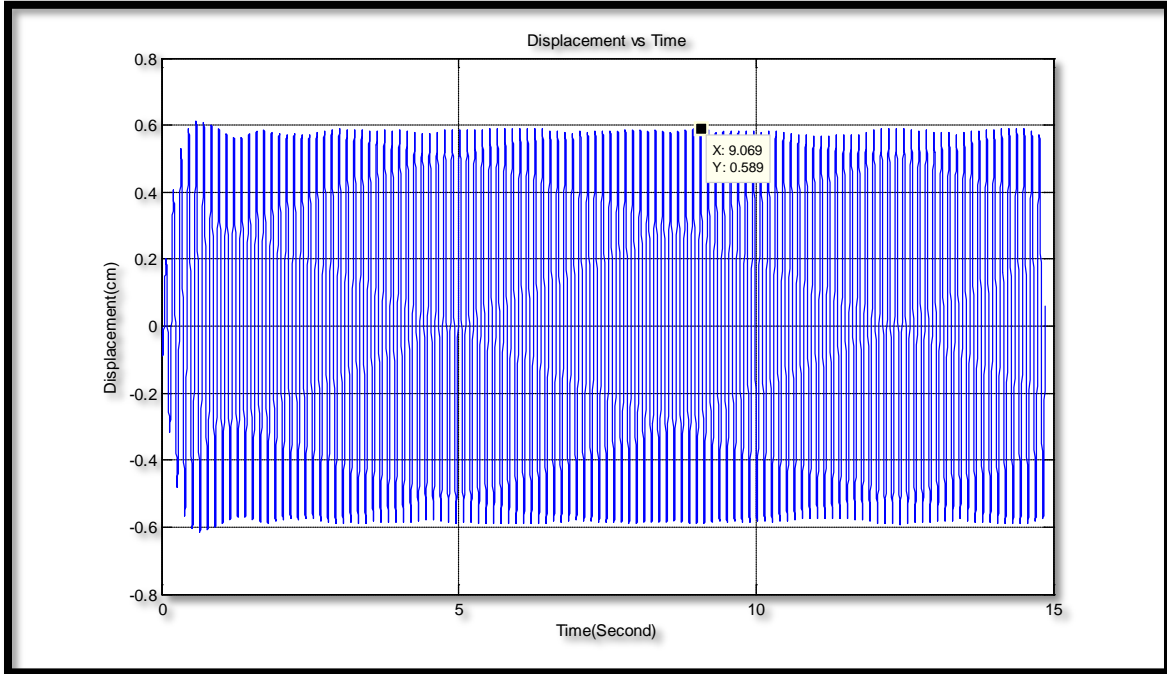
B_3200_20050_S05_D06_A50_7.80 Hz



B_3200_20050_S05_D06_A50_7.85 Hz



B_3200_20050_S05_D06_A50_7.90 Hz



Appendix D Damper design curves (Cheng et al, 2010)

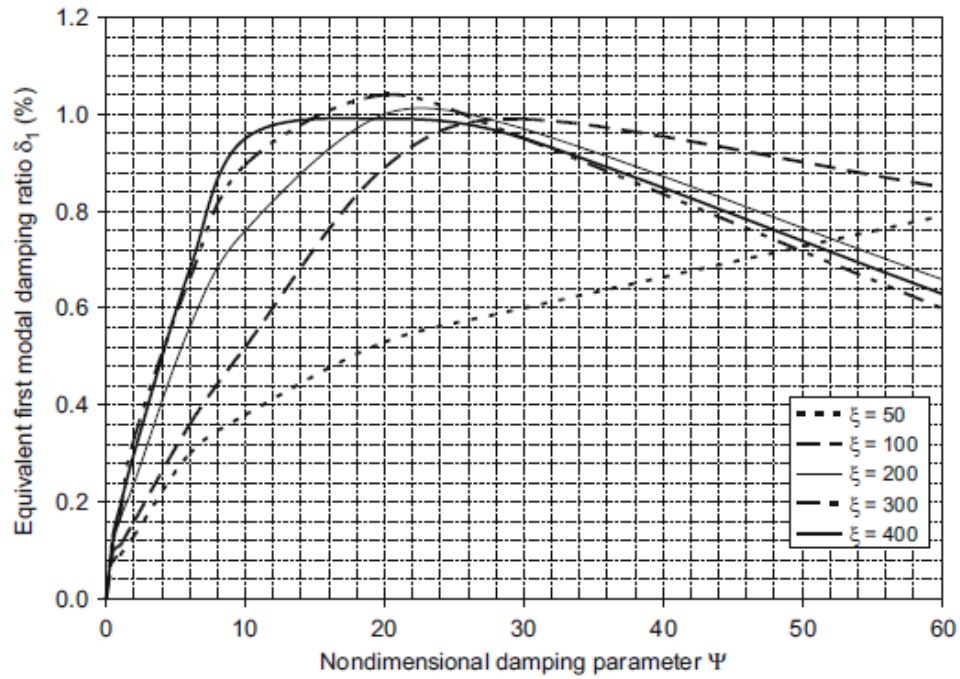


Figure D-1 Equivalent 1st modal damping ratio of a damped cable when damper at 2% L

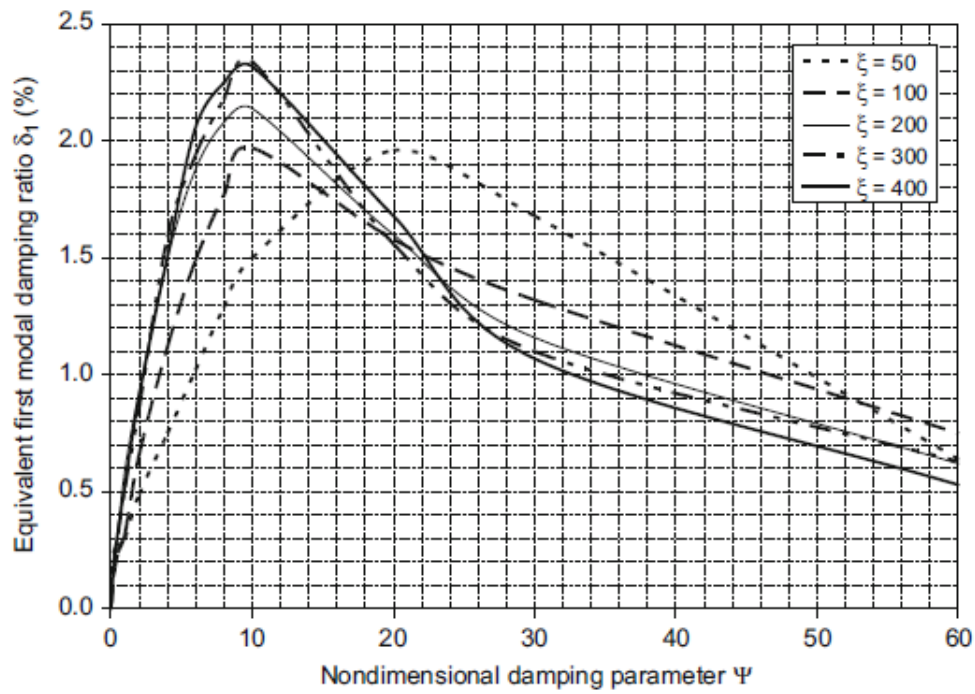


Figure D-2 Equivalent 1st modal damping ratio of a damped cable when damper at 4% L

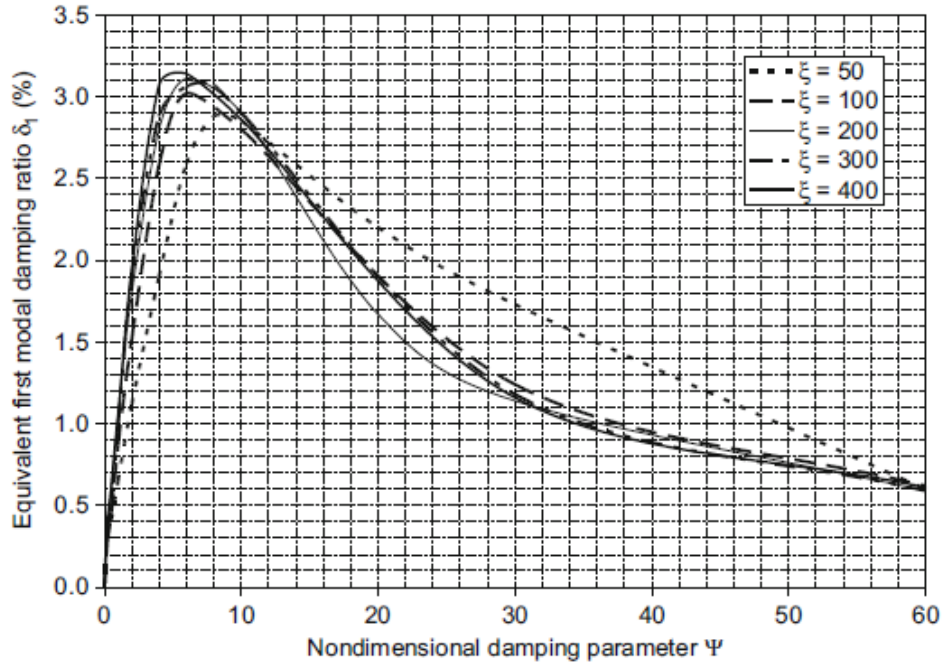


Figure D-3 Equivalent 1st modal damping ratio of a damped cable when damper at 6% L

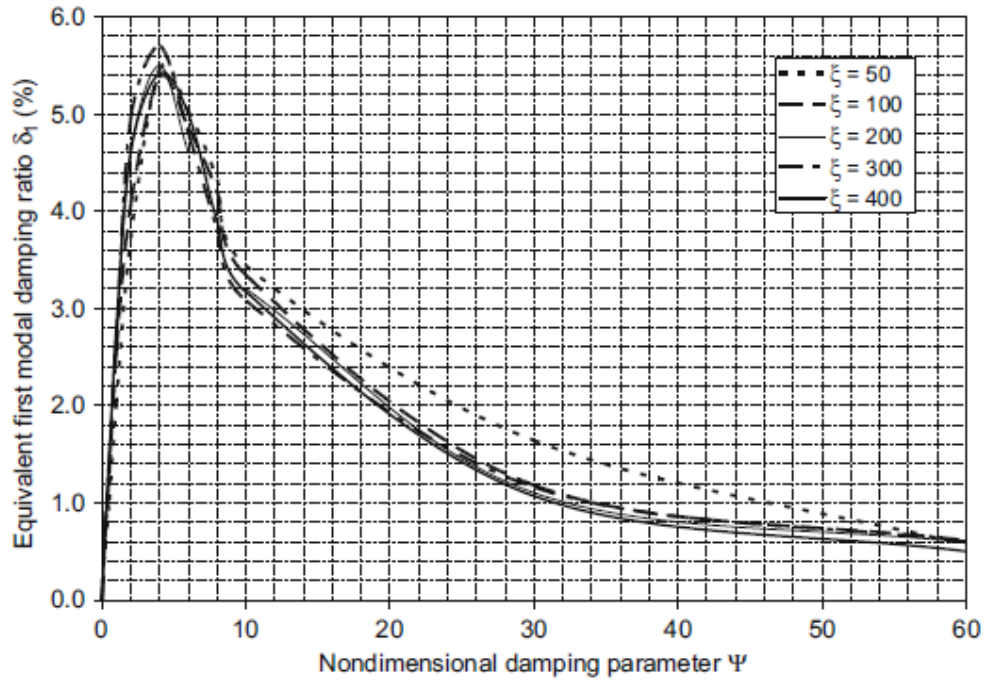


Figure D-4 Equivalent 1st modal damping ratio of a damped cable when damper at 10% L

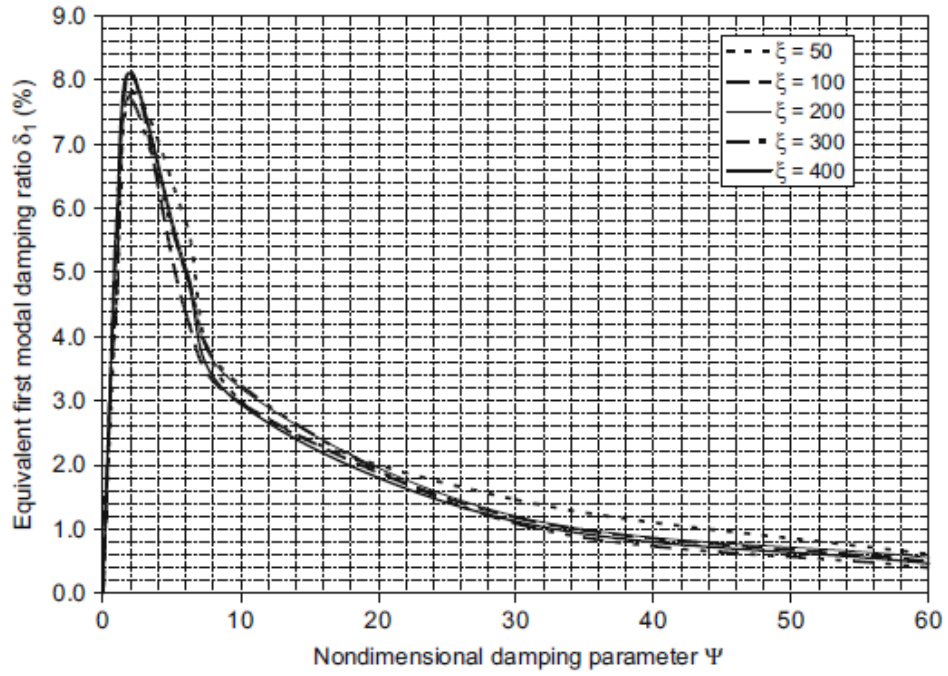


Figure D-5 Equivalent 1st modal damping ratio of a damped cable when damper at 15% L

VITA AUCTORIS

NAME: Le Huang

PLACE OF BIRTH: Nanjing, Jiangsu, China

YEAR OF BIRTH: 1983

EDUCATION: 2004- 2009 B.A.Sc University of Windsor, Windsor, Ontario

2009- 2011 M.A.Sc University of Windsor, Windsor, Ontario